ANTI-COKING MATERIALS FOR STEAM CRACKERS

A Dissertation
Presented to
The Academic Faculty

by

Shilpa Mahamulkar

In Partial Fulfillment
of the Requirements for the Degree
DOCTOR of PHILOSOPHY in the
SCHOOL OF CHEMICAL AND BIOMOLECULAR ENGINEERING

Georgia Institute of Technology
May 2017

ANTI COKING MATERIALS FOR STEAM CRACKERS

Approved by:

Prof. Christopher W. Jones, Advisor
School of Chemical & Biomolecular Engineering
Georgia Institute of Technology

Prof. Athanasios Nenes
School of Earth & Atmospheric Sciences
Georgia Institute of Technology

Prof. Pradeep K. Agrawal, Co-advisor
School of Chemical & Biomolecular Engineering
Georgia Institute of Technology

Dr. Andrzej Malek
Hydrocarbons R&D, Midland
The Dow Chemical Company

Prof. Thomas Fuller
School of Chemical & Biomolecular Engineering
Georgia Institute of Technology

Date Approved: 20th March, 2017

To my wonderful parents Suresh and Vasanti Mahamulkar
& my loving husband Ravi Kumar Kovvali

ACKNOWLEDGEMENTS

Foremost, I would like to extend my sincere thanks to my advisors Dr. Christopher Jones and Dr. Pradeep Agrawal for their continuous support throughout these five years. I am grateful for their invaluable advice, constructive criticism and the positive appreciation. Their enthusiasm and dedication towards work has been really inspiring. I thank the Dow Chemical Company, for funding the project and giving me an opportunity to acquire hands on experience in an industrial setting. I would like to thank our collaborators from University of Virginia, Prof. Robert Davis and Dr. Kehua Yin for the fruitful discussions and suggestions which have been instrumental in the work.

I had the pleasure to work with Dr. Hyuk Taek Kwon and would like to thank him for mentoring me in a new field of coatings. I am extremely thankful to my advising committee; Dr. Andrzej Malek, Dr. Hirokazu Shibata, Dr. Athanasios Nenes, Dr. Thomas Fuller for their assistance and suggestions throughout the duration of the project. I would particularly like to thank Dr. Micaela Taborga and Taylor Sulmonetti for performing XAS experiments for me. I would like to thank all Jones' group members for the stimulating discussions during group meetings and all the help in the laboratory.

Finally, my warmest thanks must be to my family and friends. I would like to thank my parents Suresh and Vasanti Mahamulkar and my sisters Swati and Dr. Shraddha Mahamulkar, for their invaluable support throughout my life, and tremendous belief in me. The major support system for me in these five years has been my husband Dr. Ravi Kumar Kovvali, and I thank him for the constant encouragement and the unconditional love and attention. I also would like to thank my professors and godparents, Prof. Anand

Patwardhan, Prof. Preeti Aghalayam for the professional and personal guidance they have provided over the years. I would like to thank my friends in India (Rohit More, Akshaya Chavan, Satyajit Sarak, Abhay Neve, Ankur Aher. Nirmit Shah, Ankita Pai, Sonali Raskar, Kaushal Sheth, Pallavi Pawar), who although were far but always just a call away. Away from India, I have my own Atlanta family (Dr. Sandeep and Sravani Kakumanu, Bhuvana Krishnaswamy, Swati Sharma, Sampath Adusumilli, Sruthi Kovvuru, Balachandra Suri, Ravi Kant, Yoshita Rathore, Raghuram Vadali, Bhanu Teerth, Srinath and Bhavya Pendyala, Madhura Joglekar, Lalit Darunte, Pradnya Samant, Akshay Korde, Jaya Arya, Rohan Awati, Sireesha Aluri) that has been especially very endearing and I thank them for making me feel at home.

TABLE OF CONTENTS

LIST OF TABLES

LIST OF FIGURES

LIST OF SYMBOLS AND ABBREVIATIONS

A	external surface area of carbon particle
CAMOL	catalyzed assisted manufacture of olefins
CVD	chemical vapor deposition
ρ	density of carbon
DFT	density functional theory
DRIFTS	diffuse reflectance infrared fourier transform spectroscopy
DTG	differential thermogravimetry
EDS	energy-dispersive X-ray spectroscopy
ESR	electron spin resonance
EXAFS	extended x-ray absorption fine structure
FTIR	fourier-transform infrared spectroscopy
NSLS	national synchroton light source
OSC	oxygen storage capacity
m	mass of carbon
r_0	radius of particle at time = 0
r_t	radius of particle at time = t
SEM	scanning electron microscopy
SOC	surface oxygen species
SOFC	solid-oxide fuel cell
t	time
TAP	temporal analysis of products
TEC	coefficient of thermal expansion

TEM	transmission electron microscopy
TEM-FIB	transmission electron microscopy – focused ion beam
TGA	thermo-gravimetric analyzer
TLE	transfer line exchanger
TOF-SIMS	time-of-flight secondary ion mass spectrometry
TPE	temperature programmed experiments
TPD	temperature programmed desorption
TPG	temperature programmed gasification
TPO	temperature programmed oxidation
TPHg	temperature programmed hydrogasification
TPR	temperature programmed reduction
UV-vis	ultraviolet – visible spectroscopy
ω	rate of mass loss ($g/cm^2 .s$)
XANES	x-ray absorption near edge structure
XAS	x-ray absorption spectroscopy
XRD	x-ray diffraction

SUMMARY

Steam cracking process is a major contributor to the industrial production of olefins. This pyrolysis process involves heating hydrocarbons to very high temperatures (800 °C – 1000 °C) in the presence of diluting steam. At these high temperatures, radical reactions play an important role in the formation of a wide range of hydrocarbons. One of the major by-products of the steam cracking process is formation of carbonaceous deposits (coke) on the wall of the reactor. The amount and type of coke formed depends on the operating conditions, nature of the feed, and nature of the reactor surface. Coke formation affects the production efficiency by increasing the pressure drop in the reactor, it reduces the reactor volume, increasing the temperature of the reactor tube by affecting heat transfer from the tube to the gas, leading to expensive shutdowns, etc. The aim of the study presented in this thesis is to develop catalysts that have the potential to minimize coke formation in steam crackers as well as help in the oxidation of these deposits at low temperatures.

In the first study, a specialized thermo-gravimetric analyzer was used for generation of *in-situ* coke. The external surface area of support was determined to be an important factor in determining the coking rate. Deconvolution of Raman spectra gave an insight into the chemical structure of the coke samples. *In-situ* generated coke was found to be more amorphous compared to an industrial coke sample. This result was attributed to the fact that industrial coke was subjected to a few months of high temperature treatment during the continuous operation of the reactor. Thermally aging the coke generated *in-situ* in an inert atmosphere increased the graphitic nature of coke. This finding was supported by temperature programmed oxidation studies and Raman analysis. *In-situ* coke deposition

was also observed to have improved coke-catalyst contact as compared to physical mixtures of coke and catalyst. *In-situ* generation of coke is more representative of the contacting conditions observed in industrial operations, than the tight contact method.

Performance of α-alumina supported ceria catalysts with varying composition was investigated for coking resistance and oxidation of coke formed *in-situ*. A larger amount of coke was deposited on bare α-alumina than on the ceria catalysts. This coking resistance was attributed to the redox property of ceria, allowing ceria to provide oxygen atoms for oxidation of coke precursors as soon as they are deposited on the ceria surface. Raman analysis on these *in-situ* coked catalysts revealed that more amorphous coke was formed on ceria-alumina catalysts as compared to bare α-alumina. The reaction rate constants for oxidation of coke were determined by fitting a first order rate equation to the mass loss data for isothermal experiments for data from 0 to 50% conversion. Ceria catalyzed oxidation was faster than un-catalyzed oxidation. In addition, ceria-alumina catalysts demonstrated faster kinetics than bulk ceria. At 350 ºC, the activity of the catalysts increased from 20 to 50 mol% Ce and then remained steady until 80 mol% Ce. TPR runs were used to measure the surface oxygen available at the temperature of oxidation for each of the catalysts. The activity of ceria-alumina oxides was related to the availability of these surface oxygen atoms. Higher surface oxygen availability increased the reaction rate.

Ceria catalysts were further developed for steam gasification of carbon deposits. This involved doping the ceria lattice with transition metals (Mn, Co, Cu), alkali metal (Sr), and rare - earth metal (Gd). Among all the different catalysts, the material containing Gd was found to be the best for steam gasification studies and was able to reduce the gasification temperature by 65 °C. In addition to steam, Gd, and Mn doped ceria catalysts

also showed improved activity for oxidation. In the presence of steam – air mixtures, oxidation due to air dominated the process and Gd showed the best activity by reducing the gasification temperature by 125 °C. Catalytic gasification of coke also took place in hydrogen atmosphere with simultaneous reduction of the catalysts. The activity of the Gd doped catalyst could be related to the presence of oxygen vacancies, small crystallite size and the high dispersion of the dopant. For Mn doped ceria, the high activity in gasification and oxidation can be attributed to the presence of active species Mn_3O_4 and oxygen vacancies. The possible incorporation of Sr into the ceria lattice and the smaller crystallite size could be the reason the high activity of the Sr doped catalyst for coke gasification in steam.

Lastly, these developed catalytic materials were used in the form of coatings on a metallic substrate to evaluate the coking as well as decoking performance. α-Alumina was first coated on an Incoloy substrate followed by a ceria layer. Sol-gel method gave smaller particles of ceria and negligible flaking than the precursor method of preparation. These catalytic coatings not only reduced catalytic coking, by acting like a barrier between the gaseous hydrocarbons and the metallic species on the Incoloy substrate, but also reduced the coke oxidation temperature by ~ 160 °C. Negligible interaction existed between the ceria layer and the Incoloy substrate, which was reflected in the same activity of supported and unsupported ceria layers. α-Alumina was found to be essential for hindering the diffusion of Cr atoms into the ceria layer and maintain the activity of the ceria layer. Over a period of four coking and decoking cycles, ceria layer exhibited slight deterioration in the performance as shown by the increased oxidation temperature by 10 °C.

The above studies will aid in the design of catalysts for low temperature gasification and oxidation of carbonaceous deposits, thus reducing the energy demand and efficiency of the steam cracking process.

CHAPTER 1. FORMATION AND OXIDATION/GASIFICATION OF CARBON

This chapter is largely adapted from 'Mahamulkar, S; Yin. K; Agrawal P. K.; Davis R.; Jones, C.W.; Malek A.; Shibata H. Formation and oxidation/gasification of carbonaceous deposits – a review. Ind. Eng. Chem. Res. **2016**, 55 (37), 9760 – 9818' and also with permission from Dr. Kehua Yin, co-author on the paper.

1.1 Steam Cracking

Carbonaceous deposits are produced during incomplete hydrocarbon combustion (soot in diesel engines),[1,2] catalytic conversion of hydrocarbons (coke deposited on catalysts),[3–6] and thermal decomposition of hydrocarbons (coke formed in steam crackers).[7–9] These deposits cause numerous problems in chemical plants and diesel engines. To this end, significant research has been focused on the development of technologies that aid the oxidation of such deposits and/or limit the coke deposition.

Two temperature ranges exist in which deposition of carbon commonly takes place namely: a low temperature regime – below 600 °C, and a high temperature regime: 800 °C – 1000 °C. Soot formation in diesel engines and coke deposition on catalysts takes place at the lower temperatures.[1] Coke formed during steam cracking reactions and soot formed in diffusion flames, however, occurs at very high temperatures.[10]

Under ideal conditions, CO_2 and H_2O are the products of complete combustion of hydrocarbons in diesel engines. However, thermodynamic equilibrium is not achieved in engines due to the limited time available for combustion and the huge temperature variation

in the combustion chamber.[2,11] Moreover, collisions among hydrocarbon fragments are common in fuel-rich atmospheres leading to the formation of soot.[12] Health hazards of soot, like chronic respiratory disorders, make it important to minimize its emission by capturing it and subsequently oxidizing it.[1,2]

Another major process contributing to carbon deposits is steam cracking, which is a widely used process for the industrial production of olefins. This pyrolysis process involves heating hydrocarbons to very high temperatures (800 °C – 1000 °C) in the presence of diluting steam.[10,13,14] The cracking units are typically made of alloys containing Ni, Fe, Cr, that are capable of withstanding very high temperatures.[14] The residence time for these reactions is around 0.5 – 1 s. At these high temperatures, radical reactions play an important role in the formation of a wide range of hydrocarbons. One of the major by-products of the steam cracking process is the formation of carbonaceous deposits (coke) on the walls of the reactor. The amount and type of coke formed depends on the operating conditions, nature of the feed, and nature of the reactor surface. Steam dilution of the feed has been observed to reduce coke formation.[15] Coke formation increases pressure drop in the reactor,[16] reduces the reactor volume, increases the temperature of the reactor tube by affecting heat transfer from tube to gas, leads to expensive shutdowns, causes carburization of steel, influences the flow in the reactor, decreases the production capacity.[17,8,10]

Coke formed in the cracking reactor is typically combusted by passing a mixture of steam and air at very high temperatures through the reactor in regeneration mode. The plant typically requires a shutdown for decoking every 20-60 days, depending on the type of hydrocarbon feed used.[18] These shutdowns are usually expensive and efforts are directed towards increasing the run length of steam crackers by minimizing coke deposition.

1.2 Reaction Mechanisms of Carbon Deposition

For scientific analysis of carbon oxidation studies, it is important to examine the mechanisms by which the carbon deposits are formed. As mentioned previously, deposition of carbonaceous compounds depends on numerous factors and hence can take place by a variety of pathways. Broadly, the mechanisms have been classified in this section based on the temperature range in which carbon deposition takes place.

Steam cracking involves thermal decomposition of hydrocarbons at high temperatures (800 – 1000 °C) to yield valuable products like olefins. At these high temperatures, radical reactions play an important role in the formation of a wide range of hydrocarbons. The major reaction for cracking of ethane involves dehydrogenation as shown in Equation 1:

$$H_3C - CH_3 \rightarrow H_2C = CH_2 + H_2 \quad (1)$$

Steam cracking reactions are highly endothermic and many of the elementary radical reactions have high activation energies. To reduce the production of undesired reactions such as formation of large hydrocarbons like poly-aromatics structure, the products are typically immediately cooled in a transfer line heat exchanger (TLE). The end product is a complex mixture of hydrocarbons. This mixture is separated by distillation and absorption processes to obtain valuable products like olefins. Paraffins from natural gas, as well as naphtha and gas oil from petroleum refineries, are the major feed-stocks for production of olefins.

The major byproduct of steam cracking is deposition of coke on the reactor surfaces. Coke deposition in steam cracking reactions is a combination of the following mechanisms namely: radical reactions in the gas phase, droplet condensation and coke formed on metallic particles. These carbon forming mechanisms are described in detail in the following sections.

1.2.1 Catalytic Coking Mechanism

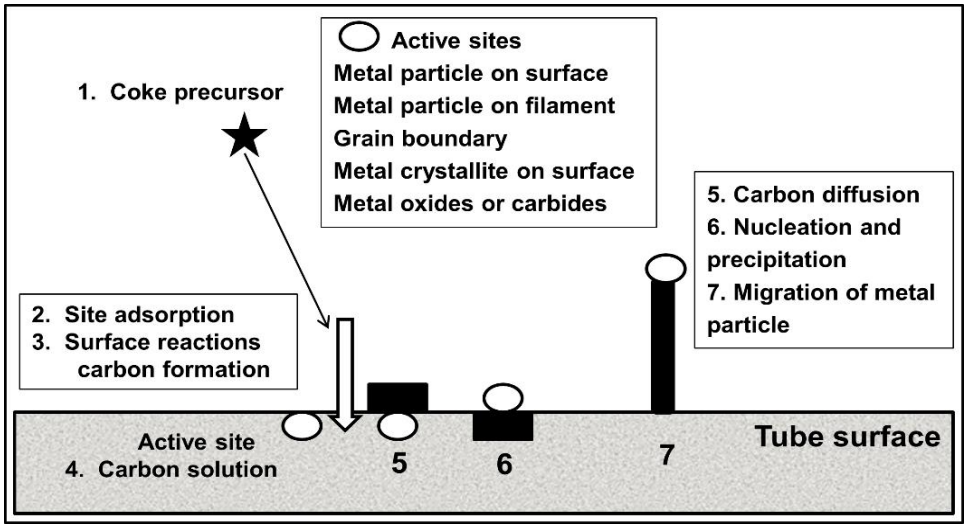

Figure 1.1 Catalytic coke formation schematic

In a steam cracker, catalytic coke formation takes place in the presence of catalytic sites, which can be the metallic walls of the reactor, more likely at grain boundaries.[10,19] Since most industrial cracking units are made of alloys of Ni, Fe, and Cr, many types of metallic sites are present on the reactor surface. These sites can catalyze coke formation at temperatures as low as 500 °C. Although the catalytic coking rate increases significantly with increasing reaction temperatures, the coking rate is also highly dependent on the reactor surface used. Due to the presence of metallic sites, coking rates are higher in reactors made of materials like stainless steels or Incoloy (superalloys made of iron-nickel-chromium having good corrosion resistance and stability at high temperatures), compared

to more inert oxide materials such as quartz.[8–10,20] Figure 1.1[19] shows a schematic of the catalytic coking process taking place on a reactor wall. Hydrocarbons adsorb on the metallic surface and form coke. This coke further dissolves and diffuses through the metallic particle. With time, carbon deposits at the end of the metal particle, raising the metal from the reactor surface. With time, additional carbon is deposited at the back end of the metal particle leading to formation of extended carbon filaments. Hence, the carbon formed by this mechanism is referred to as filamentous coke. The presence of metallic tips on the filaments makes them grow faster than the structure less coke deposits described earlier. Carbon migration can take place on the surface of the metal in some cases, blocking the metal sites and preventing further growth of the filament. This reduces the rate of dehydrogenation of the hydrocarbons thereby reducing the rate of coke formation. This mechanism is most important after the decoking step when the reactor wall is clean, devoid of any coke exposing the metallic sites on the surface for reaction.[21]

The ease of carbon deposition on a metal particle depends on the thermochemical stability of the bulk metal carbide phase.[22] Kock et al. concluded that formation of a metal carbide phase is a prerequisite for the synthesis of filamentous carbon.[23] Figure 1.2 shows the various ways in which carbon can be deposited on a Co catalyst during Fischer-Tropsch synthesis.[24] In the rate limiting step, CO dissociates to form adsorbed atomic carbon (C_α), amorphous carbon (H-containing carbon) (C_β), vermicular carbon (C_v), carbidic carbon (C_γ) and graphitic carbon (C_c).[3] A few studies show a distinction between coke and carbon based on the source of formation. The product of the Boudouard reaction (Figure 1.2) is termed as carbon while that of reactions involving hydrocarbons is termed as coke.[3]

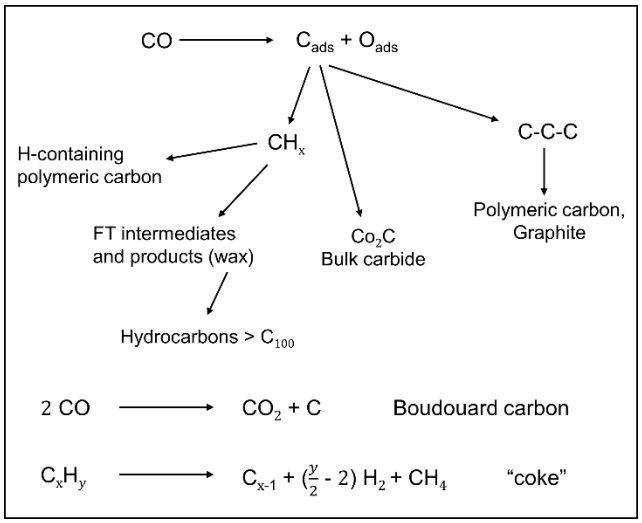

Figure 1.2 Coke formation pathways on a Co catalyst

Similar mechanisms of coke formation are observed on Ni catalysts.[25] The coke formed either blocks the catalytic sites on the surface or blocks the catalyst pore entrance, which can weaken the structure, causing its breakdown.[4,25,26] Rostrup-Nielsen et al. claimed that concentration driven dissolution-precipitation was the most likely mechanism for the growth of carbon filaments. There is a difference between the solubilities of carbon in metal from the hydrocarbon side and from the carbon whisker side. Radical reactions in the gas phase lead to carbon deposition on the metal particles. This carbon dissolves into the metal and the presence of dislocations on the metal particle causes the precipitation of carbon, as shown in Figure 1.3 where C_1 is the solubility of carbon in Ni with respect to C_nH_m and C_2 with respect to graphite (Figure 1.3).[25] Earlier studies by Yang et al. have shown the importance of a temperature driven carbon diffusion mechanism.[27] They demonstrated that methane and n-hexane, which have endothermic heats of decomposition, formed a layer of coke on the face of Ni exposed to hydrocarbon. However, benzene and toluene, whose decomposition is exothermic in nature, formed a layer of coke on the Ni

face that was not exposed to hydrocarbon. This suggested that carbon diffusion took place through a temperature-driven diffusion process.

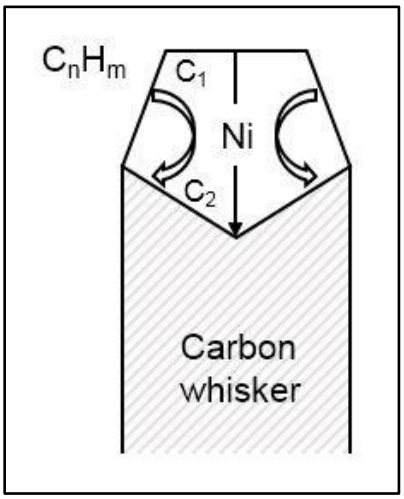

Figure 1.3 Carbon diffusion model

1.2.2 Radical Coking Mechanism

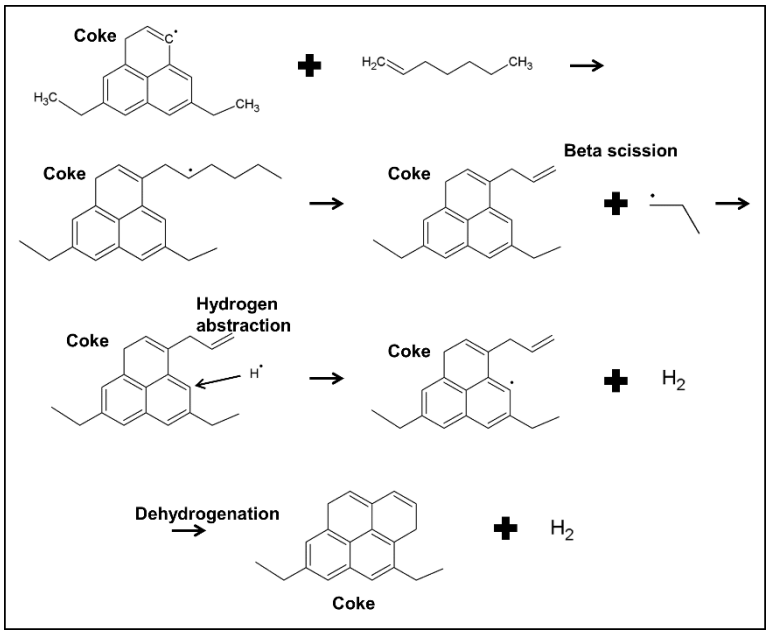

Figure 1.4 Radical mechanism for coke formation

At very high temperatures in the steam cracker, radicals are formed in the gas phase producing pyrolytic coke, which deposits on the reactor surface.[10,19] These endothermic

reactions require significant energy input to form the radical intermediates and hence take place only at high temperatures. Figure 1.4 shows a pathway for the formation of coke by the radical mechanism.[19] Coke radicals in the gas phase react with the hydrogen present in unsaturated hydrocarbons. Decomposition of the aliphatic chain gives rise to new radicals. Further dehydrogenation of such molecules results in increase in the aromatic nature of the coke and also regeneration of radicals. Coke formed by this mechanism has very low hydrogen content because of the dehydrogenation of molecules during the coking reactions. The coke formed is typically very hard (graphitic) due to the cross-linking of aromatic molecules under the reaction conditions.

The rate of coke formation is highest for acetylene and lowest for paraffins and follows the order: acetylene > olefins > aromatics > paraffins.

1.2.3 Droplet Condensation Coke

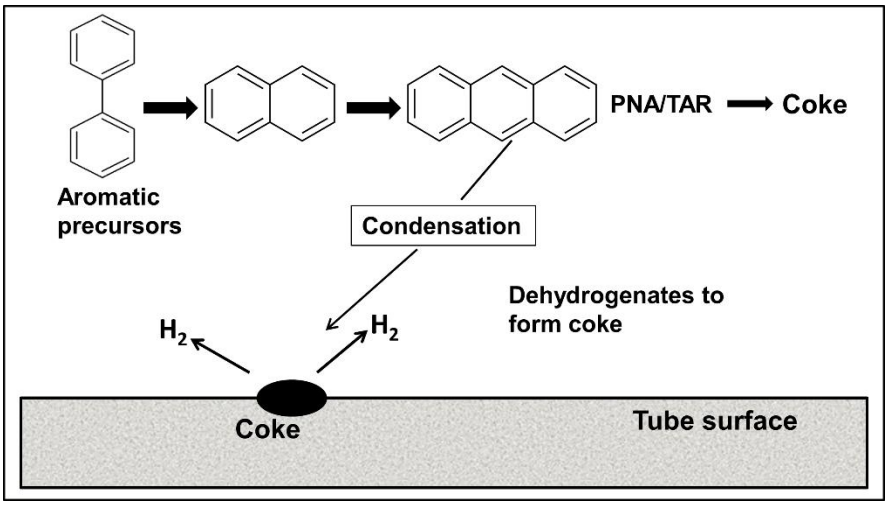

Figure 1.5 Droplet condensation mechanism

Aromatics with one or two rings act as coke precursors and condense by dehydrogenation to form tar-like particles after striking the reactor surface.[28] This

condensation takes place downstream of the cracking reactor where the temperature is lower than that in the reactor furnace. A schematic of the droplet condensation mechanism is shown in Figure 1.5. At elevated temperatures, molecules undergo dehydrogenation, aided by radicals. This mechanism helps in further growth of the coke layer. Some molecules undergo hydrogen abstraction in the gas phase itself and are deposited on the reactor surface. The coke formed in the transfer line exchanger results from the condensation of polyaromatics.[9] Since the mechanism involves condensation of aromatic molecules at lower temperature, the coking rate is independent of the chemical characteristics of the reactor surface.[9]

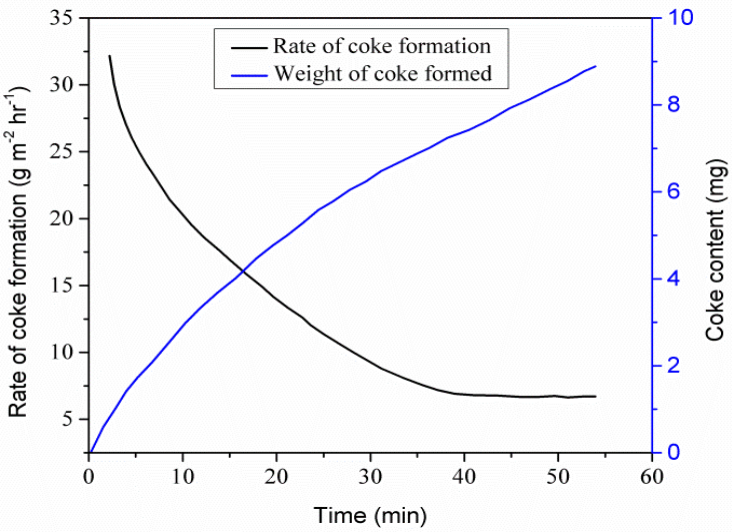

Figure 1.6 Rate of coke formation and weight content on a metallic cylinder

Figure 1.6 shows the rate of coke formation on a stainless steel surface as a function of time. The rate is initially high and decreases with time.[18] Coke formation takes place both by catalytic and radical mechanism in the region where the coking rate changes with time. Deposition of coke on the metal surface decreases the rate of catalytic coke formation until all of the sites are blocked. At this point, the rate of coke formation becomes

approximately constant and only radical coke is formed. Hence, at any given point of time, both catalytic and radical coke deposits are found on the reactor surface. After understanding the mechanisms of coke formation, the next step towards developing new technologies for minimization of coke would be to know what currently exists in the market and how successful they have been. This topic is summarized in the next section.

1.3 Inhibition of Coke Formation in Steam Cracking

Various researchers have undertaken different novel routes to reduce the coke formed due to the catalytic mechanism. The main approach to reduce the coke formed by this method is to create a barrier between the metallic reactor surface and the gas phase in the reactor. For example, an aluminum coating was used to passivate the cracking reactor surface before the reaction began, which reduced the amount of catalytic coking.[17,29] Addition of magnesium to aluminum further reduced the coking rate. It was observed that the coke deposition reduced significantly due to these coatings, as the metal reactor surface sites were blocked. Zinc coatings were found to be effective in the oxidation of the coke formed on the reactor surface.[17] Thermal spraying,[29] plasma spraying,[17] packed cementation[17,29] and chemical vapor deposition (CVD) techniques were used for coating of ceramic powders on the cracking furnace.[14] TiC and SiC coatings proved to be effective in reducing the rate of coke formation for n-hexane cracking.[14]

A coating of sulfur or phosphorous on the cracking furnace was shown to passivate the reactor surface, leading to decreased coke formation. This involved formation of metallic sulfides or metal phosphorous complexes that coordinated with the metal sites and reduced their catalytic activity. Addition of SiO_2/S to the S/P coating further enhanced the

coke reduction.[30–32] Dimethyl disulfide and carbon disulfide are other sulfur compounds used as coke inhibitors.[17] Annealing of the cracking furnace in the presence of a H_2/H_2O mixture was applied at higher temperatures to reduce the presence of metallic sites (Ni, Fe) and enrich the surface with chromia.[33]

Westaim Surface Engineered Products Inc. developed a coating called CoatAlloy™ for use in ethylene pyrolysis furnaces. The coating consists of three layers: to prevent catalytic coking, gasify radical coke and stop carbon deposits from penetrating the metal surface to cause carburization. After one year of service, no carburization was observed on the surface of the coating.[34] SK Corporation developed a coating called PY-Coat that serves similar purposes.[35] The coating formulation is immediately injected into the hot furnace after the decoking step. The formulation vaporizes and deposits on the reactor inner surface and acts as a barrier. The basic components of the coating are Si, Cr, Al, Ti, and alkali and alkaline-earth. In a pilot plant set-up for ethane cracking at 65% conversion, the coating showed no pressure drop and temperature drop. The uncoated reactor showed a pressure drop of 27 psi and temperature difference of 26 °C higher than the start of the operation.

Another furnace coil coating technology called catalyzed assisted manufacture of olefins (CAMOL) by BASF aims to have a coke-free environment in cracking furnaces.[36–38] This technology proposed to increase the run-length of the reactor and has been undergoing commercial trials since 2006. These coatings have the ability to be used in high temperature furnaces above 1130 °C, and they can potentially reduce the amount of steam required for dilution to keep coke formation to an optimum. The coatings act as a barrier between the metal sites from the reactor and the hydrocarbon gases and usually exist as an oxide layer < 10 µm in thickness. The coating also has a catalytic layer that can gasify the

coke formed on the surface of the coating. Around 1 – 2 furnace run-lengths have been achieved with this technology for lighter feedstocks and around 100 days for higher feedstocks. The coating was reported to have no impact on the product distribution and a positive impact on the yield of products, by mitigating the formation of filamentous and amorphous coke. Two types of coatings have been developed, including one for low-level catalytic gasification for lighter feeds and another for high-level catalytic gasification coating for heavier feeds.

The Alcroplex® diffusion coating from Alon Surface Technologies Inc., which is a surface modified HP material (heat resistant alloy made of iron-nickel-chromium), has been reported to reduce the coke formation rate up to 90% in the cracking of ethane.[39] It is a technology that uses a CVD mechanism for creating a stable coating on the surface of the reactor. Commercially, it has performed well by reducing the carburization of the steel and also the surface-induced catalytic coking.

NOVA Chemicals developed a technology called ANK 400 over the past 10 years.[40,41] They claim to have increased run lengths in the crackers around 10 fold with the help of an inert, nanocrystalline spinel coating that reduces both catalytic and radical coke. They also have various pretreatments that could be carried out on stainless steel reactors that can help passivate the reactor surface and reduce coke formation.[42]

Schietekat et al. recently developed a coating called YieldUp based on a perovskite catalyst system for reducing coke formation during steam cracking.[40] These coatings reduced the coke formed on Incoloy 800HT drastically by aiding the reaction of coke with steam. A reduction of 76% in the coke deposition on Incoloy was reported. Performance

of the coating in an industrial reactor was checked by a simulation of the reactor. It was estimated that a 525% increase in the run length could be achieved by application of the coating.

In other work, an H_2PtCl_6 additive lowered the rate of coke formation during steam cracking of ethane or propane, both on a quartz and a stainless steel reactor.[8] Quartz is inert in nature due to the absence of metallic sites on its surface. The coke formed on quartz surfaces is mainly gas phase coke. Stainless steel has presence of metallic sites which can catalyze coke formation. Both pyrolytic and catalytic coke species are formed on stainless steel surfaces. The addition of H_2PtCl_6 was able to reduce both pyrolytic and catalytic coke.

The coatings of materials on cracking furnaces develop cracks after prolonged use at higher operating temperatures. These cracks might then serve as the sites for catalytic coke formation. Thus, efforts are underway to increase the stability of the coatings used to passivate the surface, thus further increasing run lengths of the steam crackers. Catalytic coke is easier to minimize by using the existing coating technologies to act as a barrier between the gas and the metallic species. The real challenge lies in minimizing the radical coke deposits that are much harder to oxidize than the catalytic coke species. Hence, this work will involve working with radical coke deposits alone.

A critical step towards development of new technologies for minimization of coke deposits and/or aiding their oxidation involves choosing the right catalyst, which needs a basic understanding of the mechanism of oxidation of the carbon as well as the kinetics in the presence and absence of a catalyst. This knowledge can help in choosing the best

catalyst for further investigations. The next section tries to provide a comprehensive overview of the different catalysts used for similar applications.

1.4 Kinetics and Mechanism of Carbon Oxidation

1.4.1 Non-catalytic Radical Carbon Oxidation

To study the catalytic activity of materials in the oxidation of carbon, it is important to understand the kinetics and nature of the non-catalytic carbon oxidation as well. Screening of catalysts can be done by comparing oxidation rates in the presence and absence of catalyst. Catalysts with the highest difference in oxidation temperature compared with the non-catalytic oxidation and/or activation energy for carbon oxidation are identified as those with the highest activity. This section discusses the oxidative behavior of carbon deposits formed by radical reactions in the absence of any catalyst. A large extent of carbon oxidation literature involves use of diesel soot as the source of carbon. Soot is also formed by radical reactions in the diesel engines and hence an excellent example for reference.

Higgins et al. studied the *in-situ* oxidation of diesel and flame soot in the presence of air.[43] They concluded that the overall kinetics of oxidation of these two types of soot were not very different, which is also supported by data obtained by Neeft et al.[44] The oxidation rate of flame soot and diesel soot were the same at a temperature of 760 °C, below which the rate of oxidation of diesel soot was observed to be higher than for flame soot. This was related to the presence of catalytically active metal particles observed in soot particles originating from diesel fuel or lubricating oil. Mechanistically, both the soot

samples are formed by a radical mechanism, the difference being the temperature at which they are formed.

The reaction order in molecular oxygen of flame soot oxidation was found to be one and slightly less than one for diesel soot oxidation.[44] The reaction order in carbon for flame soot was observed to be 0.7 according to the power law model. The authors reported that the reaction order depended on the carbon conversion; however, no correlation was determined. The activation energy for flame soot oxidation was determined to be 164 kJ mol^{-1}. Dernaika et al.[45] found the peak oxidation temperature of diesel soot to be 565 °C with an activation energy of 164 kJ mol^{-1} similar to that of flame soot.

López-Suárez et al. showed that the non-catalytic oxidation of soot yielded mainly CO, indicating incomplete oxidation of the carbon.[46] The selectivity towards CO_2 did not change when NO_x/O_2 was used instead of air for oxidation. However, the onset temperature for the non-catalytic soot oxidation decreased in presence of NO_x/O_2.

For surface reactions between oxygen and carbon, a shrinking core model has been used for analysis of the oxidation data. The model is given by Equation 2 & 3:

$$-\frac{dm}{dt} = \omega A \tag{2}$$

$$\omega = \frac{\rho}{t}\,(r_0 - r_t) \tag{3}$$

where A is the external surface area of the particle, ω is the rate of mass loss (g/s-cm^2), m is the mass burned in time t, r_0 is the diameter of the particle at time zero and r_t is the diameter at time t. The density of most carbons is between 1.8 and 2.0 g/cm^3.[47] In this

model, the rate of combustion is proportional to the surface area of the carbon.[48] The total surface area of a particle shrinks slower than the volume leading to an increase in specific surface area. The reaction order with respect to carbon for this model is 0.67.[49,50] Burning of carbon follows a shrinking core model at high temperatures (> 800 °C), whereas at low temperatures the oxidation differs according to the reactivity of the carbon species. Darcy et al. found a reaction order of 0.5 under 5 - 20% O_2 between 500 °C – 560 °C in the conversion range of 15 – 90%, and claimed it to be close to the value of the shrinking core model.[51]

According to a few researchers, OH radicals instead of molecular oxygen, are responsible for soot oxidation. Fenimore et al. found that the oxidation rate of flame soot was independent of the partial pressure of oxygen.[52] They claimed that the oxidation of soot involved OH radicals rather than molecular oxygen. Neoh et al. published a similar result and proposed that oxidation by OH radicals was of primary importance and by O_2 was of secondary importance.[53] The size of the soot particles was measured using light scattering methods. The authors claimed that neglecting oxidation of soot under fuel-rich flame conditions underestimated the oxidation behavior. Puri et al. used laser induced fluorescence to measure the concentration of OH radicals during soot oxidation[54] and the concentration reduced significantly in the presence of soot particles. Evidently, a higher concentration of soot led to an increased collision efficiency for $OH^{\cdot}$ radicals. CO is more reactive than soot; however, the presence of large concentration of soot suppresses CO oxidation. In laminar flames, oxygen diffusion allows for oxidation of soot particles, CO or hydrogen. Feugier studied a fuel-rich flame system and calculated the activation energy for soot oxidation to be 138 kJ mol^{-1}.[55]

Fragmentation of soot particles is another mechanism by which oxidation can take place in addition to surface reactions with OH or O_2. In this mechanism, the oxidizing species can penetrate the soot particles causing a breakdown of big particles into smaller ones. Neoh et al. showed that in lean flames, after a burnout of 80% of the soot, the breakdown of the soot particles takes place.[56] This phenomenon has been attributed to the internal burning of particles by O_2. This breakdown is absent in rich flames where the major oxidant is OH radicals. OH is more reactive than O_2 and causes less internal burning. Fragmentation of particles can take place in two ways; breakdown of aggregates or of a single particle.[57] In the case of aggregates, the fragmentation occurs at the contact points of the primary particles. For single particles, the fragmentation depends on the internal structure of the particle. The rate of fragmentation can be related to the oxidation rate, as oxygen causes the fragmentation. This model was used to accurately predict the burnout of particles in non-premixed flames.[57]

In our recent review paper, the activation energies and reaction orders with respect to oxygen and carbon during the oxidation of various types of carbon materials are listed. The activation energy values vary in the range 130 – 170 kJ mol^{-1}. The reaction order in oxygen for low temperature oxidation of soot has been widely accepted to be nearly one.[44] However, some researchers do report a lower value of the reaction order in oxygen.[50] The reaction order in carbon has scattered values in literature due to the different sources of carbon and varied reaction conditions used by different researchers.

1.4.2 Catalytic Oxidation of Radical Carbon

Although there is an abundance of literature on catalyzed carbon oxidation, most research reports qualitative observations rather than quantitative ones. Majority of the results are obtained from temperature programmed oxidation reactions, in which specific temperatures of oxidation are reported and compared. The most common characteristic temperatures used are T_{50} (temperature at which 50% of the carbon is oxidized) and T_{max} (peak temperature of the temperature programmed oxidation (TPO) curve). The wide variety of reaction conditions, including variations of carbon type, catalyst to carbon mass ratio, heating rate, and oxygen concentration, make comparing catalyst performance difficult. The oxidation temperature of non-catalytic carbon oxidation is often reported to be different in the literature even when the same carbon and similar reaction conditions are applied. The non-catalytic oxidation temperature, T_{50}, in different reports varies between 586 °C and 651 °C. Therefore, one may surmise that the relative decrease of the oxidation temperature of the catalyzed reaction compared with the non-catalytic reaction may better represent catalyst activities than the absolute catalyzed carbon oxidation temperature. In our recent review paper,[58] the type of temperature is reported along with its decrease as compared to the non-catalytic oxidation.

Despite the relatively few efforts reported in the literature to obtain quantitative reaction rates from isothermal reactions, one can calculate reaction rates from TPO results reported in the literature when enough information is provided. The recent review also includes reaction rates based on the total surface area of the catalysts, which may be used for simple reaction modeling. The comparison of reaction rates is complex for catalyzed carbon oxidation reactions. The most important parameter to use as a reference for

quantitative comparisons is likely the non-catalytic reaction temperature. A small shift in the TPO curves can cause a large change in the calculated reaction rates. Ideally, these changes are associated with variations in use of a well-characterized catalyst, and not other factors.

1.4.2.1 Cerium Oxide Based Catalysts

Cerium based oxides are used in the three-way catalytic converter for elimination of CO, hydrocarbons and NO_x in engine exhaust gas due to their excellent oxygen storage capacity.[59] These oxides have also gained much attention for diesel soot oxidation.

Early studies used cerium salts as fuel additives in diesel engines. Cerium oxides were formed in the combustion process and entered the soot particles, which significantly lowered the ignition temperature of the soot and increased the oxidation rates by 20 fold.[60,61] However, the exhaust of cerium nanoparticles poses potential environmental, health and ecological effects, which need to be taken into consideration, disfavoring use of these species as fuel additives.[62]

Bueno-López et al. studied the CeO_2 catalyzed soot oxidation reaction with labelled oxygen in an advanced temporal analysis of products (TAP) reactor.[63] They found that the oxygen from CeO_2 reacted with soot, and the direct reaction of the gas-phase oxygen with soot did not occur under the conditions used. They defined such oxygen as "active oxygen", which was induced from the chemisorption of gas-phase dioxygen on CeO_2. Such "active oxygen" may be oxygen superoxide ions (O_2^-), which were detected by ESR[64] and FTIR experiments.[65,66]

However, these measurements were not performed under *in-situ* soot oxidation reactions. Density functional theory (DFT) calculations have also confirmed the formation of superoxide and peroxide ions on ceria-based catalysts.[67,68] Machida et al. concluded that active oxygen could be formed by either the lattice oxygen at the CeO_2/soot interface or gas-phase oxygen adsorbed at the boundary of soot + reduced CeO_2 + the gas phase, with the former being much more important.[64] The active oxygen was not only localized at the CeO_2/soot interface, but also transferred to the soot surface by spillover through surface diffusion.[69] However, the distance of spillover for active oxygen species was still not clear. The active oxygen species then reacted with soot to form surface oxygen species, followed by their decomposition to form CO and CO_2. Figure 1.7 shows a scheme of the proposed active oxygen mechanism for CeO_2 catalyzed carbon oxidation.

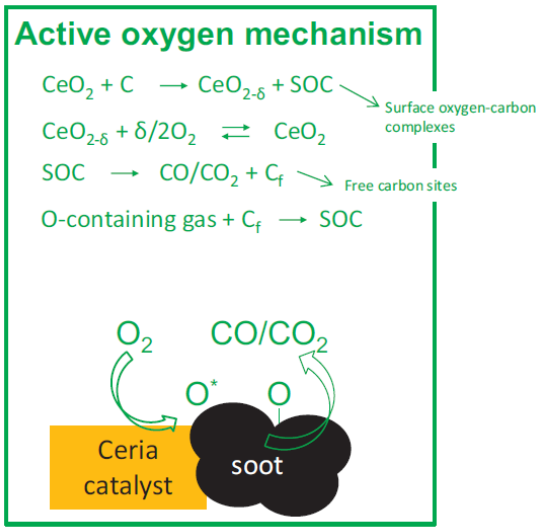

Figure 1.7 Scheme of active oxygen mechanism for CeO_2 catalyzed carbon oxidation

Shape-dependent activity of ceria has been observed in soot oxidation.[70,71]Aneggi et al. synthesized ceria nanocubes displaying (100) surfaces, ceria nanorods with a mixture of (100), (110) and (111) surfaces exposed, and conventional polycrystalline ceria with the

majority of the surface displaying (111) faces. The nanoshaped ceria showed higher soot oxidation activity than the polycrystalline ceria. The authors concluded that the activity order of the surface was: (100) > (110) > (111).[71] Such surface sensitivity may be caused by the different stability of active oxygen species on each face. Keating et al. concluded that peroxide defects on the (100) and (110) surface were more stable than oxygen vacancies under an oxidizing environment through DFT+U calculations.[68] Surface transformations can occur through high temperature calcination.[70,66] Aneggi et al. found that more reactive (100) and (110) surfaces were exposed while less reactive (111) surfaces decreased after thermal aging.[70] However, due to a decrease of the surface area, the overall activity of CeO_2 decreased, although the specific rate increased. Shen et al. prepared CeO_2 with a modified precipitation method, in which the metal salt solution was treated by HNO_3 solution.[72] The resulting CeO_2 showed higher soot oxidation activity and became even more active after thermal aging, which can be related to the preferential exposure of more reactive (100) planes. Such surface sensitivity may also depend on the reaction conditions employed. Piumetti et al. compared a set of ceria-based catalysts with different textural properties (ceria nanocubes, ceria nanorods, ceria nanocubes/ZSM-5, mesoporous ceria, and a comparative mesoporous ceria prepared by solution combustion synthesis).[73] The ceria nanocubes showed the highest total soot oxidation activity, while the high-surface-area ceria catalysts had lower onset oxidation temperatures. Thus, they concluded that the soot oxidation reaction over ceria catalysts was surface-sensitive at high temperature, but was surface-insensitive at low temperature.

The reaction rates for soot oxidation over different cerium oxides are summarized in our recent review paper.[58] There are several things one can learn from the collected

results. First, the reaction rates under isothermal conditions are very close to the rates calculated from the TPO experiments, which are always within 3 fold of each other. This demonstrates that the methods used to calculate rates from TPO curves are reasonable and should be able to give a good estimate of reaction rates. Second, most of the cerium oxide catalysts decreased the T_{50} by about 200 °C relative to non-catalytic oxidation, which confirms their high activity for soot oxidation. Third, the order of catalyst activity based on the reaction rates may be different from that based on the changes in T_{50}. Fourth, both of the nanocube and nanorod cerium oxides showed higher activity than conventional cerium oxides, while their relative activity order depended on their surface area.

Although ceria is active for the soot oxidation reaction, it suffers from sintering under high temperatures and thus a loss of activity. Therefore, modification of ceria with other metal ions has been explored to improve its thermal stability, enhance the reducibility of Ce^{4+}/Ce^{3+} and improve the bulk oxygen mobility. These elements include La,[74–76] Zr,[77–80] Hf,[79] Co,[81] Mn,[82] Pr,[83,84] Sm,[83] Tb,[83] Nd,[85] Fe,[86] Gd,[87] and Lu.[88] Among those parameters, surface reducibility is thought to be the most important. Mixed oxides can be prepared by various methods: coprecipitation,[80] sol-gel,[89–91] thermal decomposition of mixed salts,[77] solid combustion,[92] formation of inverse micromulsion,[92] and with poly(methyl methacrylate) (PMMA) colloidal crystal templates.[93] The carbon oxidation reaction mechanism of carbon oxidation is thought to remain the same after the doping of rare-earth metals, while the reaction mechanism may change after modifications with alkali metals, transition metals and noble metals. These mechanisms are discussed in a recent review by Liu et al.[94]

It is well established that the doping of cerium oxide with Zr^{4+} leads to the formation of solid solutions, which increases the thermal stability, reducibility and enhances the oxygen storage capacity of the oxide.[95] Aneggi et al. investigated the roles of lattice/surface oxygen in cerium-zirconium oxide catalysts for soot oxidation. They found that there was an inverse correlation of total available surface oxygen and T_{50}. Furthermore, the oxygen storage capacity was only important in the absence of gaseous oxygen.[80] Hurtado et al. found that the cerium zirconium mixed oxides prepared from $(NH_4)_2Ce(NO_3)_6$ showed higher activity than those made from $Ce(NO_3)_6 \cdot 6H_2O$.[96] The cubic structure of the cerium zirconium mixed oxides gradually turned into a tetragonal structure with an increased amount of zirconium. The ceria-rich mixed oxides showed higher catalytic activity than the corresponding zirconium-rich mixed oxides. The optimal molar fraction of Ce in the mixed oxides was between 0.7 and 0.8.[80,97,96] The morphology of cerium zirconium mixed oxides was found to affect the soot oxidation activity.[98] Hierarchically porous cerium zirconium mixed oxides were synthesized with a biotemplate method: pine sawdust was impregnated with a solution of cerium and zirconium nitrates and the dried sample was calcined at 600 °C to give a mixed oxide with predictable porosity. The resulting mixed oxides showed higher soot oxidation activity than the corresponding ones made from a co-precipitation method, which was attributed to higher amount of mobile lattice oxygen, as characterized by the lower temperature peak in H_2-TPR and the higher oxygen storage capacity.

La-doped CeO_2 showed higher soot oxidation activity than CeO_2 (ΔT_{50} = 25 °C) under tight contact conditions, with the best catalyst having 5 wt% La (ΔT_{50} = 200 °C). The promotion effect was related to the increase of surface area and the enhancement of the

sample's redox properties.[76,99] However, it is difficult for catalysts with low surface area to saturate the carbon. This was likely the case in this study due to the low catalyst surface area of CeO_2, (~2 m^2 g^{-1}), therefore the dramatic increase in activity after doping of La may be related to both physical and chemical changes in the catalyst. The lanthanum on the surface of CeO_2 could also improve the soot oxidation activity by introduction of a carbonate pathway.[100] Katta et al. compared Zr and La doped ceria solid solutions for soot oxidation and found that La doped ceria solid solutions (Ce/La = 2/1, ΔT_{50} = 165 °C) gave much higher activity than the Zr doped ceria solid solutions (Ce/Zr = 1, ΔT_{50} = 110 °C) and undoped ceria (ΔT_{50} = 30 °C). More oxygen vacancies and lattice defects existed in the La doped solid solution, which were detected by Raman and XPS experiments. The authors claimed that the introduction of La provoked the formation of active oxygen on the surface.[101] Similarly, Hf doping (ΔT_{50} = 177 °C) was also more effective than Zr doping (ΔT_{50} = 64 °C).[79] Such effects are due to the aliovalency of La and Hf, which leads to more oxygen vacancies.

Krishna et al. studied four rare-earth (10 wt% La, Pr, Sm, Y) modified ceria catalysts for soot oxidation.[74] There was an increase in activity for La (ΔT_{50} = 160 °C), Pr (ΔT_{50} = 140 °C) and Sm (ΔT_{50} = 100 °C) doped mixed oxides while there were no effects derived from Y doping (ΔT_{50} = 50 °C) compared with undoped cerium oxide (ΔT_{50} = 50 K) under tight contact conditions. They claimed that the increased activity was due to the increased meso/micro pore volume and the stabilization of the external surface area. The role of the catalyst was to enhance the "active oxygen" transfer to the carbon surface, but not to change the rate-determining step, which was suggested to be the chemisorption of the spillover oxygen on the carbon active sites to form the surface oxygen species (SOC).

A Mn-doped ceria solid solution improved the soot oxidation activity under both tight and loose contact conditions, which was attributed to increased oxygen vacancies and improved oxygen chemisorption.[91] $Ce_{0.9}Mn_{0.1}O_2$ had a T_{max} of 365 °C and 500 °C for tight and loose contact conditions, respectively, while CeO_2 had a T_{max} of 390 °C and 555 °C, respectively. Highly dispersed MnO_x species were formed when the Mn molar percentage was 25%. Mn^{2+} and Mn^{3+} were the two Mn species existing in the solid solution. Shan et al. observed that the solution pH during precipitation of MnO_x-CeO_2 affected the materials' soot oxidation activity.[82] The best catalyst was prepared at pH = 4. The high soot oxidation activity was attributed to the ability to activate oxygen over the MnO_x-CeO_2. The addition of Ba to the MnO_x-CeO_2 mixed oxides increased the hydrothermal stability, which was due to the formation of $BaMnO_3$ perovskite nanoparticles at the surface.[102] Escribano et al. studied a $Ce_{0.75}Zr_{0.25}O_2$ supported Mn catalyst for soot oxidation.[103] The manganese species on the surface were a highly dispersed monolayer of α-Mn_2O_3 and carboxylic ions were identified as intermediate species during catalysis by FTIR spectroscopy.

Cobalt was not effective in forming a solid solution with ceria, but the Co_3O_4-CeO_2 mixed oxides showed higher soot activity than the individual oxides (CeO_2: ΔT_{50} = 216 °C, Co_2O_3: ΔT_{50} = 220 °C).[104] The best catalyst composition was $Co_{0.93}Ce_{0.07}O_2$ (ΔT_{50} = 271 °C). Zou et al. detected the active oxygen species (superoxide and peroxide) and carbon-oxygen intermediates (carbonyl and formate species) with *in situ* Raman spectroscopy during Co_3O_4-CeO_2 catalyzed soot oxidation reactions. Harrison et al. prepared ceria-supported cobalt oxide catalysts by co-precipitation of an aqueous solution of Co^{2+} and Ce^{3+}, and impregnation of a ceria gel with cobalt (II) nitrate or cobalt (II) acetate precursors. The cobalt species in the catalysts were found to be Co_3O_4. The material

prepared by impregnation showed the highest soot oxidation activity, which could be related to its smallest Co_3O_4 particle size. The authors concluded that the reduction of cobalt associated with the oxygen spillover on CeO_2 was the reason for the high activity observed.[105]

Cu-doped ceria did not form a solid solution, but the copper oxide was highly dispersed on the ceria surface. The strong interaction between dispersed copper oxide and CeO_2 may enhance the rapid release of the lattice oxygen of ceria, leading to higher soot oxidation activity.[91,106] As noted above, the morphology of ceria can affect the soot oxidation activity. Nakagawa et al. synthesized rod and ellipsoid shaped ceria with the assistance of amine surfactants as templates and used the resulting materials as supports for copper.[107] The observed better soot oxidation activity than the conventional ceria supported Cu catalysts was attributed to the enhanced surface reducibility and the improved soot contact on the shaped catalysts. Reddy et al. also found that copper could promote the soot oxidation activity of CoO/CeO_2-ZrO_2 and NiO/CeO_2-ZrO_2 catalysts.[108] Rao et al. studied soot oxidation catalysts with copper supported on three ceria-based mixed oxides, CeO_2-Al_2O_3, CeO_2-ZrO_2, and CeO_2-SiO_2.[109] Various copper species were formed on the surface, such as highly dispersed CuO nanoparticles, isolated Cu^{2+} ions, and large particles CuO. The soot oxidation activity followed the order CuO/ CeO_2-ZrO_2 (T_{50} = 338 °C) > CuO/ CeO_2-Al_2O_3 (T_{50} = 386 °C) > CuO/ CeO_2-SiO_2 (T_{50} = 409 °C). The generation of oxygen vacancies with higher incorporation of Cu into the cerium zirconium mixed oxide was responsible for the high activity of such samples. Muroyama studied the effects of different metal dopants in ceria for soot oxidation reaction.[110] The addition of rare-earth metals (La, Nd) enhanced the activity slightly, while the addition of transition metals (Mn,

Fe, Cu) significantly increased the activity. The best catalyst was associated with Cu doping (ΔT_{max} = 295 °C) and was attributed to the large amount of surface active oxygen species. Cousin et al. found that a Cu-V/CeO_2 (ΔT_{max} = 199-224 °C, S_{CO2}= 94.8-99.4 %) catalyst showed both enhanced soot oxidation activity and CO_2 selectivity compared with V/CeO_2 (ΔT_{max} = 181 °C, S_{CO2}= 87.4 %).[111]

The wide applicability, as mentioned above, and the low cost of cerium oxide was the reason for choosing it as the base catalyst in our studies. As mentioned earlier, the steam cracker operates at very high temperatures and catalyst stability in this range is quite critical. Deciding the support for the ceria materials hence was an important step towards developing the catalysts. This issue is discussed in a later section.

1.4.2.2 Oxygen Storage Capacity (OSC)

The total oxygen storage capacity is defined as the oxygen stored under thermodynamic control. It is typically measured by carrying out temperature programmed reduction (TPR) or by reducing the sample at a fixed temperature and then reoxidizing it.[112,113] Thermo-gravimetric analysis has also been used to measure the total OSC by measuring the weight loss of the sample under a reducing atmosphere such as a dilute hydrogen stream.[80] The observed weight loss can be attributed to the loss of oxygen, which combines with hydrogen to form water. Reddy et al. and Katta et al. used a TGA to calculate the OSC under cyclic heat treatments in flowing nitrogen and dry air.[101,114] They found out that the OSC of mixed oxides was higher than that of pure ceria. Ceria-zirconia mixed oxides showed the highest OSC. These experiments may not correlate directly with

catalytic activity under working conditions. Hence, the idea of measuring OSC under transient conditions emerged.[115]

Katta et al. showed that ceria-lanthana mixed oxides act as better catalysts for soot oxidation compared to ceria-zirconia oxides, owing to the their higher oxygen storage capacity.[101] Aneggi et al. observed a correlation between the T_{50} in inert atmosphere and the OSC for ceria-zirconia materials, as shown in Figure 1.8.[80] However, in the presence of oxygen as the oxidizing gas, no correlation was found between OSC and catalytic activity.

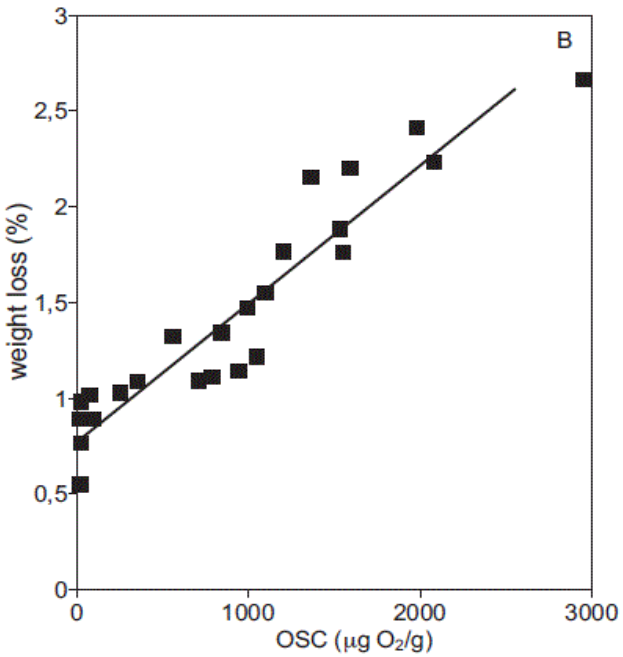

Figure 1.8 Relation between OSC and catalytic activity in an inert atmosphere at 400 °C

1.4.2.3 α-Alumina as the Support for Ceria Catalysts

Overall, a support material should be inert, stable under operating conditions and cheap. γ-alumina has been used widely as a catalyst support due to its low cost, robustness

at low temperatures and good textural properties of high surface area, pore volume. However, γ-alumina has acidic properties which makes it unsuitable as a coke inhibitor. Alumina exists in various transition states. The order of transition is as follows:

γ-Al_2O_3 → δ-Al_2O_3 → θ-Al_2O_3 – α-Al_2O_3

The transition temperatures depend on the aluminum precursor used for synthesis of alumina. α-alumina is the thermodynamically stable phase of alumina. Hence, it can be used at high temperatures. It has very low surface area but a high corrosion resistance. Industrial steam cracking takes place at high temperatures and the reaction continues for months together. Hence, a catalyst that is stable at these operating conditions should be chosen for this application. α-alumina is a good candidate for catalyst support. This project will involve use of ceria-alumina catalysts for oxidation of the coke formed during the cracking reaction

1.4.2.4 Non-ceria Based Catalysts

Alkali metals have been shown to be active catalysts for soot/carbon oxidation reactions. The observed activity order was Cs > K > Na >> Li under tight contact and full contact conditions.[116,117,118] BaO showed similar activity as the alkali metal oxides and the activity order of alkaline-earth metal oxides was Ba >> Ca > Mg under full contact conditions. However, alkaline-earth metal oxides were not active under loose contact conditions because of their poor mobility.[119]

Mul et al. screened metal chlorides and oxychlorides for soot oxidation.[120] Most of the studied chlorides and oxychlorides were not converted to oxides at the reaction temperature for soot oxidation. They observed a correlation between the melting points and

the catalytic soot oxidation activity. They found that $PdCl_2$, $CuCl_2$ and CuCl were very active catalysts, lowering the oxidation temperature by 200~275 °C, which was due to their low melting points and thus the wetting of soot by the catalyst. The DRIFT's results showed that surface oxygen complexes were formed and that active oxygen species were transferred from the catalyst to the soot surface.

Hleis et al. compared the promotion effects of different alkali metals (M/Zr=0.14, M=Li, Na, K, Rb, Cs) over a ZrO_2 catalyst during carbon oxidation and the order was Cs (ΔT_{max} = 242 °C) > Rb (ΔT_{max} = 215 °C) > K (ΔT_{max} = 208 °C) > Na (ΔT_{max} = 187 °C) > Li (ΔT_{max} = 116 °C).[121] Doggali et al. synthesized mesoporous ZrO_2 by using chitosan as a template and used it as a support for a set of transition metals (10 mol% Fe, Co, Ni, Cu and Mn).[122] Co/ZrO_2 (ΔT_{50} = 118 °C) was the most active soot oxidation catalyst while Ni/ZrO_2 (ΔT_{50} = 37 °C) showed little catalytic activity. An alumina supported Co-K-Mo catalyst lowered the soot oxidation temperature by 190 °C under loose contact conditions, exhibiting higher activity than the individual components supported on alumina.[123]

Perovskites have a general formula ABO_3, where A and B represent two cations. The A cation can be a lanthanide, alkaline, or alkaline-earth cation while the B cation can be a 3d, 4d or 5d transition metal. The combination of A and B cations and also the partial substitution of A or B cations enables the tuning of the physical and chemical properties of the perovskites, which makes them widely studied in heterogeneous catalysis.[124] The application of perovskites in carbon oxidation has received much attention over the past ten years or so.

Fino et al. compared the soot oxidation activity of different lanthanum containing perovskite catalysts and they found that the activity followed: $LaCrO_3$ (ΔT_{max} = 142 °C) > $LaFeO_3$ (ΔT_{max} = 126 °C) ≈ $LaMnO_3$ (ΔT_{max} = 126 °C).[125] The highest activity associated with the chromite catalyst was attributed to the high concentration of suprafacial (weakly chemisorbed) oxygen species from temperature programmed desorption (TPD) experiments, which transferred from the catalyst to the soot by spillover. Such oxygen species were defined as α-type oxygen with a desorption temperature in the range of 300 °C – 600 °C. Wang et al. found using *in situ* Raman spectroscopy that the active oxygen species on a $LaMnO_3$ perovskite catalyst were O_2^{2-}, O_2^{n-} ($1 < n < 2$) and O_2^{m-} ($0 < m < 1$).[126] Ifrah et al. observed that thermal treatment of $LaCrO_3$ perovskites (ΔT_{max} = 162 °C) could lead to the formation of La_2CrO_6 or La_2O_3 phases.[127] The measured order of activity for soot combustion was: $LaCrO_3$ (ΔT_{max} = 162 °C) ≈ 94% $LaCrO_3$-6% La_2O_3 (ΔT_{max} = 162 °C) > La_2CrO_6 (ΔT_{max} = 156 °C) > 86% $LaCrO_3$-14% La_2CrO_6 (ΔT_{max} = 140 °C) > La_2O_3 (ΔT_{max} = 160 °C, not all of the carbon was reacted). They concluded that both the mobility of the surface oxygen species and the presence of active Cr species (Cr^{3+} and Cr^{6+}) were important for the soot oxidation activity. Xiao et al. compared the soot oxidation activity of bulk, supported and macroporous perovskite $LaFeO_3$ catalysts under loose contact conditions and found that the highest activity on macroporous $LaFeO_3$ was related to its better contact with soot, rich active oxygen species and better surface reducibility.[128]

1.4.2.5 Carbon-Catalyst Contact Conditions

Due to the nature of the solid-solid-gas reactions that occur for catalyzed carbon oxidation with an oxidizing gas, the contact between the carbon and the catalyst is very important. During the early studies of diesel soot oxidation, Neeft et al. defined two types

of contact between carbon and catalyst – tight contact and loose contact.[129] The loose contact mixture was obtained by mixing with a spatula while the tight contact mixture was achieved by mixing the catalyst and carbon in a mechanical mill for an extended time. A loose contact mixture can also be obtained through other methods: filtration with a soot aerosol, shaking in a sample bottle, and dipping in a soot dispersion.[130] The catalysts that are in tight contact with carbon have higher oxidation activity than those in loose contact conditions.[116] In fact, the activity ranking of an array of catalysts may be different under tight contact and loose contact conditions. Shimokawa et al. compared the carbon oxidation activity over TiO_2 and CeO_2 supported Ag and K catalysts.[131] Supported Ag catalysts were more active under tight contact conditions and supported K catalysts were more active under loose contact conditions. Thus, the carbon oxidation activity of different catalysts should be compared under the same contact conditions. The contact of soot with diesel particulate filters under practical conditions resembles loose contact conditions.[132,130] However, to achieve reproducible results and compare the carbon oxidation activity of different catalysts, the experiments should be performed with samples under tight contact conditions. Therefore, most researchers have used tight contact samples for the evaluation of catalysts.

Clearly, to improve the catalytic oxidation activity, good contact of the carbon and catalyst is desired. One method to achieve good contact of the carbon and catalyst is to use a liquid phase catalyst at reaction temperature, like a eutectic salt mixture with a low melting point. Jelles et al. observed a significant increase in carbon oxidation activity over $CsVO_3$-MoO_3 and Cs_2MoO_4-V_2O_5 molten salts at 347 °C or higher and attributed it to the melting of these salts, which resulted in the wetting of the soot by liquid-phase catalyst.[133]

These two salts also showed high stability at 752 °C in air. Despite their high activity for carbon oxidation and high stability at elevated temperature, their practical applications for diesel soot oxidation are limited due to the liquid phase transformation at reaction temperatures, making the deposition of molten salts on proper supports desired. $CsVO_3$-MoO_3 and Cs_2MoO_4-V_2O_5 molten salts were deposited on α-alumina, γ-alumina, cordierite, diatomaceous earth, silica, silicon carbide and silicon nitride.[134,135] These catalysts showed similar carbon oxidation activity as their corresponding molten salts under loose contact conditions and the highest soot oxidation rate obtained was similar to that of the best catalytic fuel additives (a combination of cerium and platinum). Considering both the reactivity and stability, Van Setten et al. concluded that an ideal support should meet three requirements: the molten salts should have an affinity for the support to wet it; the wetted support should enforce a stable liquid distribution; and the supports should stabilize the molten salts in such a way that even after prolonged heating, the molten salts should remain accessible for carbon, e.g. low-porous materials are required.[134]

Efforts have also been made to study the contact between carbon and catalysts during the oxidation reaction. Bassou et al. evaluated ceria/soot contacts through temperature programmed experiments (TPE) and successive adsorption of O_2.[136] In a typical experiment, the mixture of ceria and carbon was first heated in helium from 27 °C to 827 °C, with the products CO and CO_2 tracked. The mixture was then cooled to 23 °C in helium, followed by a switch from He to O_2 for ceria to adsorb O_2. The consumption of O_2 was quantified and used to represent the amount of oxygen transferred from ceria to carbon. Successive TPE/O_2 adsorption cycles were repeated on the same sample to mimic

the progressive oxidation of carbon. They found that the amount of oxygen transferred remained constant and concluded that the contact area remained constant during the reaction. These results are consistent with conclusions from the ceria catalyzed carbon oxidation studied with *in situ* TEM by Simonsen et al.[137]

Besides tight and loose contact conditions, mixtures with full contact conditions were obtained by impregnating carbon with the aqueous alkali metal (Na, K, Cs) and alkaline earth metal (Mg, Ca, Ba) acetate solutions.[119,138] These mixtures were heated at 500 °C in He to turn the salts to oxides, followed by carbon oxidation tests. The intrinsic reactivity of the alkaline and alkaline-earth metal oxides was thus determined under full contact conditions, showing higher activity than the tight contact mixtures. There was a good correlation between the electronegativity of these elements and their carbon oxidation activity: the lower the electronegativity, the higher the activity.

Although the contact conditions can significantly affect the carbon oxidation activity, the direct contact between soot and catalyst may not be necessary as long as the catalyst has high intrinsic activity and the materials between them allow diffusion of active oxygen species. Yamazaki et al. separated the catalyst layer and carbon particles with an ash layer of either alumina or calcium sulfate.[139] CeO_2 did not show any catalytic activity while the Ag/CeO_2 (CeO_2 supported Ag catalyst) and CeO_2-Ag (Ag nanoparticles surrounded by aggregated of CeO_2 particles) catalysts showed remote carbon oxidation activity even when the ash layer thickness was more than 50 μm. Based on results from $^{18}O/^{16}O$ isotopic exchange reaction and electron spin resonance techniques, they proposed a reaction mechanism in which the superoxide ion (O_2^-) species generated on the catalyst

surface migrated to the ash layer and then to the carbon particles, where they oxidized the carbon.

While diesel soot oxidation reactions have been extensively studied, the interest in catalytic coating materials for steam crackers is growing, whereby there is intimate contact between the catalyst and carbon through *in-situ* coke formation. Obeid et al. deposited carbon on yttria-stabilized zirconia powder by propylene cracking, which showed higher oxidation activity than the tight contact mixture, confirming the importance of contact area for catalytic carbon oxidation reactions.[140] Mahamulkar et al. deposited coke directly on catalytic powders by ethylene pyrolysis in a specialized TGA, where the coke oxidation properties could be modified by thermally aging the coke.[141] The *in-situ* coke-catalyst contact was close to the tight contact condition.

1.5 Kinetics and Mechanism of Steam Gasification of Carbon

Steam is widely used in industrial operations and could be of use in gasification of carbon deposits. However, steam exposure can affect the physical properties of various catalysts and investigation of the stability of catalysts under such conditions is necessary. Steam has been used in the literature as a gasifying agent, in the presence or absence of oxygen. The following section gives a brief overview of the catalysts that are active in the presence of steam as well as the effect of steam on the gasification of carbon.

1.5.1 Oxygen Assisted Steam Gasification of Carbon

The effect of steam addition to oxygen has been investigated by a few researchers and there seems to be no unanimous relation between the addition of steam and activity.

Neeft et al. found no dependence of water on the non-catalytic oxidation of diesel soot.[44] However, addition of water in the range of 4-10 vol% to oxygen increased the oxidation rate of flame soot while keeping the activation energy constant (168 kJ mol^{-1}). The apparent reaction order in carbon increased with addition of water. Jeguirim et al. studied the effect of water on non-catalytic carbon black oxidation in the presence of NO_2. They found that water vapor increased the oxidation rate, but the mechanism of oxidation remained the same, irrespective of the presence or absence of water vapor. The activity of water vapor was attributed to the formation of nitric and nitrous acids, which allowed reaction between carbon and NO_2.[142] The effect of water vapor on the oxidation rate was found to decrease with an increase in temperature. The reactions forming acidic active intermediates involved in soot oxidation in the presence of NO_2 and H_2O were given by Equations 4 & 5:

$$2NO_2 + H_2O \rightarrow HNO_3 + HNO_2 \quad (4)$$

$$3HNO_2 \rightarrow HNO_3 + 2NO + H_2O \quad (5)$$

Arnal et al.[143] observed similar results as Neeft et al. for the influence of water vapor on the non-catalytic oxidation of a commercial carbon sample. The dominant reaction in the presence of water vapor was the gasification of carbon. Oxidation in presence of water vapor resulted in more complete oxidation to CO_2 than for oxidation using only oxygen. The stability of carbon surface oxygen complexes was higher in the presence of water vapor, causing the formation of CO_2 instead of CO.

Peralta et al. observed that Ba,K/CeO_2 catalyst showed no change in activity towards soot oxidation in the presence of water at 400 °C.[144] However, when the

temperature was increased to 800 °C, the presence of water led to a significant decrease in activity. For Cu-K-V-Cl catalysts, Badini et al. found a similar effect and hypothesized the reason for the effect as an increase in the volatility of chloride compounds in the presence of water vapor at high temperatures.[145] However, they found that binary catalysts like $CsVO_3$ + KCl and KVO_3 + KCl showed different behavior, wherein water vapor did not affect the catalytic activity.

1.5.2 Steam Gasification without Gaseous Oxygen

McKee et al. suggested that during steam gasification using potassium, the hydroxide of potassium was formed.[146] Reduction-oxidation cycles involving reduction of metal and oxidation of carbon, were suggested to be the pathway for gasification. Sodium and potassium salts showed similar catalytic activity for the gasification of graphite. However, the activity shown by lithium was an order of magnitude higher than that of the K and Na salts. This was hypothesized to be because of the lower melting point of the lithium salt. The suggested reaction mechanism for gasification for all these three salts was given Equations 6, 7 & 8:

$$Na_2CO_{3(l)} + 2C_{(s)} \rightarrow 2Na_{(g)} + 3CO_{(g)} \quad (6)$$

$$2Na_{(g)} + 2H_2O_{(g)} \rightarrow 2NaOH_{(l)} + H_{2(g)} \quad (7)$$

$$2NaOH_{(l)} + CO_{(g)} \rightarrow Na_2CO_{3(l)} + H_{2(g)} \quad (8)$$

Freriks et al. showed that dispersed potassium was more active than bulk potassium during the gasification of carbon deposited from poly(fufuryl alcohol) pyrolysis.[147] Also,

the activity was found to be dependent on the dispersion level of potassium. They suggested formation of a potassium surface complex as the active species and claimed that the earlier prediction of formation of hydroxide was not probable. At low temperatures, this complex reacted with water vapor to form potassium carbonate and a primary alcohol. Mouljin et al.[148] also showed that no intercalation compounds of K were formed during gasification. A renewed mechanism that supports most results from the literature at that time was proposed in the form of Equations 9, 10 &11:

$$CO_2 + K_xO_y \leftrightarrows CO + K_xO_{y+1} \quad (9)$$

$$K_xO_{y+1} + C \rightarrow K_xO_y + (CO) \quad (10)$$

$$(CO) \leftrightarrows CO \quad (11)$$

where the structure of K_xO_y is not clear. A similar mechanism can be written for the use of H_2O and O_2 as well. Meijer et al. found that increasing the K/C ratio increased the gasification reactivity.[149] The activation energy for the gasification of the carbon support was reduced from 256 kJ mol^{-1} to 160-190 kJ mol^{-1} on addition of alkali. This activity decreased by 40% when 10% CO_2 was fed along with steam. A similar effect was also observed with addition of hydrogen to the feed. Increasing the H_2/H_2O ratio reduced the gasification activity. The gasification rate for catalysts with Na, K, Rb, Cs remained fairly constant due to the similar dispersion of these materials.

The effect of Ca on carbon gasification in CO_2 was related to chemisorbed CO_2 on the Ca surface.[150] The carbon in this study was obtained by pyrolysis of a phenolformaldehyde polymer resin. Ca was found to be more active in a CO_2 atmosphere

than in steam. With time, the gasification activity decreased in the CO_2 atmosphere due to the enlargement of the Ca particles, leading to decreased surface area. The active species were identified to be $CaCO_3$. This species was converted to CaO in the presence of steam and hence, lower activity was achieved.

The above sections summarized the wide range of catalysts that have been used for oxidation as well as gasification of carbon deposits. With this knowledge the next step towards achieving our goal would be to define clear research objectives with a definite focus. The next section states the objectives and hypotheses for the work carried out.

1.6 Research Objectives

The aims of the proposed work are to study the performance of ceria-alumina catalysts to aid the oxidation of the coke formed by the radical coking mechanism (homogenous coke) during the cracking of propylene or ethylene gas.

The specific objectives of the project are:

Aim 1 (CHAPTER 2): To understand what type of coke structures (graphitic or amorphous) are present in the coke formed during gas phase cracking reactions and be able to identify operating conditions to form radical coke.

A custom-made thermos-gravimetric analyzer (TGA) is used for formation of coke. The structure and properties of the *in-situ* coke formed are compared to industrial coke.

Hypotheses: Graphitic carbon is formed at high temperatures, while amorphous carbon is formed at low temperatures. The coke structure also depends on the hydrocarbon

concentration in the feed, the reaction time and the residence time of the inlet gases. Since the concentration of hydrocarbon used is high (steam – HC ratio – 0.8 to 1) and the run time is a few months in industrial operations, a high proportion of graphitic structures as compared to amorphous ones are expected in industrial coke.

The reaction conditions used in the TGA (2% hydrocarbon, reaction time – 1hr) are not harsh enough to create graphitic structures in large proportions. Hence, a larger amount of amorphous structures are expected in these coke samples. The flow reactor system designed in the laboratory is capable of handling larger concentrations of hydrocarbon feed. This system can be expected to give coke that has a similar nature to that of industrial coke.

Aim 2 (CHAPTER 3): To determine the structure-activity relationships of ceria-alumina catalysts in the oxidation of coke

Ceria-alumina catalysts with different ceria loadings will be synthesized and characterized. Coke and catalyst are then physically mixed. The performance of the catalysts will be investigated by studying the oxidation kinetics of coke.

Hypothesis: The redox capacity of ceria has recently been used for oxidizing carbonaceous materials like soot. Based on the same redox principle, ceria-alumina composites should be able to aid the oxidation of coke formed in gas phase reactions in cracking reactors.

Aim 3 (CHAPTER 4): To determine if use of steam, as an oxidizing gas, will aid the oxidation of coke.

Industrially, a mixture of air and steam is used for decoking the reactor. To have similar conditions for decoking in the reactor, steam will be introduced as an oxidizing gas.

Hypotheses: Steam has been known to oxidize hydrocarbons by steam reforming (SR) reactions and to oxidize carbon monoxide by the water gas shift (WGS) reaction. The coke is a mixture of hydrocarbons whose partial oxidation may give rise to carbon monoxide. Hence, it can be expected that steam will aid the oxidation of these species in the coke by WGS and SR reactions. Ceria slightly enhances the performance of steam reforming reactions.[6] The adsorption of water has been found to increase in the presence of ceria, leading to increased gasification of carbonaceous deposits.[6]

Aim 4 (CHAPTER 5): To synthesize ceria coatings on a metallic substrate that minimize catalytic coking and also reduce the temperature of oxidation of deposited coke

The ultimate application of the catalytic powders that will show good activity towards oxidation of coke would be to be used as coatings in industrial cracking furnaces. Hence, it is necessary to be able to develop a methodology for synthesizing thermally stable catalytic coatings on a metallic substrate and determine their activity towards coke oxidation.

Hypotheses: The catalytic coating on the metallic substrate will act as a barrier between the hot hydrocarbons and the catalytic metal species in the substrate and thus help in reducing catalytic coking. Synthesizing ceria coatings on the substrate will help in oxidizing the coke precursors as soon as they are deposited, as well as reduce the temperature of oxidation, behaving similarly to the catalytic powders.

1.7 Research Impact

The following presented work provides a comprehensive way to understand the changes in the coking rates and coke structure with changing reaction conditions. This work is one of the few studies in the literature using α-alumina, the most thermally stable phase of alumina, as a support for ceria in the oxidation/gasification of coke. The ability to work with 100% steam in the TGA can help understand the mechanism of coke gasification under pure steam and also evaluate the stability and activity of catalysts in a realistic industrial environment during the decoking phase. Understanding the structure-activity relationships of the catalysts can help in designing better coke oxidation and gasification catalysts. These catalysts will help oxidize coke faster and decrease the down time of the reactor for decoking. By burning the coke off at low temperatures, these catalysts may also help in decreasing the energy required for coke removal in industrial steam cracking operation, making the process energy-efficient. This work can also potentially help in reducing the carbonaceous deposits responsible for deactivation of catalytic activity. Synthesizing catalytic coatings will be the pre-final step towards the real application of coating the industrial furnaces with a catalyst that can not only reduce catalytic coking but also minimize radical coke deposition and hence increase the run length of the industrial furnaces.

CHAPTER 2. IN-SITU GENERATION OF RADICAL COKE

This chapter is largely adapted from 'Mahamulkar, S; Yin. K; Davis R.; Shibata H., Malek A.; Agrawal P. K.; Jones, C.W. *In-situ* generation of radical coke and the role of coke-catalyst contact on coke oxidation. *Ind. Eng. Chem. Res*. **2016**, 55 (18), pp 5271 – 5278.

2.1 Background

As mentioned in the last chapter, coke deposition on reactor walls or other process equipment in the steam cracking process, affects the process efficiency and reduces the rate of heat transfer.[8,10] The amount and type of coke deposits formed depend majorly on the operating conditions such as the nature of the feed and characteristics of any surfaces present. To restore the normal operation of such processes, expensive process shutdowns are typically carried out. Shutdowns often involve combustion of these carbon deposits using steam and air mixtures. Hence, significant research has focused towards development of technologies that can aid the oxidation or gasification of such deposits.

Coke deposits can vary in structure and chemical composition based on the mechanism of coke formation. The two most common mechanisms of formation of coke identified in the literature are (i) catalytic and (ii) radical, as mentioned earlier. Catalytic coke formation as the name suggests is catalyzed by the metallic species in the walls of the reactor, likely at grain boundaries.[10,19] At higher temperatures, radicals are formed in the gas phase that can produce pyrolytic coke, which then deposits on the surface of the cracking furnace.[10,19] Coke formed by the radical mechanism has very low hydrogen

content due to the dehydrogenation of precursor molecules during the coking reactions. The coke formed is typically very hard due to the cross-linking of aromatic molecules under the reaction conditions. Catalytic coke is filamentous in nature and easier to oxidize as compared to radical coke due to the high hydrogen content. There has been lot of research done to minimize catalytic coking as stated in the previous chapter. Minimization and oxidation of radical coking is an issue that needs to be addressed to be able to increase the life of the cracking furnace and hence reduce maintenance costs. Hence, the work presented in this thesis revolves around the formation and oxidation of radical coke species only. It is assumed that the commercial coatings available in the market will be enough to create a barrier between the hydrocarbon gases and the metallic walls thus avoiding catalytic coking.

The reactivity of catalysts towards carbon oxidation has been reported to depend on the degree of contact between the carbon and the catalyst.[118,129,151] In the literature, the catalysts that were in tight contact with carbon have shown higher oxidation activity than those in loose contact conditions.[74,90,116,152] Also, the reproducibility of loose contact results in the literature has been comparatively poor.[140] In such cases, a comparison of catalytic activity under different contact conditions can give rise to misleading results. For achieving reproducible results, most researchers use tight contact samples for the initial screening of catalysts. However, tight contact may not be a true representation of the contact conditions that might occur realistically in reactors, catalytic converters, or other process equipment.

For effective comparison between activities of different catalysts towards oxidation of coke, it is important to have a realistic coke–catalyst contact. In this work, emphasis is placed on the '*in-situ* deposition' mode of contact between coke and catalyst. To determine

the effect of *in-situ* coke–catalyst contact on the oxidation of coke, alumina-supported ceria have been used as model catalysts since ceria has been found to be effective for a number of catalytic oxidation processes. The important characteristic of ceria is its redox capability under oxidizing and reducing conditions. Its most significant use lies in its application as a three-way catalyst for treating exhaust gases from automobiles.[153,154] Ceria catalysts are promising candidates for many catalytic applications where redox cycles are important such as soot oxidation,[63,64,71,155–157] the water gas shift reaction,[158] steam reforming,[159] and CO oxidation.[160]

The present work focuses on generating *in-situ* radical coke, which oxidizes at high temperature, in the laboratory on powder catalyst samples. A specialized TGA was used for coking experiments. The mechanism of *in-situ* coke deposition (catalytic vs. radical) was investigated thoroughly. The effect of thermal aging treatments on the hardness of the coke deposit was also examined. The nature of the coke deposits was determined using a combination of thermal analysis and spectroscopic techniques. A specific focus was placed on ascertaining the effect of coke – catalyst contact on the oxidation of coke. It was observed that *in-situ* radical coke generation in the laboratory showed better coke-catalyst contact than physical mixtures and is more representative of realistic coke-catalyst contact conditions that might occur in process equipment.

2.2 Materials and Methods

2.2.1 Material Synthesis

Mesoporous γ-alumina was prepared via a surfactant-mediated self-assembly method.[161–163] A mixture of nitric acid (Sigma Aldrich, 70%) and deionized water (200

mL) was used for peptization of 13.75 g of pseudo-boehmite. This was followed by sonication of the suspension at room temperature for 90 min and stirring at 60 ºC for 17 h. The peptized alumina sol was cooled to room temperature and added to a stirred solution of ethanol and Pluronic® P-123. P-123 is used as a template to create mesoporous γ-alumina. During synthesis, Pluronic P-123 interacts with species that is present in boehmite dispersion and forms a polymer – alumina mesostructured composite. Upon calcination, the polymer is removed and mesoporous alumina is formed.[163] The mixture was stirred for 24 h at room temperature. The next step involved heating of the solution at 60 ºC for 60 h to remove the solvent. Heating the mixture at 75 ºC for 24 h carried out drying of the P-123-alumina. Residual water and ethanol were removed by heating the composite at 150 ºC for about 1 h. The composite was then heated to 700 ºC at a heating rate of 1 ºC/min and kept at 700 ºC for four hours for removal of the P-123 template. Θ-alumina was obtained by heating commercial γ-alumina at 1100 ºC for 8 h using a heating rate of 1 ºC/min.

A commercial α-alumina support was procured from Sigma Aldrich. Ceria loaded α-alumina materials were prepared by a wetness impregnation method using cerium nitrate hexahydrate ($Ce(NO_3)_3.6H_2O$) as the cerium precursor and α-alumina as the support (Sigma Aldrich, corundum). The cerium precursor is dissolved in distilled water and α-alumina is added to the solution in the appropriate amount. The mixture was dried at 110 ºC and calcined at 1100 ºC for 8 h using a heating rate of 1 ºC/min. They are denoted as x-CeO_2-Al_2O_3 where x denotes the mol% of Ce in the catalyst sample while Al is present in (1-x) mol%.

An industrial coke sample was obtained from The Dow Chemical Company.

2.2.2 Coke-Catalyst Contacting

A customized thermogravimetric analyzer (TGA, NETZSCH, STA449F3 Jupiter®) was used for *in-situ* generation of coke and to study coke oxidation. This TGA can be operated with reactive gases like hydrocarbons at high temperatures. For safety reasons, flammable gas concentrations were kept below their flammability limits in the TGA. In these experiments, 2 mol% of propylene or ethylene was used. The internal components of this TGA were designed to work efficiently in the presence of corrosive atmospheres. The measurement head, made of alumina, was stable at high temperatures and resistant to corrosive gases.

For *in-situ* coke deposition, the TGA furnace was heated to the desired temperature in helium flow. Once the desired temperature was reached, 2 mol% hydrocarbon in helium was introduced into the system for 1 h. After 1 h, the hydrocarbon flow was stopped and the furnace was allowed to cool while under helium flow. The coking rate and the amount of coke deposited were measured by the TGA. Coke deposited on the measurement head was removed completely prior to oxidation of the coked catalysts, by temperature programmed oxidation in air up to 900°C.

For tight contact experiments, small amounts of industrial coke and catalyst or support were ground in a mortar and pestle for 45 minutes in the ratio 1:9. Loose contact experiments involved physical mixing of the above two materials in the same ratio with the help of a spatula where the coke particles were reduced to a size of 500 µm using a Wiley mill.

2.2.3 Materials Characterization

Nitrogen physisorption isotherms were collected at -196 °C using Micromeritics Tristar II after the samples were heated to 200 °C under vacuum for 10 h prior to the analysis. The data obtained were used to calculate surface areas and pore characteristics for the various solids. A Witec confocal Raman microscope (Alpha 300R) was used to obtain Raman spectra for the reaction-aged catalysts with an Ar^+ ion laser (λ = 513.998 nm) using a 1.5 mW excitation source intensity and 1800 grating with < 0.9 cm^{-1} pixel resolution. A magnification of 50x was used. A dense sample layer of about 1 mm thickness was pressed onto a cover slip with the help of a spatula. This coverslip was then placed on the microscope sample holder. A white light source was used to focus on the surface of the sample. After focusing on a spot, the sample was exposed to the laser beam and the Raman spectra were recorded. First order Raman spectra were de-convoluted using the peak analyzer function of the OriginPro 8.5 software.

2.2.4 Thermal Coke Aging Experiments

Thermal aging experiments were performed on an Autochem II 2920 instrument from Micromeritics. A small amount of an *in-situ* coked sample from the TGA was placed in a quartz U-tube. This tube was mounted on the Autochem machine and the sample was pretreated under a helium atmosphere by heating to 150 °C at a rate of 10 °C/min, to remove traces of volatile matter. The sample was then aged for longer times at the same temperature used for coking, under helium atmosphere. Inert atmosphere was used to study the effect of aging independently of the coking process.

2.2.5 Temperature Programmed Oxidation

Temperature programmed oxidation (TPO) experiments were also performed on the NETZSCH TGA. TGA was used to determine the reactivity of the coke. The temperature was raised from room temperature to 950 °C at a rate of 10 °C/min in the presence of air (100 mL/min). The rate of mass loss was used to compare the oxidation of different coke and coked-catalyst samples. The temperature, at which the rate of oxidation was maximum, was denoted as the peak oxidation temperature.

2.3 Results and Discussion

The first series of experiments conducted was used to investigate the mechanism of coke formation in the TGA in the presence of an oxide support. The rationale for doing these experiments was to verify if the coke formed in the TGA was generated from homogeneous radical reactions, and that heterogeneous coke was not involved. Furthermore, conducting thermal cracking experiments in the TGA provided a quantitative measurement of the coking rate and the amount of coke formed.

A blank coking experiment, with no support or catalyst present, showed some (~ 0.6 mg) coke deposition on the measurement head of the TGA (Figure A1, Appendix A). When coking was carried out in the presence of a support, the amount of coke deposited increased. Further experiments were carried out to determine the mechanism of formation of this deposited coke. To determine if the total surface area of the support was a factor determining the coking rate, two different samples (100 mg) of γ-alumina with different surface areas were chosen for analysis. These samples were exposed to 2 mol% propylene atmosphere at 950 °C for 1 h. From Table 2-1 one can see that the synthesized mesoporous

γ-alumina (203 ± 2 m^2/g, particle size 14 μm) had a total surface area nearly twice that of the commercial γ-alumina (84 ± 2 m^2/g, particle size 16 μm). Nonetheless, the coking rate on the synthesized alumina was very similar to that on the commercial alumina (Table 2-2). The typical TG curve for coke deposition is shown in Figure A2, Appendix A. Clearly, the coking rate was not proportional to the total surface area and one can conclude that the total surface area of the support did not play a significant role in the coking process. Pore blockage was investigated by nitrogen physisorption studies on the coked commercial γ-alumina. The coked sample showed a lower surface area (77 ± 2 m^2/(g-alumina) of coked sample) as compared to the pristine commercial γ-alumina (84 ± 2 m^2/g). To find the source of this reduction in surface area, commercial γ-alumina was subjected to the same thermal treatment as the coking experiment but without exposing it to the hydrocarbon. This thermal treatment caused sintering of the commercial γ-alumina that reduced its surface area to 68 ± 2 m^2/g (Table 2-1). Hence, the possibility of pore-blocking due to deposition of coke was ruled out. This also suggests that coke deposition primarily took place on the outer surface of the support.

Table 2-1 Textural properties of oxide supports and catalytic materials

Sample	**Total surface area (m^2/g)**	**Pore volume (cc/g)**
γ-alumina (commercial)	84	0.42
γ-alumina (synthesized)	203	1.10
Coked commercial γ-alumina	77	0.37
Thermally treated commercial γ-alumina	68	0.36
θ-alumina (synthesized)	34	0.22

Table 2-2 Effect of total surface area on coke deposition

Material	Weight of material (mg)	Total surface area (m^2/g)	Coke deposited in 1 h (mg)
γ-alumina (commercial)	100	84	10.6 ± 0.25
γ-alumina (synthesized)	100	203	12.1 ± 0.3

As mentioned earlier, coke deposition increased in the presence of a support. One possible explanation for this observation could be the increased external surface area provided by the supports. A second explanation could be that the support induced coking via a heterogeneous mechanism. To probe these possibilities, two supports of equivalent external surface area were selected for exposure to hydrocarbon at 950 ºC for 1 h. An inert support that would not induce catalytic coking, SiC, was utilized along with θ-alumina, a support that might induce some catalytic coking. The total external surface area of both samples was ~0.06 m^2 (SiC is non-porous, BET surface area of θ-alumina – 0.34 m^2; 1.4 g of SiC with a particle size of 50 μm; 10 mg of θ-alumina with a particle size of 10 μm). Figure 2.1 shows that the same quantity of coke was formed on the θ-alumina and on the SiC. The coking rate on SiC was 4.6 mg/hr, which was very similar to that on θ-alumina (4.5 mg/hr). Similar behavior is also seen in the case of γ-alumina. For the same weight, commercial γ-alumina with larger particle size (16 μm) showed lower coke deposition as compared to synthesized γ-alumina with smaller particle size (14 μm, higher external surface area). This observation clearly indicates that the quantity of coke deposited in the TGA depends on the external surface area of the support and not on the chemical nature of the support, suggesting that coking occurs primarily by a homogeneous, radical mechanism under the conditions used.

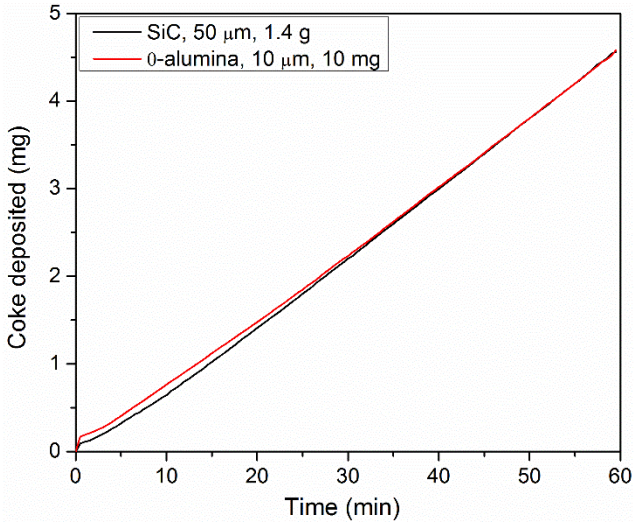

Figure 2.1 Coke deposition (950 °C, 1 h) on support materials with equal external surface area (sample masses were adjusted to equalize external surface area)

2.3.1 Kinetics of In-situ Coke Deposition

Kinetic parameters can give additional insight in to the mechanism of coke deposition. Hence, to determine the reaction order in hydrocarbon for deposition of coke on α-alumina, during thermal decomposition of ethylene, three different concentrations of ethylene were used (1.4 mol%, 1.6 mol% and 1.8 mol% in He). The reaction temperature was maintained at 950 °C for a period of 1 h. The coking rate was measured by the TGA and a log plot of coking rate (mol sec^{-1}) vs ethylene concentration yielded a reaction order of 1.2085 (Table A1, Figure A3 – Appendix A). A similar analysis was carried out with 2% propylene as the hydrocarbon and we achieve an order of 1.03 (Figure A4, Appendix A). The thermal cracking kinetics of propane and ethane have previously been found to be first order in the hydrocarbon concentration.[18,164] Thermal cracking involves a large number of radical reactions. A reaction order of approximately one suggests that coke formation in the TGA took place by radical reactions.

The apparent activation energy of the coke deposition process was calculated by measuring the coking rate at the reaction temperatures of 850 °C, 950 °C and 1050 °C. Assuming Arrhenius law, the log of the rate constant ($(m^3)^{1.2}\,sec^{-1}\,mol^{-0.2}$) as plotted against the inverse reaction temperature which gave an activation energy of 91 kJ mol^{-1} (Table A2, Figure A5 – Appendix A). This value is significantly lower than the C-C bond dissociation energy[165] for ethylene which is 727.8 kJ mol^{-1} and also the bond dissociation energy of the sp^2 C-H bond which is 456 kJ mol^{-1}.[165] The apparent activation energy for ethylene cracking is 323 kJ mol^{-1}.[166] This apparent activation energy is calculated based on the disappearance of the reactant (ethylene). However, in the current study, the activation energy is calculated based on the coking rate. Similar studies on other reactions have been done in the literature, which yield activation energy values in the same range as found in the current study (refer Table A3). Hydrogen abstraction and addition reactions are known key steps in the formation of radical coke.[19,167] From the literature values, we can infer that involvement of larger hydrocarbon molecules in the formation of coke has a low apparent activation energy. Thus, the coke formed in this study is a result of the combination of radical reactions taking place because of hydrogen abstraction and addition.

2.3.2 Raman Spectroscopy

Structural information about carbon materials can be obtained by Raman spectroscopy. The amorphous and graphitic carbon content of the sample can be inferred by deconvolution of the Raman peaks.

Table 2-3 Assignment of peaks in Raman spectra

Peaks	Raman shift (cm^{-1})	Type of carbon
G	1585	Ideal graphitic
D_1	1350	Disordered graphitic edges, in-plane imperfections
D_2	1620	Disordered graphitic surface
D_3	1500	Amorphous carbon, sp^2 bonded
D_4	1200	Disordered graphite lattice, ionic impurities

Table 2-3 relates the Raman shift to the type of carbon in the sample [168]. A higher wavenumber corresponds to a higher energy required for excitation of bonds, with amorphous carbon species requiring lower energy for excitation than graphitic species. The amorphous carbon species typically consist of poly-aromatic precursors of graphene layers. The amount of graphite formed in the sample depends on operating conditions that produced the carbon/coke sample, e.g. reaction temperature, reaction time and residence time.

Sadezky et al. found that fitting the G, D_1, D_2, D_4 peaks as Gaussians and the D_3 peak as a Lorentzian gave the best fit for their spectra[168]. A similar deconvolution analysis was used here for obtaining Raman parameters for different coke samples. The heterogeneity of the industrial coke samples was studied by measuring Raman spectra at different spots on the sample. Table 2-4 shows the deconvolution results at different spots in the industrial coke sample. Negligible differences were observed in the coke composition values at different spots, indicating homogeneity of the sample. From Figure 2.2, it can be inferred that the industrial coke has significantly more graphitic species than amorphous species. The large contribution of the D peaks indicates a highly disordered

structure. In contrast, *in-situ* coke deposited in the TGA was more amorphous than the industrial coke. This might be due to the short reaction time (1 h).

Table 2-4 Homogeneity of industrial coke sample by Raman deconvolution analysis

Spots	G (%)	D_1 (%)	D_2 (%)	D_3 (%)	D_4 (%)
Spot 1	20.0	49.0	14.0	7.00	10.0
Spot 2	18.5	47.5	14.9	7.50	11.6
Spot 3	21.0	47.7	14.4	6.00	10.8

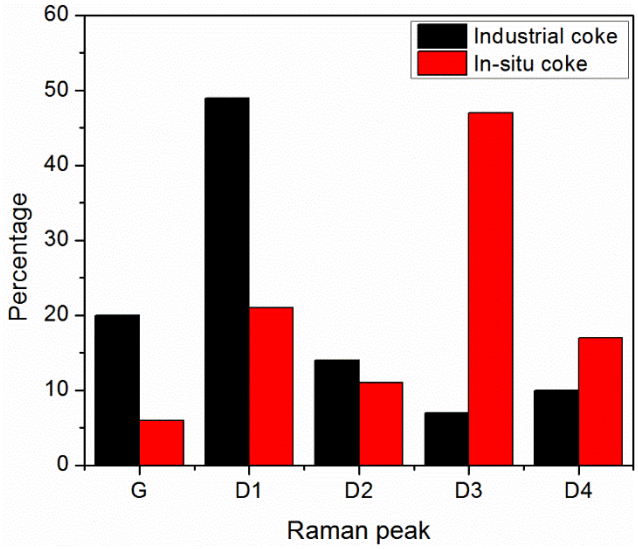

Figure 2.2 Deconvolution analysis of Raman spectra for *in-situ* and industrial coke showing amorphous nature of *in-situ* coke

2.3.3 Thermal Aging

It would be useful to be able to produce coke in the TGA, where excellent coke-catalyst contact can be achieved (vide infra), with similar oxidizing nature as an industrial coke. To this end, the ability to thermally age an *in-situ* coke to increase its graphitic content was explored. Specifically, the exposure time to ethylene was increased during an *in-situ* coking experiment using an α-alumina sample (500 mg). The degree of coke graphitization was determined by the Raman analysis. The relative intensity of the D_3 peak

given by equation 12, denoting amorphous carbon, was used as a measure of the graphitic nature of the coke samples.[169]

$$Relative\ intensity\ of\ D_3 = \frac{I_{D3}}{I_{D3} + I_G + I_{D2}} \quad (12)$$

A decrease in the relative intensity of the D_3 peak denotes a decrease in the amount of the amorphous coke. Figure 2.3 shows a plot of the relative intensity of the D_3 peak with that of the peak oxidation temperature for coke deposited on a bare α-alumina support. An increase in the reaction time from 1 to 2 to 4 h yielded coke with decreased amorphous carbon content. This decreased amorphous carbon led to a higher peak oxidation temperature (sample size for TPO: 1 h – 37 mg, 2 h – 21 mg, 4 h – 10 mg). Repeating the measurements showed minimal error in the de-convolution results, suggesting good reproducibility.

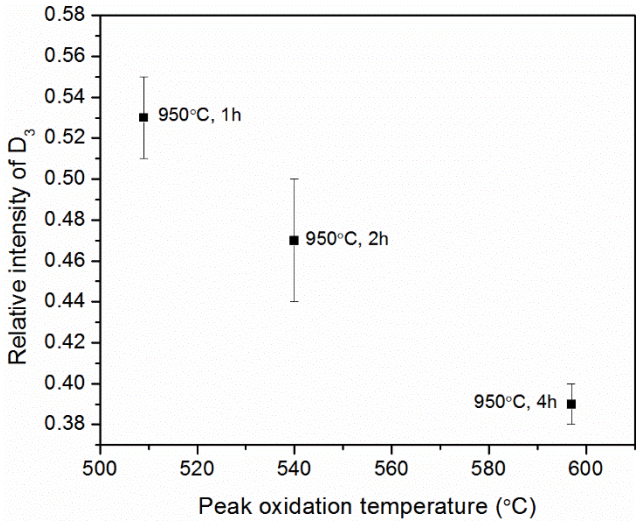

Figure 2.3 Relation between amorphous nature of coke and its oxidation behavior

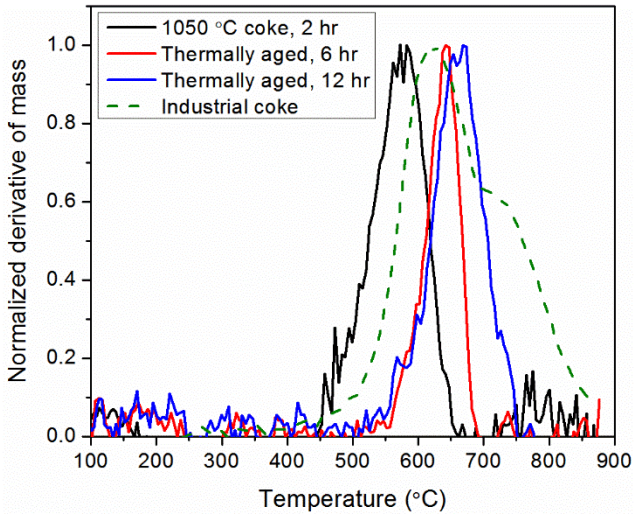

Figure 2.4 Comparison of TPO curves of thermally aged coke with industrial coke with following coke content: industrial – 2.7 mg, *in-situ* coke – 0.34 mg

To harden the coke, a thermal aging treatment was used in further studies. The coke generated *in-situ* on α-alumina (500 mg) at 1050 °C for 2 h was considered as a reference sample. The coke sample formed at 1050 °C, 2 h had lower amorphous content (0.34) than the coke formed at 950 °C, 2 h (0.47). A higher reaction temperature was chosen as the hardness of the coke increased with temperature. This reference coke was thermally aged under helium for a period of six and twelve hours. Figure 2.4 shows that thermal aging caused the TPO curve to shift right and oxidize the coke at higher temperatures. The industrial coke had some carbon species oxidizing at higher temperatures (> 800°C) which was not reflected in the thermally aged coke. However, it was demonstrated that increasing the time for thermal aging is a suitable way of producing harder coke samples. Industrial coke shows two peaks in TPO while *in-situ* coke shows one peak because industrial coke is more graphitic according to Raman analysis (Figure 2.5). The higher temperature peak seen is for the oxidation of graphitic species. *In-situ* coke is less graphitic and more amorphous than industrial coke. The *in-situ* coke made in the laboratory with a reaction time of few hours cannot match the reaction time the industrial coke was exposed to

possibly a few months. This increased high temperature exposure has caused the industrial coke to harden and oxidize at much higher temperature than the *in-situ* coke.

Figure 2.5 shows that thermally aging the coke for 6 h increases the T_{50} (temperature at which 50 wt% of the carbon content is oxidized, sample size 25 mg) without a significant change in the amorphous content of the coke. This could be attributed to the increase in the structural order of the graphitic species or morphology of the coke, which is not discussed in this paper. Further studies are required to probe this observation. However, increasing the thermal aging time from 6 to 12 h, decreased the amorphous carbon content and increased the T_{50}. Thus, we observe that thermally aging the coke in an inert atmosphere made it more difficult to oxidize. The thermally aged coke oxidized at a similar temperature as the industrial coke and thus, radical coke with similar oxidizing characteristics as industrial coke was generated in the laboratory.

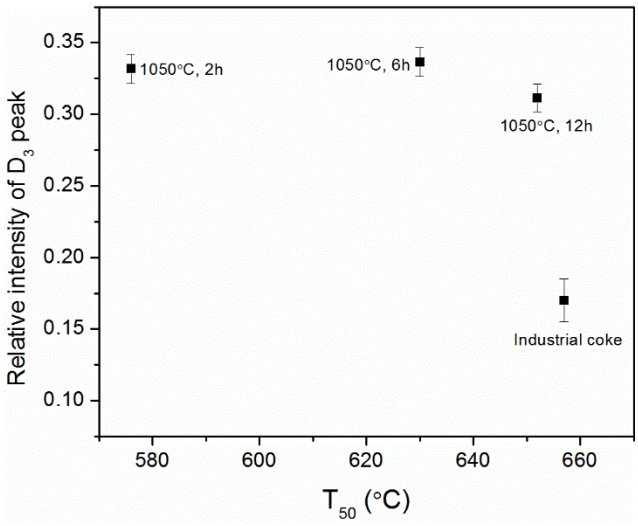

Figure 2.5 Evolution of amorphous carbon content with thermal aging

2.3.4 Coke – Catalyst Contact

Contact	Schematic Coke Catalyst
(a) Loose	
(b) Tight	
(c) In-situ	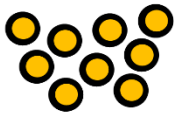

Figure 2.6 Schematic of coke - catalyst contact under different conditions: a) Loose contact b) Tight contact c) *In-situ* deposited coke

Ceria-alumina catalysts were used as model catalysts for studying the coke-catalyst contact created via *in-situ* coke generation. Nitrogen physisorption revealed the highly non-porous nature of the commercial α-alumina support used in the catalyst preparation. Impregnation of ceria onto the α-alumina increased the surface area slightly, though the catalysts remained non-porous in nature.

Figure 2.6 shows a schematic of different contact conditions. In loose contact conditions (Figure 2.6a), very few contact points exist between the coke particles and the catalyst particles, leading to modest catalytic activity for oxidation. When the coke and catalyst samples are ground together to create tight contact, the particle size of the coke and catalyst particles may be reduced, increasing the contact area of the coke and catalyst particles (Figure 2.6b). As a result, the oxidation activity under these conditions is higher than under loose contact. During *in-situ* coke deposition on catalysts, it was demonstrated

above that coke was deposited externally on the individual catalyst or support particles as a coating, leading to intimate contact between the carbon particles and the catalyst (Figure 2.6c).

To study coke-catalyst contact, four different contact conditions were examined. The first set of samples involved deposition of *in-situ* coke (950 °C, 1 h) on a series of ceria-alumina catalysts with varying cerium content. These coked catalysts were then ground to simulate a tight contact mixture as a second set of samples. For comparison, loose and tight contact samples were obtained using the industrial coke with the same catalysts as mentioned above. To quantify the effect of coke-catalyst contact, TPO experiments were carried out on all the samples. Figure 2.7 shows that *in-situ* coke oxidized with a peak oxidation temperature at 410 °C. Grinding the *in-situ* coke and the catalyst before the TPO experiment led to appearance of a smaller peak at a lower temperature of 350 °C. This showed that for oxidation of *in-situ* coke, tight contact (grinding) enhances the catalytic activity of the supported ceria slightly. This effect could be attributed to the increased contact between the coke and catalyst particles due to grinding. The tail observed at higher temperatures could be due to the detachment of coke from the catalyst over α-alumina in which case uncatalyzed oxidation takes place causing it to oxidize at higher temperature. In contrast, tight contact for the industrial coke with the ceria-alumina (50-CeO_2-Al_2O_3) catalyst showed a significant improvement in catalytic activity as compared with the loose contact conditions (Figure 2.7).

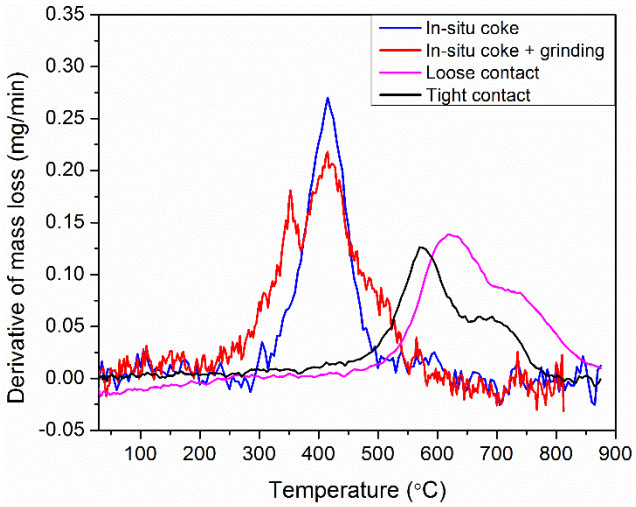

Figure 2.7 TPO curves showing coke – catalyst (50-CeO_2-Al_2O_3) contact under different contacting conditions

Quantification of these results is given in Table 2-5 . For instance, for a catalyst with 20 mol% Ce (20-CeO_2-Al_2O_3), grinding after *in-situ* coke deposition showed very little (1 °C) reduction in the T_{50} value (Table 2-5). For the same catalyst, the difference between loose and tight contact with the industrial coke was significant, with a reduction in T_{50} of 76 °C (ΔT_1). This behavior was observed for other catalysts (50-CeO_2-Al_2O_3 and 80-CeO_2-Al_2O_3) as well, demonstrating that grinding to create tight contact conditions is important to improve coke-catalyst contact using physical mixtures of separate coke and catalyst particles.

Table 2-5 T_{50} values for industrial coke in contact with ceria-alumina catalyst (ΔT_1 – difference between T_{50} of loose and tight contact, ΔT_2 – difference between T_{50} of *in-situ* coke and *in-situ* coke followed by grinding)

Coke – catalyst contact	**T_{50} (°C) / 20-CeO_2-Al_2O_3**	**T_{50} (°C) / 50-CeO_2-Al_2O_3**	**T_{50} (°C) / 80-CeO_2-Al_2O_3**	**T_{50} (°C) / 50-CeO_2-Al_2O_3 (thermally aged coke)**
Loose contact	657	657	657	-
Tight contact	581	565	601	-
ΔT_1	76	92	56	-
In-situ coke	406	412	403	506
In-situ coke (followed by grinding)	405	398	394	507
ΔT_2	1	14	9	1

The effect of coke-catalyst contact was also investigated on a harder coke deposited *in-situ* on the 50-CeO_2-Al_2O_3 catalyst. Coking was carried at 1050 °C for 2 h on the 20-CeO_2-Al_2O_3 material and the coked sample was thermally aged for 12 h. TPO yielded a T_{50} value of 507 °C. Grinding the coke sample yielded a similar T_{50} value with a ΔT_2 of 1 °C, indicating no improvement in coke – catalyst contact on grinding. This observation suggests that *in-situ* coke deposition leads to intimate contact between coke and the catalyst, irrespective of the hardness of the coke. This demonstrates that coke – catalyst contact after grinding *in-situ* coke remains the same as before grinding. The coke-catalyst contact for *in-situ* coke generation shows catalytic activity similar to tight contact conditions and is also more representative of the realistic contact that takes place in industrial operations. *In-situ* coke forming methodology also helps in improving the reproducibility and reliability of data as compared to vague descriptions of loose and tight contact, where the mixing time can affect the catalytic activities.

2.4 Conclusions

The present work demonstrated that radical coke can be generated in the laboratory and deposited on catalyst or support samples in a specialized TGA. Deconvolution of Raman spectra gave an insight into the chemical structure of the coke samples. *In-situ* coke was found to be more amorphous compared to an industrial coke sample. Temperature programmed oxidation experiments were employed to study the oxidation behavior of the coke deposits. Thermal aging has important effects on the oxidation characteristics of the coke deposits. Thermal aging of the coke increased the hardness of the *in-situ* coke, as shown by Raman analysis and TPO experiments. Coke – catalyst contact in the *in-situ* coke samples was improved as compared to the physical mixtures of coke and catalyst, suggesting that coke generated on catalyst samples *in-situ* may be representative of coke catalyst contact found in actual reactors where coke is produced by a homogeneous radical process.

CHAPTER 3. CERIA CATALYZED COKE OXIDATION

3.1 Background

As described in the previous chapter, radical coke was successfully made on the catalytic supports. The next step towards achieving the project goal is to develop catalysts that can aid the oxidation of these radical carbon deposits at temperatures lower than uncatalyzed oxidation, thereby reducing the energy requirements of the process. While choosing catalysts, it is also important to choose materials that do not contribute to catalytic coking. For example, metals like Ni, Fe, Pt should be avoided to minimize catalytic coking. In this work, catalytic materials that are resistant to coking and are active towards oxidation of carbon deposits are explored. These catalysts are active after high temperature treatment and cannot only be used in steam cracking but also in other high temperature applications such as pyrolysis reactions and in solid oxide fuel cells, where coking is a major issue.

Coke deposited in industrial reactors or on catalysts is typically combusted by passing air, other oxygen-containing gases, or mixtures thereof (e.g. steam and air) at high temperatures through the reactor in regeneration mode. For instance, the steam cracker plant or process usually requires a shutdown for decoking every 20 – 60 days, depending on the type of feed used.[18] The physical structure and chemical nature of the carbon deposits depends on a number of factors, namely the operating temperature, pressure, residence time in the reactor and hydrocarbon feed composition. These aspects and others are summarized in an extensive review on different mechanisms of carbon formation and technologies used for reducing coke formation as well as for oxidation.[58] In parallel, materials that can reduce the rate of deposition of carbon deposits are also sought-after,

especially in solid oxide fuel cell (SOFC) applications. In SOFCs, coking is a major problem on the Ni based anode. Coke can block the pores of the anode or cause micro-cracking, affecting cell performance.[170]

Due to the nature of the solid-solid-gas reactions that occur for catalyzed carbon oxidation with an oxidizing gas, the contact between the carbon and the catalyst is very important. In this paper, catalytic activity under another type of coke – catalyst contact, *in-situ* coke – catalyst contact, where coke is directly deposited on the catalyst, has been measured. This method of coke deposition has been described in detail in chapter 2. [141] This contact method is a near exact representation of how carbon and catalyst would come in contact in an industrial setting.

Over the last decades, cerium oxide and mixtures of cerium-containing oxides have been found to be effective for a number of oxidative catalytic processes. An important characteristic of ceria is its redox capability under both oxidizing and reducing conditions. Cerium based oxides have been used in the three-way catalytic converter for elimination of CO, hydrocarbons, and NO_x in engine exhaust due to their excellent oxygen storage capacity. Their highly active surface crystal facets and redox behavior allow cycling between Ce^{3+} and Ce^{4+} states with the formation and elimination of oxygen defects.[64,171] Such materials have also received wide attention for diesel soot oxidation. A comprehensive review of ceria materials for carbon oxidation has been done in our previous work[58] and also mentioned in some depth in chapter 1. Oxygen vacancy defects are known to be one of the most reactive sites on metal oxides.[154,172] The redox chemistry of ceria can be written as Equation 13:

$$2CeO_2\ (s) \rightarrow 2CeO_{2-y}\ (s) + yO_2\ (g) \quad (13)$$

where, CeO_{2-y} is a non-stoichiometric phase. The oxygen storage capacity of ceria can be enhanced by doping it with other rare earth elements.[158] Ceria catalysts are promising candidates for applications like soot oxidation,[63,64,71,155–157] the water gas shift reaction,[158] CO oxidation,[160] and in solid oxide fuel cells.[173–175]

Doping of ceria with zirconium has been observed to increase the oxygen storage capacity of ceria and enhance catalytic activity towards oxidation of soot.[64,77,80,114] Most of the soot oxidation studies involving ceria work with temperatures below 800 °C, above which compositional changes might take place affecting the properties of the catalyst.[114] However, steam crackers units operate at temperatures around 1000 °C and hence the thermal stability of the catalytic materials is of high importance. Therefore, any support material used should be inert, stable under operating conditions and low cost. γ-Alumina has been used widely as a catalyst support due to its low cost, robustness at low temperatures and good textural properties like high surface area and pore volume. However, it is not stable at high temperatures (> 800 °C) and can transition to other phases of alumina.[112,176] α-Alumina is the most thermodynamically stable phase of alumina, has very low surface area but high corrosion resistance, which makes it an appropriate candidate for high temperature applications.

In this work, the aim was to apply the knowledge that exists in the literature for oxidation of soot in designing catalysts that are active for coke oxidation. Accordingly, the objective of this study was to develop catalytic materials that aide coke oxidation and minimize coke deposition in high temperature applications and investigate the properties

responsible for their activity. Ceria dispersed on a commercial α-alumina support at various loadings was used to explore coke deposition as well as oxidation of coke. Two types of coke – catalyst contact were examined, (i) traditional tight contact and (ii) *in-situ* contact. The alumina-supported cerium oxides were also characterized by various analytical techniques, allowing for their oxidation performance to be correlated with their composition and structural properties.

3.2 Experiments

3.2.1 Catalyst Synthesis

Ceria loaded α-alumina materials were prepared by a wetness impregnation method using cerium nitrate hexahydrate ($Ce(NO_3)_3.6H_2O$, Sigma Aldrich) as the cerium precursor and α-alumina as the support (Sigma Aldrich, corundum, -100 mesh, 99%). The mixture was dried at 110 °C overnight and calcined at 1100 °C for 8 h at a heating rate of 1 °C/min in air. The synthesized catalysts are denoted as x-CeO_2-Al_2O_3, where x denotes Ce/(Ce+Al) atomic ratio in the catalyst sample. An industrial coke sample was obtained from the Dow Chemical Company.

3.2.2 Catalyst Characterization

Catalyst samples were characterized by nitrogen physisorption, X-ray diffraction, Raman spectroscopy, UV-Vis spectroscopy, and temperature programmed reduction. Nitrogen physisorption isotherms were collected at -196 °C using a Micromeritics Tristar II. The samples were heated to 200 °C under vacuum for 10 h prior to the analysis. The data obtained were used to calculate surface areas for the various powders. The powders

were characterized by X-ray diffraction (XRD) using Cu K α radiation. The instrument was operated at 40 mA and samples were packed into a horizontally mounted sample holder. The crystallite sizes were estimated using the Scherrer equation. A Witec confocal Raman microscope (Alpha 300R) was used to obtain Raman spectra for the fresh and coked catalysts with an Ar+ ion laser (λ = 513.998 nm) using a 2 mW excitation source intensity and 1800 grating with < 0.9 cm^{-1} pixel resolution. A magnification of 50x was used. A dense sample layer of about 1 mm thickness was pressed onto a cover slip with the help of a spatula. This coverslip was then placed on the microscope sample holder. A white light source was used to focus on the surface of the sample. After focusing on a spot, the sample was exposed to the laser beam and the Raman spectra were recorded at ambient temperature. First order Raman spectra were de-convoluted using the peak analyzer function of the OriginPro 8.5 software.

X-ray absorption near edge structure (XANES) was performed at beamline X18B of the National Synchrotron Light Source (NSLS), Brookhaven National Laboratory. The X-ray absorption spectroscopy (XAS) data were obtained in transmission mode at the Ce L_{III} edge (5723 eV). The Ce L_{III} edge spectra were measured at room temperature in air. The XANES samples were prepared by spreading a thin layer of material on pieces of transparent tape. CeO_2, obtained from Sigma Aldrich, was used as the standard. Two scans from 5,573 to 6,187 eV were collected for each sample. The XAS data were then processed with Athena software for background removal, and edge-step normalization.

The ceria lattice oxygen species available for oxidation reactions at different conditions were measured by temperature programmed reduction (TPR) experiments on a Micromeritics AutoChem 2920. The samples were pretreated at 150 °C in He for 1 h to

remove volatile species. Approximately 40 – 50 mg of the sample was heated at a constant rate (5 °C/min) from room temperature to 900 °C in 10% hydrogen in argon (30 mL/min), in a U-shaped quartz tube. The water produced was removed by passing the effluent gas through a cold trap (a mixture of acetone and liquid nitrogen). Hydrogen consumption was monitored by a thermal conductivity detector. For quantitative analysis, the instrument was calibrated with the reduction of Ag_2O. UV-Vis spectroscopy measurements were performed in the wavelength range of 200 – 800 nm using a Cary UV-Vis NIR spectrophotometer. The instrument was calibrated using $BaSO_4$ as the standard.

3.2.3 Coke – Catalyst Contact

3.2.3.1 *In-situ* Coke – Catalyst Contact

A customized thermogravimetric analyzer (TGA, Netzsch, STA449F3 Jupiter®) was used for *in-situ* generation of radical coke (coke formed in gas phase) and to study coke oxidation. This TGA could be operated with reactive gases like hydrocarbons at high temperatures. For safety reasons, flammable gas concentrations were kept below their flammability limits in the TGA. In these experiments, 2 mol% of ethylene was used. The internal components of this TGA were designed to work efficiently in the presence of corrosive atmospheres. The measurement head, made of alumina, was stable at high temperatures and resistant to corrosive gases.

For *in-situ* coke deposition, the TGA furnace was heated to the desired temperature in helium flow. Once the desired temperature was reached, 2 mol% ethylene in helium was introduced into the system for 1 h. After 1 h, the ethylene flow was stopped and the furnace was allowed to cool while under helium flow. The coking rate and the amount of coke

deposited were measured by the TGA. Coke deposited on the measurement head was removed completely prior to oxidation of the coked catalysts, by temperature programmed oxidation in air up to 900 °C after removal of the coked catalyst sample.

3.2.3.2 Tight Contact

For tight contact experiments, an industrial coke sample obtained from the Dow Chemical Company was used. A small amount of industrial coke and catalyst in the ratio 1:9 were ground in a mortar and pestle for 45 min to achieve tight contact conditions.

3.2.4 Catalytic Activity

3.2.4.1 Temperature Programmed Oxidation

Temperature programmed oxidation (TPO) experiments were also performed on the Netzsch TGA. The TGA was used to determine the reactivity of the coke deposited on various catalyst materials. For these measurements, 15 mg of the coke – catalyst mixture was placed in an alumina crucible. The temperature was raised from room temperature to 950 °C at a rate of 10 °C/min in the presence of air (100 mL/min). The rate of mass loss was used to compare the activity of catalysts for both the industrial and *in-situ* coke samples.

3.2.4.2 Isothermal Oxidation

Isothermal oxidation was carried out on the Netzsch TGA by heating the coke – catalyst sample to the desired temperature under helium flow. Once the desired temperature was reached, air was introduced into the furnace. Rate constants were obtained by fitting

the mass loss data to a first order rate equation. The data from 0 – 50% conversion were used to calculate the rate constants. Isothermal studies were also performed in the absence of any oxidizing agent under helium flow to establish a baseline or to study the effect of surface oxygen species present on the ceria.

3.2.4.3 Isothermal Reduction of Catalysts

Isothermal reduction of catalysts was carried out at the reaction temperature (950 °C) to determine the amount of oxygen released during the pyrolysis reaction where hydrogen is produced. The TGA furnace was heated to the desired reaction temperature in nitrogen flow. Once the desired temperature was reached, 1.5 mol% hydrogen in nitrogen was introduced into the system for 1 h. After 1 h, the hydrogen flow was stopped and the furnace was allowed to cool while under helium flow.

3.3 Results and Discussion

3.3.1 Catalyst Characterization

Figure 3.1 compares the XRD patterns for α-alumina supported ceria catalysts along with unsupported ceria and the α-alumina support. No significant change was observed in the crystallinity of the ceria domains as well as the α-alumina structure. All α-alumina supported ceria composites showed distinct ceria peaks. Diffraction peaks corresponding to fluorite structure of CeO_2 (28.6°, 33.3°, 47.5°, 56.4°) [177] were well defined in the diffractograms of the composites. Peak broadening was used to determine crystallite size based on the (111) plane of ceria. These sizes are in the range of 30 – 60 nm, as summarized in Table 3-1.

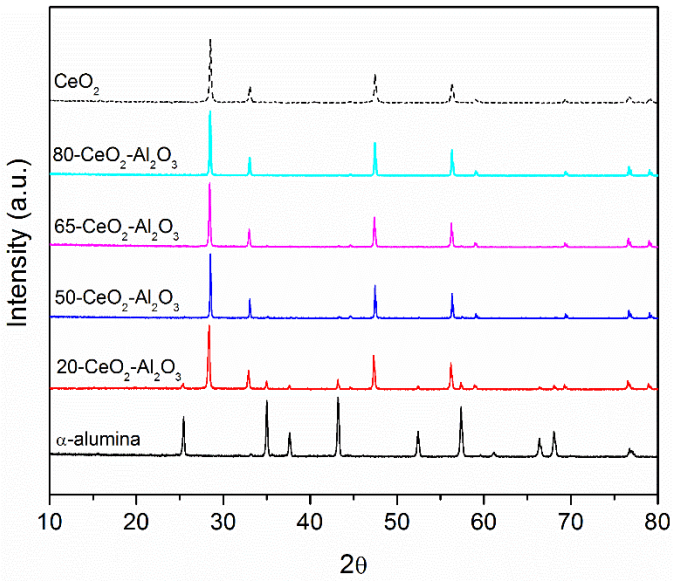

Figure 3.1 XRD patterns of α-alumina, unsupported ceria and ceria -alumina composites with different ceria loading

Table 3-1 Crystallite sizes of the ceria (111) plane at θ ~ 28°

Sample	**XRD crystallite size 111 peak (nm)**
CeO_2	42
20-CeO_2-Al_2O_3	32
50-CeO_2-Al_2O_3	57
65-CeO_2-Al_2O_3	47
80-CeO_2-Al_2O_3	53

The surface areas of the various materials are summarized in Table 3-2. Since, the surface areas are very low, around 1.5 – 2 g of the catalysts were used for physisorption analysis. Catalysts with 20 and 50 mol% Ce had slightly higher surface areas than bare α-alumina. Higher ceria loadings of 80 mol% reduced the surface area. From the physisorption experiments, it was observed that the catalytic materials were highly non-porous in nature. This is attributed to the non – porous nature of the commercial α-alumina support that was used, as well as the high calcination temperature. Both aspects make these

catalysts thermally stable so they can be used in high temperature applications. Unsupported ceria showed higher surface area than the supported ceria samples, but it had a similar non-porous nature.

Table 3-2 Textural properties of α-alumina, unsupported and supported ceria catalysts

Support	Surface area (m^2/g)
α-alumina	1.5
20-CeO_2-Al_2O_3	1.9
50-CeO_2-Al_2O_3	2.1
65-CeO_2-Al_2O_3	1.9
80-CeO_2-Al_2O_3	1.0
CeO_2	7.0

Figure 3.2 shows that XANES spectra for bulk ceria and α-alumina supported ceria are similar to the reference ceria sample obtained commercially. Two major peaks at 5731 eV (A) and 5738 eV (B) are present in all the catalysts' spectra. These peaks have been associated to the +4 oxidation state of Ce [178]. The difference in the intensity of the peaks for various catalysts is related to the crystallite size of the catalysts. The larger the crystallite size of the materials, the higher the intensity of the A and B peaks, which is also consistent with the sizes obtained from XRD analysis (Table 3-1). A minor peak (C) at 5727 eV indicates the presence of Ce species in the +3 oxidation state. The presence of the +3 and +4 oxidation states of Ce is consistent with the well-known redox nature of the catalysts, and also demonstrates that chemical nature of the unsupported ceria and ceria supported on alumina is the same. Hence, there are no interactions between ceria and alumina species in the supported materials that would change the electronic structure of the ceria.

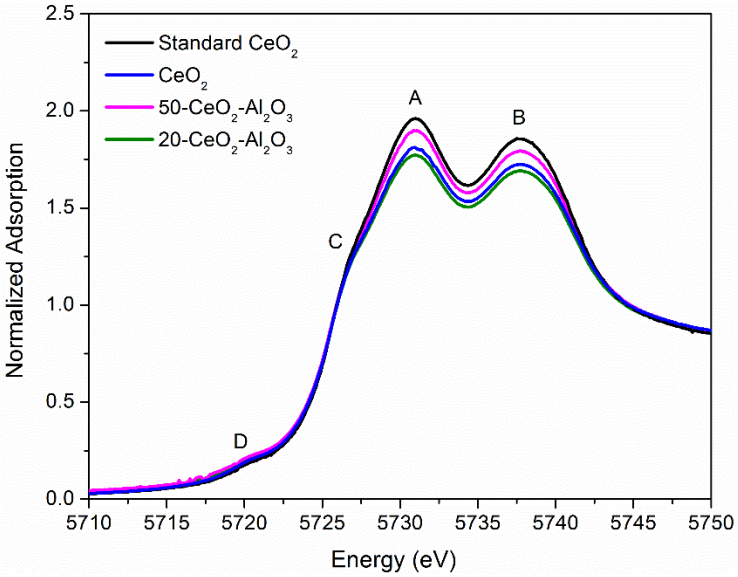

Figure 3.2 Ce L_{III}-edge XANES spectra of unsupported and supported ceria

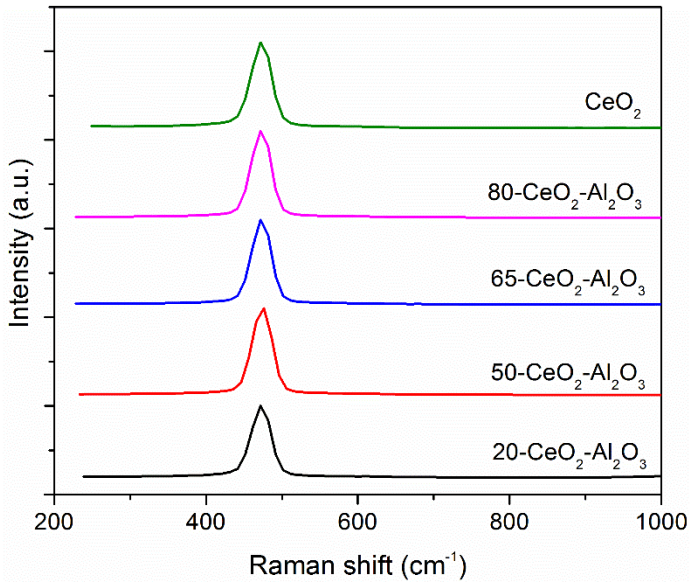

Figure 3.3 Raman spectra of the ceria catalysts; 514 nm, 2 mW

Figure 3.3 shows Raman spectra of the supported and unsupported ceria catalysts. A peak at ~ 470 cm^{-1}, characteristic of CeO_2 (F_g mode), was observed for all samples.[179] This indicates presence of characteristic CeO_2 domains in the catalysts. The absence of spectral features at 250, 268, 288, 383, 558 cm^{-1} denotes the absence of any interaction between Ce and Al species. These features have been observed on ceria dispersed on γ-

alumina investigated by Shyu et al.[179] and have been associated with a $CeAlO_3$ species. Thus, results from XANES and Raman spectroscopy demonstrate the presence of independent CeO_2 domains on the surface of α-alumina, without any intermixing with the alumina species, for all the α-alumina supported ceria samples.

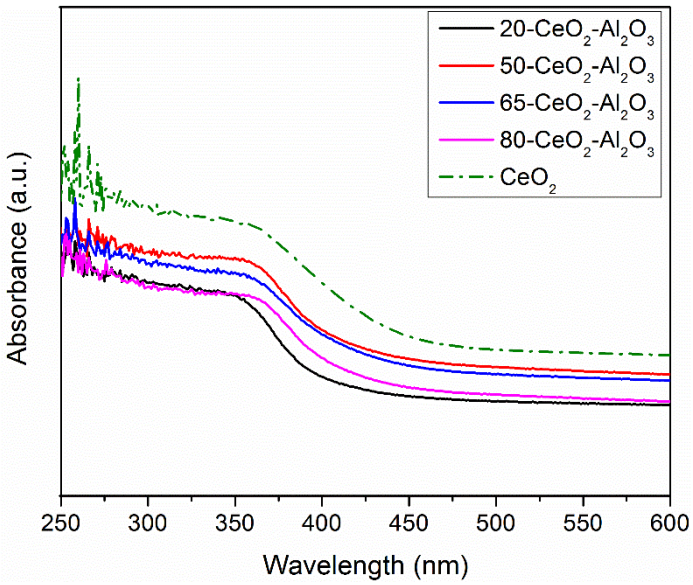

Figure 3.4 UV-VIS spectra of the ceria catalysts with different Ce loadings

Nano-crystallites in a material can escape XRD detection due to their small crystal size. In such cases, UV absorption of materials can be used to detect their presence. Figure 3.4 shows the UV spectra of both the supported and unsupported ceria catalysts. An absorption band at around 370 – 380 nm was observed for all the catalysts and has been attributed to inter-band transitions, which is in agreement with values in the literature for transmission on single ceria crystals.[180] This observation is again an indication of no significant interactions between ceria and alumina species in the α-alumina supported ceria catalysts. Absorbance at lower wavelengths ≤ 375 nm indicated the presence of smaller crystallites (≤ 4 nm) that were not detected by XRD.[180]

TPR experiments of the alumina supported ceria materials and unsupported ceria were performed to analyze the reduction properties of the catalysts. Two major peaks were observed for both the unsupported and supported ceria, referred to here as the low temperature and the high temperature peak, respectively whose values are shown in Figure 3.5. This is consistent with the reduction profiles for ceria reported by others in the literature.[76,177] Unsupported ceria has higher temperature values for both the peaks than the α-alumina supported ceria (Figure 3.5). The presence of two peaks depicts the step-wise reduction of CeO_2. The low temperature peak has been typically associated with the removal of surface oxygens of CeO_2. The higher temperature peak is then associated with the progressive reduction of the bulk CeO_2 after all the surface species have been reduced. Bulk ceria, when reduced, leads to formation of Ce_2O_3.[177] Visually this compound appears bluish black in color. All samples after the TPR runs turned bluish black, indicating the reduction of bulk ceria.

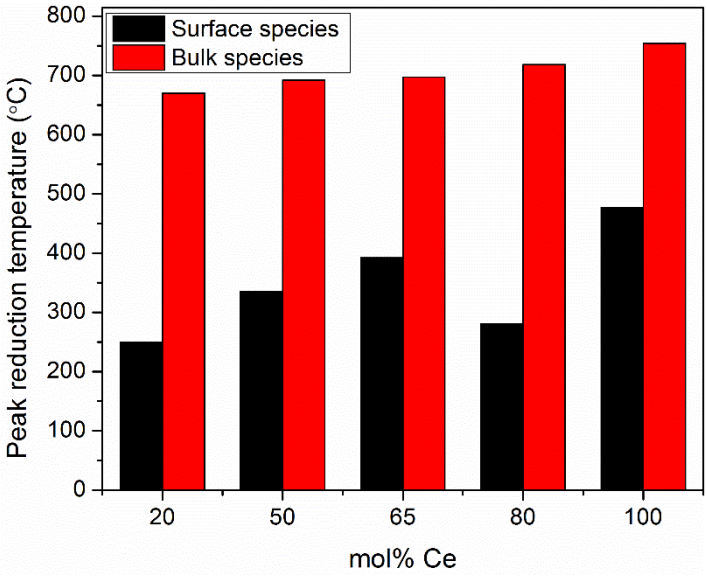

Figure 3.5 Peak reduction temperature of unsupported and supported ceria materials from TPR analysis

3.3.2 Coking Resistance of α-Alumina Supported Ceria Catalysts

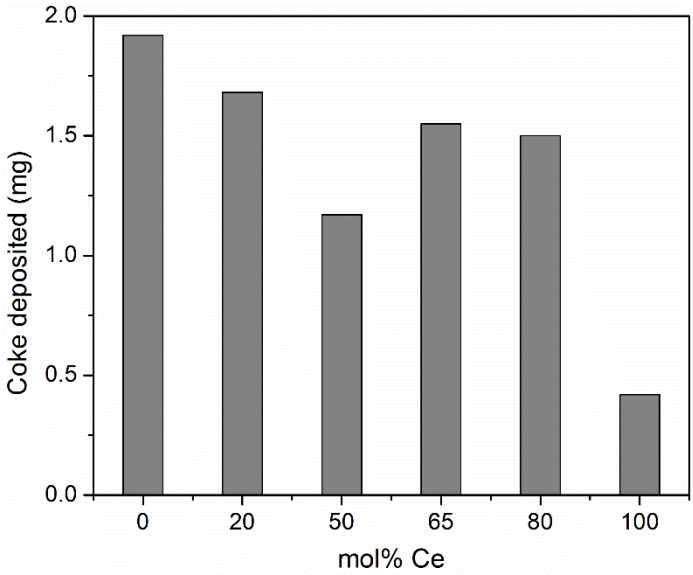

Figure 3.6 Comparison of coking resistance of the supported ceria catalysts with unsupported ceria and the α-alumina support

Metallic and acidic catalysts are well known to catalyze coke formation.[25,181] Inhibition of coke deposition requires the catalysts to also be coke – resistant. To demonstrate the coke resistance abilities of the ceria catalysts, *in-situ* coke deposition was performed in the TGA. Coke deposition on α-alumina (0 mol% Ce) was used as a reference case. In the previous study, it was demonstrated that *in-situ* coke deposition was independent of the catalytic support and that radical coke was deposited on the supports. Here, the support materials of equal surface areas were exposed to 2% ethylene in helium at 950 °C for 1 h. The amount of coke deposited on these supports is shown in Figure 3.6. The maximum amount of coke deposition was observed on the reference α-alumina support. All the ceria catalysts showed lower amounts of coke deposition. This observation can be attributed to the ability of ceria to provide oxygen to the deposited coke precursors for *in-situ* oxidation of coke species, slowing coke deposition to a degree. The bulk ceria

material had the least amount of coke deposited on its surface. To calculate the amount of oxygen that may be labile and thus given up by the ceria catalyst in the presence of the reducing hydrogen produced during pyrolysis of ethylene, the catalysts went through the same thermal treatment as the pyrolysis reaction in the presence of 1.5 vol.% hydrogen alone. Table 3-3 shows the values for isothermal reduction of the catalysts and the amount of coke deposition observed on them. For the highest (20 mol% Ce) and lowest (CeO_2) amounts of coke deposited, there is a clear correlation with the weight loss of catalysts, which may be related to reduction of the catalysts, and correlates with the amount of oxygen released by the catalyst under pyrolysis conditions. For the other catalysts, the resolution between the values for the weight loss of catalyst in presence of hydrogen is quite low and hence comparison is difficult.

Table 3-3 Weight loss of catalysts during exposure at 950 °C, 1.5 vol.% H_2 in N_2

Catalyst	Weight loss (%) in H_2 atmosphere	Coke deposition (mg)
20-CeO_2-Al_2O_3	1.17	1.7
50-CeO_2-Al_2O_3	1.90	1.2
65-CeO_2-Al_2O_3	1.88	1.5
80-CeO_2-Al_2O_3	1.95	1.6
CeO_2	2.06	0.44

Raman analysis is an effective way to determine the type of carbon species in the coked samples. Deconvolution of the Raman peaks reveals interesting information on the amorphous carbon content in the coke samples. Raman spectra of *in-situ* coke was deconvoluted into five peaks (G, D_1, D_2, D_3, D_4), where D_3 is the amorphous carbon peak observed at 1500 cm^{-1}.[168] Sadezky et al. found that fitting the G, D_1, D_2, D_4 peaks as Gaussian and the D_3 peak as Lorentzian gave the best fit for the spectra.[168] Similar deconvolution analysis was used for obtaining Raman parameters for the different coked

samples. The heterogeneity of the coke samples was studied by measuring the Raman spectra at different spots on the sample. The relative intensity of the amorphous carbon is given by equation 12:[169]

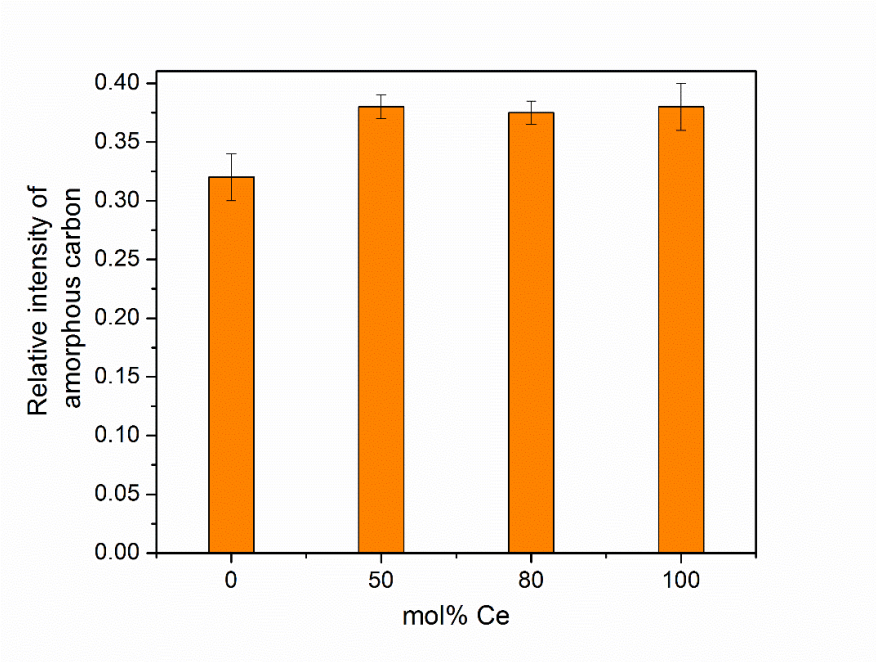

Figure 3.7 Deconvolution of Raman spectra of coked catalyst samples comparing the relative amorphous nature of the coke deposited *in-situ* on the various materials.

Figure 3.7 shows the amount of amorphous carbon in the coke deposited on the ceria catalysts in comparison with the bare α-alumina support. Coke formed on the α-alumina had lower amorphous content than the coke formed on the ceria catalysts. These data demonstrate that ceria catalysts not only reduced the amount of coke deposition relative to the α-alumina, but the deposited carbon also formed less hard coke under the conditions used. This observation can be attributed to the ability of ceria to oxidize coke precursors as they become deposited on the surface of the powder catalyst. Ceria catalysts thus appeared to not only reduce the amount of coke deposited but also to reduce the hardness of the deposited coke.

3.3.3 Temperature Programmed Oxidation Studies of Coke using α-Alumina Supported Ceria

To investigate the activity of the ceria catalysts towards oxidation of coke, temperature programmed oxidation studies were performed under two coke – catalyst contact conditions. For the tight contact conditions (Figure 3.8a), uncatalyzed (0 mol% Ce) industrial coke oxidized at a very high T_{50} (temperature at which 50% of the coke was oxidized) value of ~ 650 °C. This value reduced significantly (by ~100 °C) in the presence of the ceria catalysts. All the ceria catalysts reduced this T_{50} value to a comparable degree, as shown in Figure 3.8a. For *in-situ* deposited coke, Figure 3.8b demonstrates that the coke deposited on α-alumina (0 mol% Ce) had the highest T_{50} value (~ 550 °C) and hence, was the most difficult to oxidize. This observation is likely related to the hardness of the coke, as seen in section 3.3.2, and the low catalytic activity of α-alumina towards coke oxidation. The presence of ceria in the catalyst reduced the T_{50} value by ~ 150 °C for all ceria-containing materials (Figure 3.8b). Oxidation of coke on α-alumina supported ceria and bulk ceria catalysts showed very little variability in the T_{50} value.

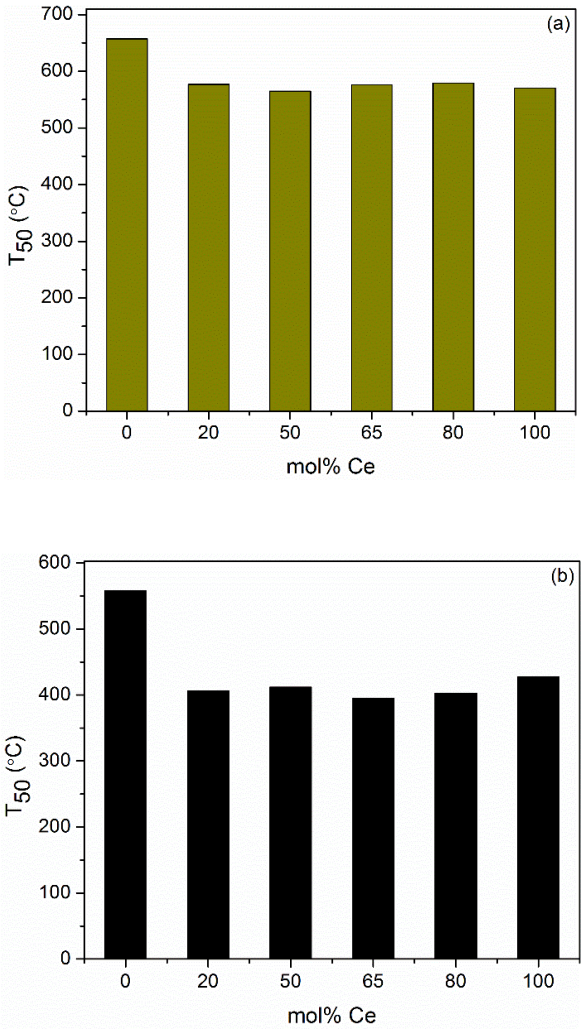

Figure 3.8 T_{50} values for oxidation of (a) industrial coke (b) *in-situ* coke

3.3.4 Catalytic Activity of Coke Combustion over Ceria-Alumina

To measure the kinetics of the catalytic oxidation of coke, isothermal experiments were performed on the tight contact coke – catalyst mixtures and the *in-situ* coked catalysts. The lower temperatures were chosen for isothermal studies such that non-catalytic oxidation of coke was kept relatively low. As shown in Figure 3.9, at 450 °C and in the presence of a ceria-containing catalyst, the catalytic activity was improved compared to experiments using the ceria-free alumina support. However, the differences in the kinetic constants for the catalysts with different ceria content were minimal. At an increased

temperature of 500 °C, the catalytic effect was significantly enhanced. The catalytic activity of the 50-CeO_2- Al_2O_3 material was five times that of the uncatalyzed oxidation. Unsupported ceria showed the lowest catalytic activity at both temperatures for the tight contact conditions. The 20-CeO_2-Al_2O_3 material showed increased catalytic activity as compared to the un-catalyzed oxidation. As the mol% Ce was increased from zero to 50%, the catalytic activity increased. However, after 50 mol% Ce loading, the activity remained steady without any further improvement. This behavior was observed for both the coke-catalyst contact conditions, indicating the similarity of *in-situ* and tight contact conditions, with both exhibiting intimate contact between the coke and catalyst particles. However, after 50 mol% Ce loading, the activity remained steady without any further improvement. Similar catalytic behavior was observed for *in-situ* catalyst contact, as observed in Figure 3.10, indicating the similarity of *in-situ* and tight contact conditions. As shown in Figure 3.10 coke deposited on the α-alumina support did not oxidize at all, which is likely primarily related to the lack of redox activity of the α-alumina. The *in-situ* coke deposited was more amorphous than the industrial coke sample and hence, the temperature chosen for kinetic studies was lower for the *in-situ* coke. As a result, the reaction rates cannot be compared for the two temperature ranges, as the nature of the carbon species used was different.[58]

Similar isothermal experiments were carried out in the absence of oxidizing gas under helium flow at 450 °C. Industrial coke did not show any weight loss in the absence of a catalyst as well or oxidizing agent. As expected, the reaction progressed significantly slower as compared to studies where air was present. In the presence of a catalyst, the weight loss followed a zero order rate model. This observation demonstrates the ability of

the ceria catalyst to provide oxygen to the carbon species in the absence of gaseous oxygen. No weight loss occurred when a similar heat treatment was given to bare catalysts without coke, indicating the weight loss observed during isothermal oxidation experiments was entirely due to loss of carbon species. The rate constants for oxidation in air were calculated for the 0-10% conversion region of the industrial coke for the uncatalyzed (no catalyst) as well as catalyzed reactions, as shown in Table 3-4. The theoretical total surface oxygen species that are available on the ceria catalysts were calculated based on the average exposure of 111, 110 and 100 crystal planes of ceria, assuming Al atoms were not reduced and one out of four Ce atoms was reduced [182]. As the theoretical amount of surface oxygens in the sample increased, the rate of gasification of carbon under inert conditions increased too, implying the importance of surface oxygen release by ceria leading to carbon oxidation. This theoretical value calculates only the contribution from surface oxygen species as opposed to bulk oxygen species, which are active at the high temperature of 950 °C used for measuring the hydrogen consumption in Table 3-3. Hence, the order of magnitude observed for values in Table 3-3 and Table 3-4 cannot be directly compared.

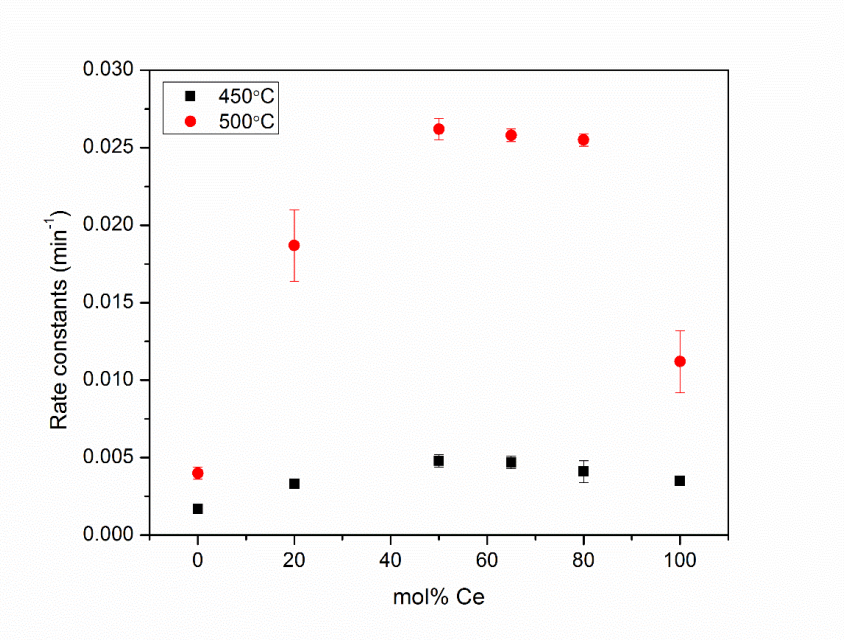

Figure 3.9 Kinetic studies for oxidation in tight coke-catalyst conditions with the industrial coke sample at 500 °C in air

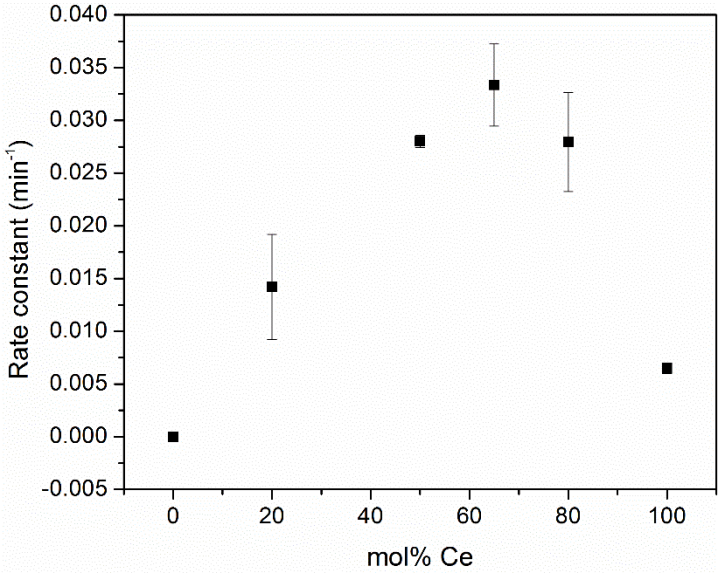

Figure 3.10. Kinetic studies for oxidation using *in-situ* coke-catalyst contact conditions at 350 °C in air

Table 3-4 Rate constants for gasification of coke in inert gas environment

Catalyst	Rate constant, industrial coke, inert gas, (g_{carbon} min^{-1}), 450 °C	Theoretical surface oxygens available, µmol/g
-	0.0000	-
20-CeO_2-Al_2O_3	0.0004	2.1
50-CeO_2-Al_2O_3	0.0008	5.7
65-CeO_2-Al_2O_3	0.0007	6.7
80-CeO_2-Al_2O_3	0.0006	4.4
CeO_2	0.0009	37.5

3.3.5 Relating Catalytic Activity to Surface Oxygen Content

Temperature programmed reduction curves showed that the α-alumina supported ceria samples had a lower overall reduction temperature than bulk ceria. Surface reduction of the ceria also improved when ceria was dispersed over alumina. The amount of surface oxygen available for reduction up to a specific temperature was calculated from the TPR data, as discussed above. This majority likely consisted of surface lattice oxygen species due to the low temperatures used for coke oxidation. However, the possibility of contribution from bulk lattice oxygens cannot be neglected. A good correlation was found between the available ceria lattice oxygen species and the kinetic rate constants calculated from the isothermal oxidation data. Interestingly, this observation was observed for both the tight contact (Figure 3.11) and *in-situ* coke – catalyst (Figure 3.12) contacting conditions. This strengthens the previous observation that *in-situ* coke – catalyst contact showed similar oxidation behavior as tight contact conditions.

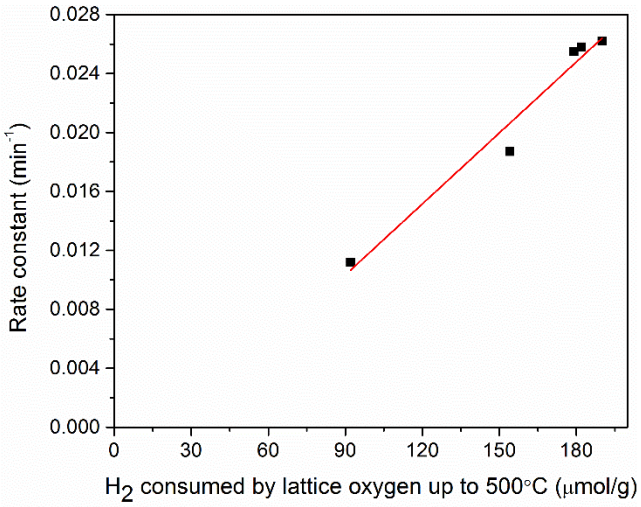

Figure 3.11 Relating the reaction rate constant to ceria lattice oxygen availability for tight coke-catalyst contact

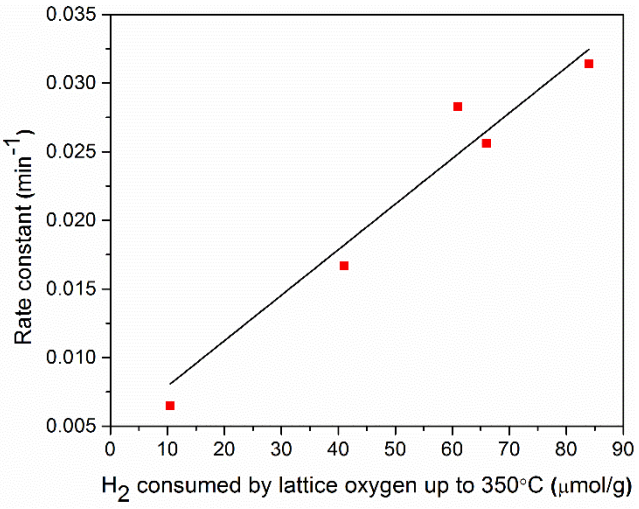

Figure 3.12 Relating the reaction rate constant to ceria lattice oxygen availability for *in-situ* coke - catalyst contact

3.4 Proposed Mechanism of Coke Oxidation over α-Alumina Supported Ceria

In the previous section, it was demonstrated that the lattice oxygens from ceria were responsible for the observed enhanced activity towards oxidation of coke. Based on this observation, a mechanism of coke oxidation is proposed.

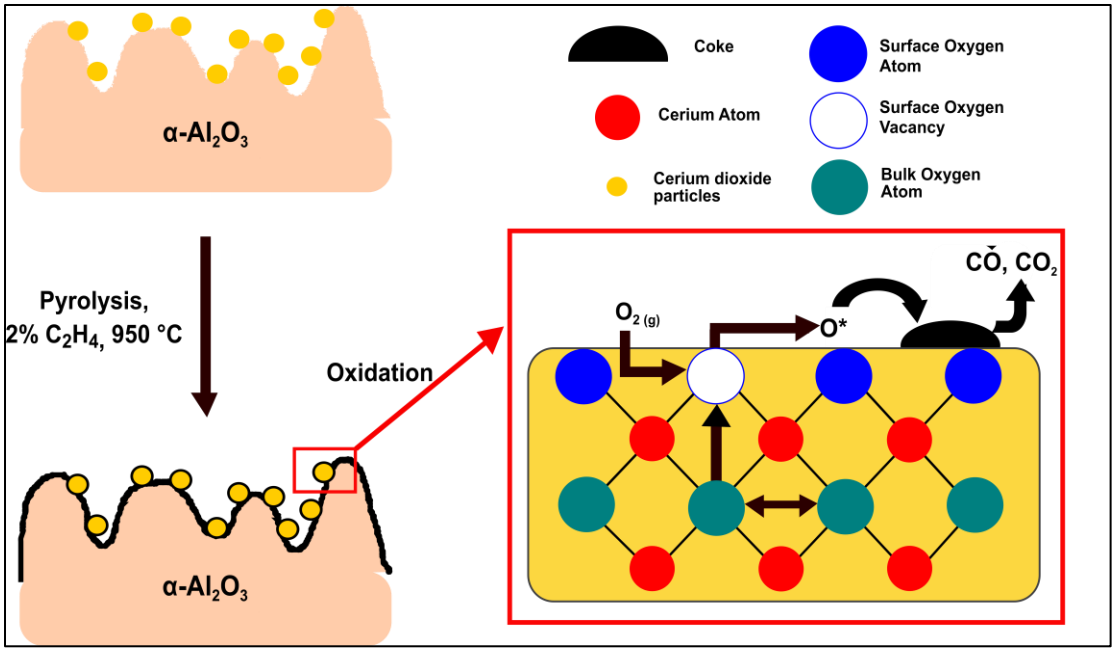

Figure 3.13 Schematic representation of the mechanism of coke oxidation on ceria and supported ceria catalysts

Figure 3.13 shows a schematic of *in-situ* coke formation and the hypothesized mechanism of coke oxidation using the ceria catalysts. During pyrolysis, coke is formed on both ceria and α-alumina. Since it has been shown that individual ceria domains of varied crystallite sizes exist on the surface of the α-alumina support, the schematic shows only ceria as the catalytic surface. As seen from the TPR results, ceria has two types of lattice oxygens available for reduction, namely surface oxygens and bulk oxygens. Based on the temperature range of coke oxidation, the contribution of bulk oxygen changes and as expected, it increases with temperature. In the proposed mechanism, under the conditions used here, primarily surface lattice oxygen are thought to participate in the oxidation reactivity. It is proposed that surface lattice oxygen from ceria forms an active species (O*) at the coke – ceria interface. This active species reacts with coke to form volatile carbon oxides. Gaseous oxygen fills the oxygen vacancy formed by the loss of oxygen. Simultaneously, there is increased mobility in the bulk of ceria and diffusion of

bulk lattice oxygens to the surface that can fill up the oxygen vacancies. This mechanism has been proposed for ceria – zirconia materials for soot oxidation,[80] and CO oxidation,[183] ceria,[172] ceria – lanthana,[75,76] copper – ceria for CO oxidation,[184] etc. previously.

3.5 Conclusions

Thermally stable ceria supported on α-alumina and unsupported ceria appeared to be resistant to coking and useful in the oxidation of coke deposits under realistic *in-situ* contact conditions. Using α-alumina as the support renders these catalysts suitable for high temperature applications like steam cracking, pyrolysis, solid oxide fuel cell for use up to ~ 1000 °C. Surface characterization of catalysts by XANES and Raman spectroscopy revealed the presence of independent CeO_2 domains with no significant electronic interactions with the alumina support. XRD gave evidence of large crystallites and smaller crystallites were inferred to exist based on UV-Vis spectroscopy. Two types of coke – catalyst contact were investigated for coke oxidation, tight contact between the catalysts and industrial coke and *in-situ* contact where carbon was deposited directly on the catalysts. Ceria catalysts were observed to show coking resistance when compared to bare α-alumina support during *in-situ* coking. This ability was qualitatively related to the ability of ceria catalyst to release oxygen in a reducing environment. The oxidation performance was probed by temperature programmed and isothermal oxidation studies. In both coke-catalyst contact conditions, α-alumina supported ceria materials were observed to have better oxidation capability towards the coke deposits than bulk ceria. The kinetics of coke oxidation were correlated to the availability of ceria lattice oxygen, which was obtained from temperature programmed reduction studies. The similarity observed for the behavior of coke oxidation activity in these two contact conditions indicates that *in-situ* coke –

catalyst contact mimics tight contact conditions. A mechanism involving lattice active adsorbed oxygen species causing oxidation of coke particles was proposed.

CHAPTER 4. DOPED CERIA CATALYSTS FOR STEAM GASIFICATION AND OXIDATION OF COKE

4.1 Background

In the steam cracking process, steam is used as a diluent to reduce coke formation during the cracking phase. As mentioned in chapter 1, many dopants have been used previously for improving the catalytic performance of ceria towards oxidation of coke. Zr has been found to be one of the best dopants that increases the oxygen vacancies and hence helps in oxidation of carbon at lower temperatures. Our collaborators from the University of Virginia have worked with Ce-Zr mixed oxide materials for coke oxidation and gasification. Hence, this work has explored other elements that could potentially help in aiding the gasification activity of ceria.

Transition metals like Cu, Co, Mn, Fe have been useful in improving the catalytic activity of ceria towards carbon oxidation, as explained earlier in chapter 1. While choosing a catalyst for this particular application of decoking in steam cracking, choosing a catalyst that does not propagate the catalytic coke formation is critical. Fe and Ni have been known to catalyze coke formation and were hence, eliminated. The transition elements considered for the specific steam cracking application include Co, Cu and Mn.

Alkali and alkaline earth materials have also been very useful in improving catalytic activity towards gasification of coke. However, elements like potassium are volatile in nature at the high temperatures (800 °C) used in steam cracking operation. Although K has the excellent property of increasing oxygen mobility, it is not feasible to use such catalysts

in this particular operation. To explore the effect of alkali metals, Sr, which is a less volatile element, is used as a dopant for ceria.

Rare-earth element doping has shown significant improvement in the oxidation properties of ceria.[74,85,100,101] However, the disadvantage of using rare-earth elements is the high cost of these materials. In this steam cracking application, if all steam cracking furnaces are coated with a catalyst that shows good activity for carbon removal, the technology must be economical. Ceria and the α-alumina support used for coke oxidation are quite inexpensive materials and the dopant should be at par with these materials in terms of cost. Despite its high cost, in this work we have explored gadolinium as the rare-earth element representative, based on its performance in initial screening experiments. Gd has been used extensively for carbon oxidation in solid oxide fuel cells (SOFC) where carbon deposition takes place on the electrodes.[174,185] Gd doped ceria catalysts are used to provide oxygen for the carbon deposits and their immediate oxidation.[186] Hence, use of Gd in this coke removal application may be appropriate due to its coke resisting capability, especially if the loadings are kept low.

In the industrial process, a mixture of steam and air is used for removal of coke from steam cracking furnaces. Steam is used for the cracking cycle and the same steam flow is continued for the decoking cycle. Air is introduced into the cracking furnace over a period of time as per need. A significant portion of the reactive gas during the decoking cycle is steam which makes it necessary to evaluate and develop catalysts that are stable as well as active in a steam rich environment.

4.2 Experiments

4.2.1 Catalyst Synthesis

Ceria loaded α-alumina materials were prepared by a wetness impregnation method using cerium nitrate hexahydrate ($Ce(NO_3)_3.6H_2O$, Sigma Aldrich) as the cerium precursor and α-alumina as the support (Sigma Aldrich, corundum, -100 mesh, 99%). The mixture was dried at 110 °C overnight and calcined at 1100 °C for 8 h at a heating rate of 1 °C/min in air. The synthesized catalysts are denoted as x-CeO_2-Al_2O_3, where x denotes Ce/(Ce+Al) atomic ratio in the catalyst sample. Doped ceria catalysts were prepared by vigorously mixing citric acid, P-123, cerium nitrate hexahydrate, dopant nitrate tetrahydrate, α-alumina. The mixture was dried at 110 °C overnight and calcined at 900 °C for 8 h at a heating rate of 1 °C/min in air. Doped ceria catalysts are represented as yZCeAl where Z denotes the dopant and y denotes the Z/(Z+Ce) atomic ratio in the sample, while Ce:Al is 1:1. For comparison, an undoped ceria – α-alumina catalyst (denoted as CeAl) was prepared in the same manner as the doped catalysts. An industrial coke sample was obtained from the Dow Chemical Company.

4.2.2 Catalyst Characterization

Catalyst samples were characterized by nitrogen physisorption, X-ray diffraction, Raman spectroscopy and measurement of the oxygen storage capacity. Nitrogen physisorption isotherms were collected at -196 °C using a Micromeritics Tristar II. The samples were heated to 200 °C under vacuum for 10 h prior to the analysis. The data obtained were used to calculate surface areas for the various powders. The powders were characterized by X-ray diffraction (XRD) using Cu K α radiation. The instrument was

operated at 40 mA and samples were packed into a horizontally mounted sample holder. The crystallite sizes were estimated using the Scherrer equation. A Witec confocal Raman microscope (Alpha 300R) was used to obtain Raman spectra for the fresh and coked catalysts with an Ar+ ion laser (λ = 513.998 nm) using a 2 mW excitation source intensity and 1800 grating with < 0.9 cm^{-1} pixel resolution. A magnification of 50x was used. A dense sample layer of about 1 mm thickness was pressed onto a cover slip with the help of a spatula. This coverslip was then placed on the microscope sample holder. A white light source was used to focus on the surface of the sample. After focusing on a spot, the sample was exposed to the laser beam and the Raman spectra were recorded at ambient temperature.

X-ray absorption spectroscopy (XANES and EXAFS) were conducted at the Advanced Photon Source (APS), Argonne National Lab (ANL) at beamline 12-BM. The data were obtained in transmission mode at the Ce L-III edge (5723 eV) in the range of 5525-6150 eV, with a spot size of 0.5 mm x 1.2 mm. Each sample was ground thoroughly and then a thin layer of powder was rubbed onto Kapton tape. The tape was folded multiple times to achieve a proper edge step. Cr K-edge (5989 eV) was utilized as the reference due to the multiple Ce edge steps between 5525-6150 eV, which make it difficult to use as a reference material. After collection, Athena software conducted background removal, edge-step normalization, and Fourier transform on each XAS spectrum. Artemis software was utilized to fit the Fourier transformed EXAFS data with a model. The Ce-O scattering path was modelled from crystallographic data obtained from CeO_2[187] and then processed using FEFF8.[188]

Temperature programmed reduction (TPR) experiments were performed on a Micromeritics AutoChem 2920. The samples were pretreated at 150 °C in He for 1 h to remove volatile species. Approximately 40 – 50 mg of the sample was heated at a constant rate (5 °C/min) from room temperature to 900 °C in 10% hydrogen in argon (30 mL/min), in a U-shaped quartz tube. The water produced was removed by passing the effluent gas through a cold trap (a mixture of acetone and liquid nitrogen). Hydrogen consumption was monitored by a thermal conductivity detector. For quantitative analysis, the instrument was calibrated with the reduction of Ag_2O.

Oxygen storage capacity measurements were performed on a Micromeritics AutoChem 2920. Approximately 40 – 50 mg of the samples were pre-oxidized at the desired temperature in 10% O_2 in He for 1 h to completely oxidize the catalytic cerium species, in a U-shaped quartz tube. Pulses of 10% Hydrogen in Ar were then passed on the sample every 4 minutes. A total of thirty pulses were used. The sum of the total hydrogen consumed in every pulse gave the oxygen storage capacity of the catalysts.

4.2.3 Coking Resistance

A customized thermogravimetric analyzer (TGA, NETZSCH, STA449F3 Jupiter®) was used for *in-situ* generation of radical coke (coke formed in gas phase) and to study coke oxidation. The methodology used for these experiments is described in detail in Section 2.2.2.

4.2.4 Catalytic Activity

The catalytic activity of these catalysts was measured for steam gasification and coke oxidation as well.

4.2.4.1 Temperature Programmed Oxidation and/or Gasification

In this work, experiments involving steam are denoted as gasification while the ones with air are called as oxidation experiments. Temperature programmed oxidation (TPO) and gasification (TPG) experiments were performed on the NETZSCH TGA. This TGA was customized for handling pure steam at temperatures up to 1200 °C. A steam generator was connected to the TGA furnace with a heated transfer line (180 °C) which also had a bypass line. The steam generator consisted of a water tank which was filled with deionized water (resistivity 18.2 MΩ.cm) with the help of a syringe. The water tank was refilled before it went empty. The steam generator was maintained at 180 °C to avoid condensation. The generator was heated for one hour before starting an experiment. The water tank was purged with helium for 20 min to remove dissolved oxygen. The steam generator consisted of a 15 μm filter which trapped the impurities in the water to avoid contamination of the weighing balance. When the desired temperature of the furnace was reached, the steam flow was initiated on the TGA software. To avoid lag caused because of the time taken for the water to evaporate, form steam and for the steam to flow through the transfer line into the furnace, the steam was bypassed into a beaker filled with deionized water for 30 min. The steam flow also took some time to stabilize and provide constant flow. Once a stable flow of steam was reached, the steam flow was directed into the furnace. To avoid condensation in the furnace, the temperature of the furnace during the

gasification measurements was always maintained above 125 °C. An extended heated line (150 °C) was attached to the outlet of the furnace to avoid condensation of steam.

An industrial coke sample obtained from the Dow Chemical Company was used as the source of carbon. A small amount of industrial coke and catalyst in the ratio 1:9 were ground in a mortar and pestle for 45 min to achieve tight contact conditions. The TGA was used to determine the reactivity of the coke deposited on various catalyst materials. For these measurements, 15 mg of the coke – catalyst mixture was placed in an alumina crucible. The temperature was raised from room temperature to 950 °C at a rate of 10 °C/min in the presence of air (100 mL/min) and at a rate of 5 °C/min in the presence of pure steam (4.4 g/h). The rate of mass loss was used to compare the activity of catalysts. The catalysts were also tested for their activity in the presence of both air and steam. As mentioned earlier, industrial operation would involve use of mainly steam mixed with air. Hence, temperature programmed studies at a heating rate of 10 °C/min were also performed in a mixture of 90% steam and 10% air. This process will also be referred to as gasification since the mixture mainly contains steam.

4.2.4.2 Isothermal Oxidation and Gasification

Isothermal oxidation and gasification experiments were carried out on the NETZSCH TGA by heating the coke – catalyst sample to the desired temperature under helium flow. Once the desired temperature was reached, air (oxidation) or pure steam (gasification) was introduced into the furnace. The steam flow rate was kept at 4.4 g/h for these measurements. Rate constants were obtained by fitting the mass loss data to a first order rate equation. The data from 0 – 50% conversion were used to calculate the rate

constants. Isothermal studies were also performed in the absence of any oxidizing agent under helium/nitrogen flow to establish a baseline or to study the effect of surface oxygen species present on the doped ceria catalysts.

4.2.4.3 Temperature Programmed Hydrogasification of Coke

In the steam cracking operation, ethane cracks at high temperature to form ethylene. In this process, large amount of hydrogen is formed in the reactor. The amount of hydrogen at the exit of the furnace is ~ 30 vol%. Hydrogen can act as a reducing agent for the catalysts and can lower the catalytic activity of the ceria catalysts. Hence, it is extremely important to understand the behavior of the catalysts in the presence of hydrogen as the gasifying agent alone. To this effect, temperature programmed hydrogasification (TPHg) experiments were performed on the NETZSCH TGA. The TGA was used to determine the reactivity of the coke deposited on various catalyst materials. For these measurements, 15 mg of the coke – catalyst mixture was placed in an alumina crucible. The temperature was raised from room temperature to 950 °C at a rate of 5 °C/min in the presence of 1.5% H_2 in N_2 (100 mL/min). Due to safety reasons, the amount of hydrogen that could be used in the experiments was limited to below the lower flammability limit of hydrogen in nitrogen. The rate of mass loss with respect to temperature was used to compare the activity of catalysts.

4.3 Results and Discussion

4.3.1 Catalyst Characterization

For undoped ceria catalysts prepared by wetness impregnation the detailed characterization has been specified in the previous chapter (Section 3.3.1). This chapter will hence summarize the characterization of doped and undoped ceria – alumina catalysts prepared by the one-pot method.

Figure 3.1 compares the XRD patterns for α-alumina supported doped ceria catalysts. No significant change was observed in the crystallinity of the ceria domains in the doped samples. Diffraction peaks corresponding to fluorite structure of CeO_2 (28.6°, 33.3°, 47.5°, 56.4°)[177] were well defined in the diffractograms of the composites. No peaks for oxides of the dopants were observed in the XRD patterns indicating either very small crystallites that have escaped the detection or high dispersity of these domains on the alumina surface. Peak broadening was used to determine crystallite size based on the (111) plane of ceria. These sizes were in the range of 25 – 45 nm, as summarized in Table 4-1. Gd and Sr doped samples particularly seemed to have lower crystallite sizes as compared to the undoped catalyst while Cu, Co and Mn materials had domain sizes larger than the undoped ceria.

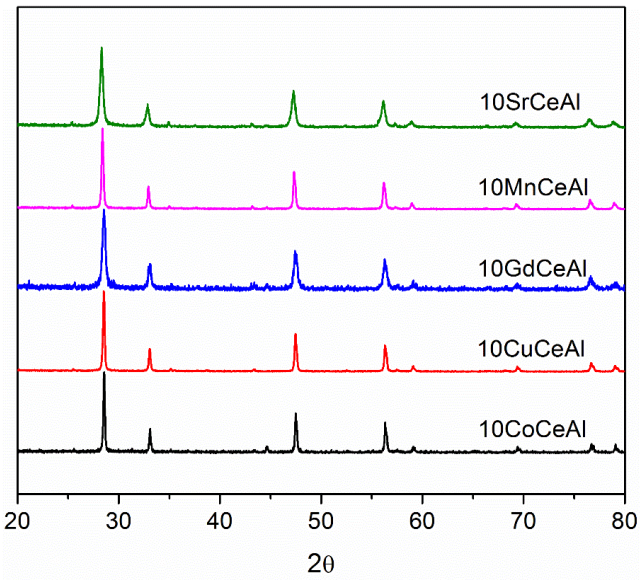

Figure 4.1 XRD patterns for doped ceria catalysts

Table 4-1 Crystallite sizes of the ceria (111) plane at θ ~ 28° for doped ceria catalysts

Catalyst	XRD crystallite size (111) peak (nm)
CeAl	32.9
10SrCeAl	25.9
10MnCeAl	37.2
10GdCeAl	23.7
10CuCeAl	42.8
10CoCeAl	42.8

The surface areas of the various materials are summarized in Table 3-2. Since, the surface areas were very low, around 1.5 – 2 g of the catalysts were used for physisorption analysis. Catalysts doped with other elements had surface area higher than the undoped catalyst. Similar to the undoped catalysts mentioned in chapter 3, from the physisorption experiments, it was observed that the catalytic materials were highly non-porous in nature. This is attributed to the non – porous nature of the commercial α-alumina support that was used, as well as the high calcination temperature. Both aspects make these catalysts thermally stable so they can be used in high temperature applications.

Table 4-2 Textural properties of doped and undoped supported ceria catalysts

Catalyst	Surface area (m^2/g)
CeAl	2.4
10SrCeAl	4.4
10MnCeAl	7.6
10GdCeAl	5.7

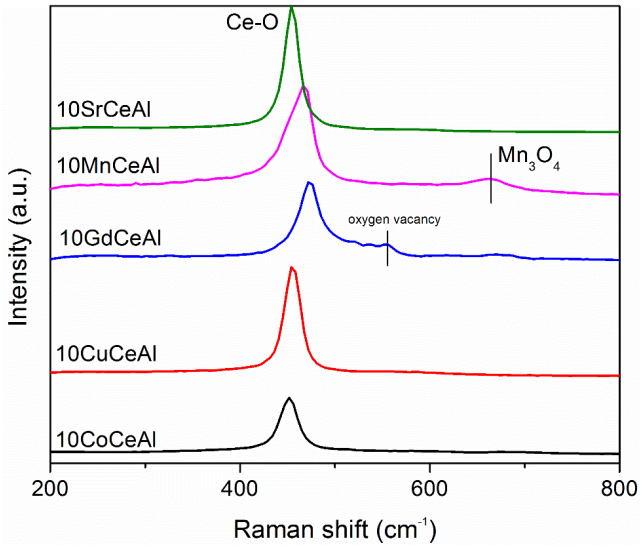

Figure 4.2 Raman spectra for doped ceria catalysts showing the dominant Ce-O interaction peak

Raman spectra for the doped catalysts are demonstrated in Figure 4.2. A peak at ~ 470 cm^{-1}, characteristic of CeO_2 (F_g mode), was observed for all samples.[179] This indicated the presence of characteristic CeO_2 domains in the catalysts. The absence of spectral features at 250, 268, 288, 383 cm^{-1} denoted the absence of any significant interactions between Ce and Al species. These features have been observed on ceria dispersed on γ-alumina investigated by Shyu et al[179] as mentioned earlier in chapter 3 and have been associated with a $CeAlO_3$ species. There was an extra peak observed for the Mn catalyst

denoting the presence of Mn_3O_4 species. The Gd sample showed an extra peak at ~550 cm^{-1}, which was attributed to the oxygen vacancies present in the sample.

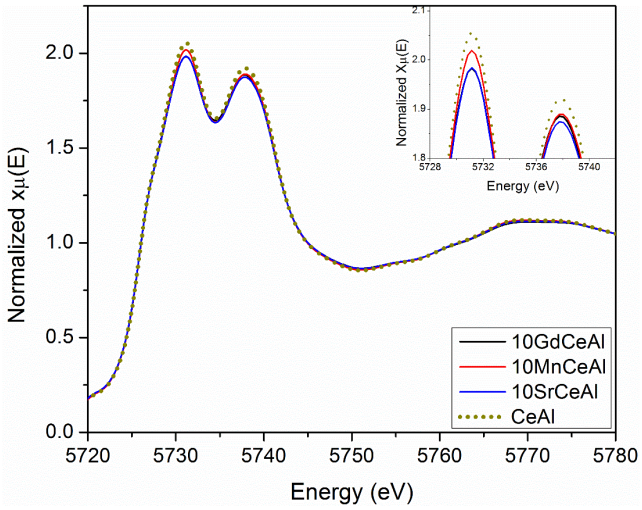

Figure 4.3 XANES spectra for doped and undoped ceria catalysts

Figure 4.3 XANES spectra for doped and undoped ceria catalysts showed that XANES spectra for doped and undoped α-alumina supported ceria were similar. Two major peaks at 5731 eV (A) and 5738 eV (B) were present in all the catalysts' spectra. These peaks have been associated to the +4 oxidation state of Ce.[178] A minor peak (C) at 5727 eV indicated the presence of Ce species in the +3 oxidation state. The presence of the +3 and +4 oxidation states of Ce was consistent with the well-known redox nature of the catalysts, and also demonstrated that the chemical nature of the unsupported ceria and ceria supported on alumina is the same. Hence, there were no significant interactions between the ceria and alumina species in both the doped and undoped materials that would change the electronic structure of the ceria. Thus, results from XANES and Raman spectroscopy demonstrate the presence of independent CeO_2 domains on the surface of α-alumina, without any intermixing with the alumina species, for all the α-alumina supported ceria samples.

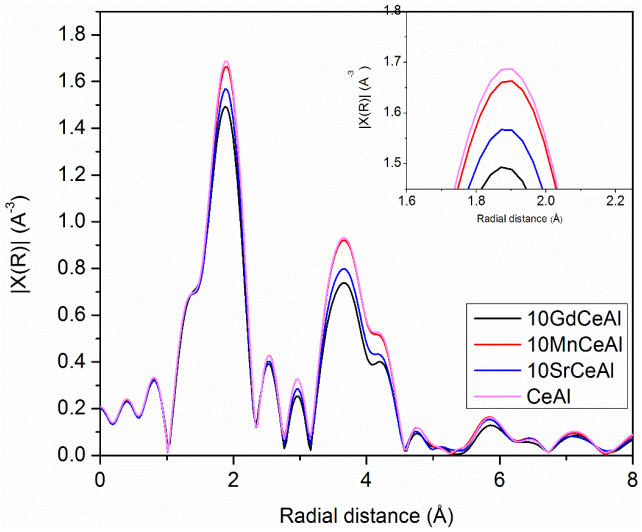

Figure 4.4 EXAFS spectra for the doped and undoped ceria catalysts

Figure 4.4 shows the EXAFS spectra for the doped and undoped ceria catalysts. After the 1st shell fitting with the spectrum, the Ce-O bond distance was calculated as shown in Table 4-3. The lower bond distance for the prepared catalysts as compared with the standard ceria implied the incorporation of either Al, Gd, Sr, Mn into the ceria matrix. The presence of α-alumina along with dopants made it difficult to interpret the results accurately and distinguish between the two elements. One notable result in this analysis was the high Debye-Waller factor for the Gd catalyst, which demonstrated the higher dispersion of Gd. The dispersion factor is also higher for the Sr catalyst. The bond distance for Ce-O was less for the Gd and Mn doped catalysts and could be attributed to the formation of oxygen vacancies. The atoms around a vacancy tend to repel away from the vacancy, distorting the lattice and pulling the neighboring oxygen atoms closer to the Ce atoms. Detailed EXAFS fittings are provided in Figure B1, Figure B2, Figure B3 and Figure B4 in Appendix B.

Table 4-3 EXAFS results for analysis of Ce-III edge[(a)]

Catalyst	Bond distance Ce-O (Å)[b]	Δσ (10^{-3} Å^2)[c]	ΔE_0 (eV)[d]	R factor
Standard CeO_2	2.328 ± 0.018	6.0 ± 3.0	6.9 ± 1.4	0.012
CeAl	2.328 ± 0.017	6.3 ± 2.8	6.5 ± 1.6	0.016
10SrCeAl	2.328 ± 0.018	6.9 ± 3.2	6.9 ± 1.5	0.014
10MnCeAl	2.324 ± 0.020	6.3 ± 2.9	6.8 ± 1.5	0.015
10GdCeAl	2.318 ± 0.022	8.0 ± 3.5	6.9 ± 1.4	0.013

[a] Fitting parameters: Fourier transform range, Δk, 2.2-10.0 Å^{-1} with weighting k^2. The R-range was 1.2- 2.4 A and the coordination number for Ce-O was maintained at 8.
[b] radius
[c] Debye-Waller Factor
[d] edge energy

4.3.2 Catalytic Activity

4.3.2.1 Temperature Programmed Gasification and Oxidation

To investigate the activity of the doped ceria catalysts towards gasification of coke in the presence of steam, temperature programmed gasification studies were performed. As can be seen in Table 4-4, the range of T_{50} (temperature at which 50% of the coke was gasified under steam) was higher by ~ 200 °C as compared to the air oxidation values seen in chapter 3. This indicated that steam was a mild gasifying agent as compared to air and might provide oxygen for combustion at a slower rate comparatively. With the undoped ceria catalyst prepared by wetness impregnation (50-CeO_2-Al_2O_3) as well as one-pot method (CeAl), a reduction of ~ 20 °C was observed for the gasification of industrial coke. This activity was further improved by incorporating dopants into the ceria matrix. Co was the least active, followed by copper. Gadolinium, strontium and manganese showed similar activity with a reduction of ~ 65 °C as compared to the uncatalyzed gasification.

Table 4-4 T_{50} values for steam gasification of industrial coke

Catalyst	T_{50} (°C)
Uncatalyzed	887
50-CeO_2-Al_2O_3	865
CeAl	869
10SrCeAl	835
10MnCeAl	835
10GdCeAl	823
10CuCeAl	845
10CoCeAl	862

These catalysts were also used for carrying out oxidation of industrial coke samples in the presence of air. The TPO curves are shown in in Figure 4.5. As can be seen, the Gd and Mn samples particularly helped in shifting the curve to the left and also helped reduce the high temperature peak at ~ 700 °C. Since, Gd and Mn showed high activities for both gasification and oxidation, they were chosen for further analysis. Sr which demonstrated good activity for gasification was also chosen as a potential candidate for the dopant since the industrial decoking step will primarily constitute steam as the gasifying agent.

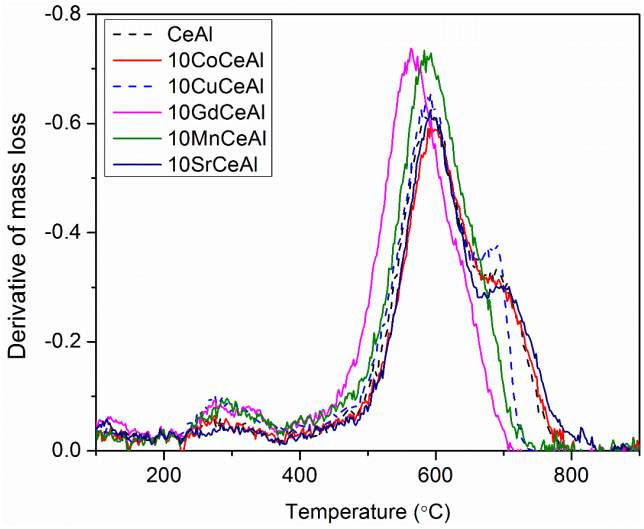

Figure 4.5 TPO curves for oxidation of coke using doped ceria catalysts

Table 4-5 Catalytic activity for gasification of industrial coke in steam-air mixtures

Catalyst	T_{50} (°C),
Uncatalyzed	716
10SrCeAl	630
10MnCeAl	627
10GdCeAl	592
CeAl	645

When a mixture of steam and air was used for gasification of coke through temperature programmed runs, once again Gd came out the best of all dopants and showed a reduction of the gasification temperature by ~ 125 °C (Table 4-5). This reduction quantity is double that seen in steam gasification and of the same order of magnitude as the air oxidation. This observation indicates that gasification in the presence of steam-air mixtures is mainly governed by air. Sr and Mn doped ceria also showed similar activity as undoped ceria. As illustrated before, Mn is more active than Sr during oxidation while Sr is more active than Mn during gasification. The similar activity shown by Sr, Mn in steam-air mixture could be due to the dominance of the faster oxidizing agent air as compared to steam.

4.3.2.2 Isothermal Oxidation and Gasification of Coke

To measure the kinetics of the catalytic gasification of coke, isothermal experiments were performed on the tight contact coke – catalyst mixtures. A relatively low temperature was chosen for isothermal studies such that the non-catalytic gasification of coke was kept relatively low. A first order rate law was used to fit the mass loss of the carbon in the catalyst-carbon mixtures. As shown in Table 4-6, at 750 °C and in the presence of a ceria-containing catalyst, the catalytic activity was improved and was almost twice when compared to experiments using the uncatalyzed coke. However, the differences

in the kinetic constants for the undoped catalysts with different ceria content were minimal. Ceria – alumina with Ce:Al ratio of 1:1, prepared by wetness impregnation, showed similar activity to the one prepared by the one-pot synthesis method. When ceria was doped with Gd or Sr, the activity towards gasification significantly improved, while Mn showed a slight improvement in activity. During air oxidation, Sr and Mn had lower reaction rates than the Gd catalyst as well as the undoped ceria catalysts. Gd doped ceria showed similar rate constants as the undoped ceria catalysts supported on alumina in the presence of air. Gd turned out to be the best catalyst for both steam gasification as well as air oxidation of coke.

Table 4-6 Rate constants for ceria catalysts for steam gasification (100% steam, 4.4 g h^{-1}) and air oxidation of coke

Catalyst	Rate constant, steam, 750 °C, (min^{-1})	Rate constant, air, 500 °C, (min^{-1})
Uncatalyzed	0.0016	0.0040
20-CeO_2-Al_2O_3	0.0028	0.0180
50-CeO_2-Al_2O_3	0.0026	0.0260
65-CeO_2-Al_2O_3	0.0029	0.0255
80-CeO_2-Al_2O_3	0.0028	0.0250
CeO_2	0.0031	0.0120
CeAl	0.0030	0.0140
10MnCeAl	0.0034	0.0152
10SrCeAl	0.0047	0.0099
10GdCeAl	0.0050	0.0248

4.3.2.3 Temperature Programmed Hydrogasification of Coke

In the hydrogasification experiments, only hydrogen was used as the gasifying agent to understand the behaviour of these catalysts under a reducing atmosphere. The Gd doped ceria catalyst was hydrogasified without coke and with coke. As seen in Figure 4.6, until 600 °C, no weight loss was observed for the sample containing no coke (black curve) indicating negligible reduction of the Gd catalyst. After 600 °C, increased

weight loss indicated catalyst reduction. When coke was mixed with the catalyst (red curve), ~ 1.5% of weight loss was seen below 600 °C implying the gasification of coke in the presence of hydrogen. After 800 °C, the weight loss was more when coke was present as compared to the case where coke was absent. This suggested coke gasification took place in the presence of hydrogen too. Carbon can combine with hydrogen at high temperatures to form volatile CH_x fragments.[58]

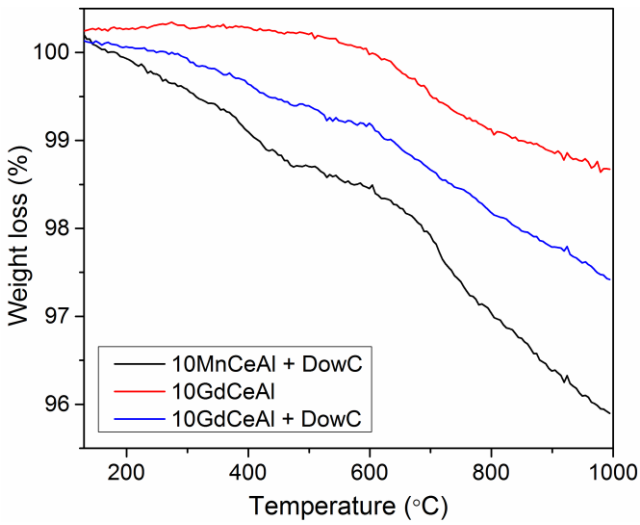

Figure 4.6 Hydrogasification of industrial coke in the presence of 10GdCeAl and 10MnCeAl

In the presence of coke, the catalyst reduction should not be neglected. For the Gd catalyst, temperature programmed reduction (TPR) studies with 10% H_2 in Ar showed a 4.7% of weight loss. The order of magnitude of this quantity is comparable to the weight loss seen in the hydrogasification experiments. The absolute quantities cannot be compared due to the lower hydrogen pressure (3%) used in the hydrogasification experiments.

For Mn catalyst, the weight loss in the presence of coke during hydrogasification was higher when compared to the Gd catalyst. This difference could be related to the higher reduction of the Mn catalyst (8.6 wt%) than the Gd catalyst (4.7 wt%) in the TPR studies.

4.3.2.4 Coking Resistance

The catalyst with the Mn dopant formed the lowest carbon amount during *in-situ* coke deposition experiments. Gd showed the next lowest coke loading (Table 4-7). When this coke formed was combusted, Gd, Mn and the undoped ceria catalyst showed low oxidation temperatures, unlike Sr, which inhibited the reaction similar to the oxidation of industrial coke, as shown in 4.2.4.1. On performing the isothermal oxidation experiments at 350 °C, Gd gave the highest reaction rate followed by the undoped ceria catalyst and the Mn doped catalyst. These rates are almost three times that of the undoped ceria catalysts prepared by wetness impregnation, shown in Section 3.3.4. As expected, Sr had a low oxidation rate, again similar to the industrial coke oxidation behaviour (4.2.4.2). In practical applications, Mn would be a better choice of catalyst due to its comparative coke gasification activity in steam, its high coke resistance, low cost and comparative coke oxidation rates in air as compared to the Gd doped catalyst.

In the presence of coke, the catalyst reduction should not be neglected. For the Gd catalyst, temperature programmed reduction (TPR) studies with 10% H_2 in Ar showed a 4.7% of weight loss. The order of magnitude of this quantity is comparable to the weight loss seen in the hydrogasification experiments. The absolute quantities cannot be compared due to the lower hydrogen pressure (3%) used in the hydrogasification experiments.

For Mn catalyst, the weight loss in the presence of coke during hydrogasification was higher when compared to the Gd catalyst. This difference could be related to the higher reduction of the Mn catalyst (8.6 wt%) than the Gd catalyst (4.7 wt%) in the TPR studies.

Table 4-7 In-situ coke deposition and oxidation on doped ceria catalysts

Catalyst	Coke deposited (mg)	T_{50} (°C), air	Rate constant, min^{-1}, air, 350 °C
CeAl	2.86	385	0.070
10GdCeAl	2.04	382	0.076
10SrCeAl	2.26	450	0.015
10MnCeAl	1.41	391	0.061

4.3.2.5 Analysis of Spent Catalysts from the TPG Reaction

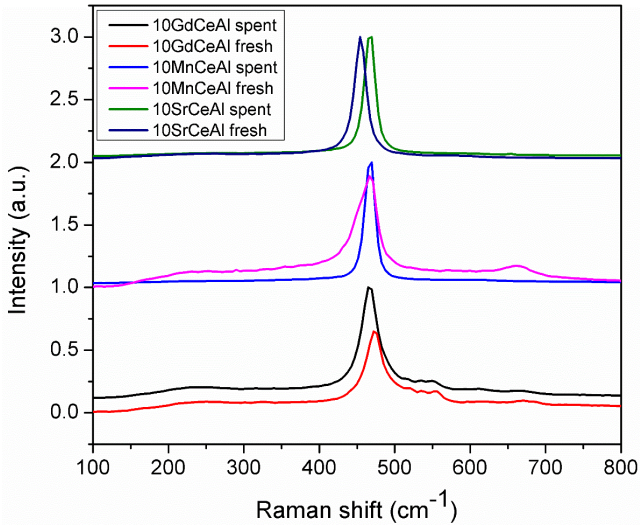

Figure 4.7 Raman spectra for spent catalysts after steam gasification of coke

Raman spectra of spent catalysts after the TPG reaction (Figure 4.7), demonstrated the stability of the Gd catalyst after exposure to pure steam at elevated temperatures. The oxygen vacancy peak for the Gd catalyst also remained after reaction although the intensity was lower than the fresh catalyst. For the Sr catalyst, the Ce-O interaction peak shifted left indicating loss of Sr from the ceria matrix. For the Mn catalyst, no shift in the ceria peak

was observed. However, the peak associated to the Mn_3O_4 species disappeared after reaction implying the chemical reduction of Mn oxides during the gasification process.

Spent catalysts were also analysed by XRD and their crystallite sizes were calculated by the Scherrer equation (Table 4-8). They showed negligible difference in the crystallite size of ceria when compared to the fresh catalysts (Table 4-8).

Table 4-8 XRD crystallite sizes of spent catalysts after TPG reaction

Catalyst	XRD crystallite size (111) peak (nm)
10GdCeAl	25.9
10MnCeAl	38.9
10SrCeAl	25.9

4.3.2.6 Oxygen Storage Capacity Measurements

As mentioned in Section 1.4.2.2, the oxygen storage capacity of ceria materials has been related in the literature to the carbon oxidation activity in the absence of external oxygen. To compare the catalytic activity to the OSC, the OSC measurements were carried out at the same temperature as the isothermal gasification experiments, i.e. 750 °C, and the values are mentioned in Table 4-9.

There was no correlation between the OSC and the catalytic activity of these catalysts, implying steam did not act like an inert gas, and was mildly oxidizing. This also suggests steam can provide external oxygen to the carbon system for gasification. However, this external oxygen transfer was less as compared to transfer from air, as evident from the lower rates of gasification.

Table 4-9 OSC values for ceria catalysts, 750 °C

Catalyst	Oxygen Storage Capacity (μmol g^{-1})
CeAl	237
10GdCeAl	225
10MnCeAl	148
10SrCeAl	102

4.4 Proposed Mechanism of Steam Gasification of Coke

The mechanism of steam gasification for different dopant types could be different. For a rare earth element, the presence of oxygen vacancies[87] has been related to their ability to provide oxygen for carbon oxidation. In this work too, Gd doped ceria showed the presence of oxygen vacancies, which could be the major reason for the high activity of these catalysts towards coke gasification in steam. The oxygen vacancies created on the surface and the bulk increased the oxygen mobility in the catalyst making it easier to provide oxygen for oxidation of coke. There existed two sources of oxygen in this case, the lattice oxygen from the Gd doped ceria and the dissociation of steam.

For alkaline earth metals, an oxygen transfer mechanism has been related to their gasification activity.[189] In the work presented here, the presence of Sr in the ceria lattice created defects, and the high dispersion of the Sr species and the small crystallite size of ceria increased the rate of oxygen transfer for the oxidation of coke. The mechanism could be generalized as follows for an alkaline element X,

$$H_2O + X_xO_y \leftrightarrows H_2 + X_xO_{y+1} \quad (1)$$

$$XO_{y+1} + C \rightarrow X_xO_y + (CO) \quad (2)$$

$$(CO) \leftrightarrows CO \quad (3)$$

The presence of active Mn_3O_4 species in the Mn doped catalyst as well as the presence of oxygen vacancies, likely would have been responsible for the supply of oxygen to the coke deposits for this catalyst.

Further studies are needed to probe the detailed mechanism of action for these catalysts.

4.5 Conclusions

Doped ceria catalysts (10 mol%) with Co, Cu, Gd, Mn, Sr were successfully prepared using a one-pot synthesis method. All the dopants showed improved activity towards steam gasification of coke. Gd, in particular, was able to reduce the peak steam gasification temperature of coke by ~ 65 °C as compared to the uncatalyzed gasification. In addition to high activity in steam, Gd and Mn dopants also demonstrated improved activity for coke oxidation in air. Sr, on the other hand, lost its activity during coke oxidation. In the presence of steam – air mixtures, oxidation due to air dominated the process and Gd showed the best activity by reducing the gasification temperature by 125 °C. When hydrogen was used as the gasifying agent, reduction of the doped catalysts took place, along with gasification of the industrial coke. The high activity of Gd could be related to the oxygen vacancies (Raman spectrum), the smaller ceria crystallite size (XRD pattern) and the higher ceria dispersion (EXAFS). No correlation was found between the oxygen storage capacity and the gasification activity. This could be due to the ability of the steam to dissociate and provide oxygen to replenish the catalysts. For Mn doped ceria, the high activity in gasification and oxidation can be attributed to the presence of active species Mn_3O_4 and the presence of oxygen vacancies. The possible incorporation of Sr into the ceria lattice

and the smaller ceria crystallite size could be the reason for the high activity of the Sr doped catalyst for coke gasification in steam.

CHAPTER 5. CATALYTIC CERIA COATINGS FOR OXIDATION OF COKE

The work mentioned in this chapter is carried out in collaboration with the Postdoctoral Research Fellow, Dr. Hyuk Taek Kwon, and the data are presented here with his permission. Reviewing literature, detailed planning of experiments, contributing intellectually was done by both researchers. Both were responsible for the operation and maintenance of the thermo-gravimetric analyzer for coking and decoking experiments while characterization and synthesis of the coatings was done by Dr. Kwon.

5.1 Background

As mentioned in chapter 1 Section 1.3, tremendous efforts have been directed to reduce the coke formed in steam crackers. Some of these efforts are in the area of coatings that act as a barrier between the hydrocarbon gases and the metallic walls of the reactor, thereby minimizing the formation of catalytic coke. In an attempt to take the project a step further, the catalytic powders (mentioned in previous chapters) that showed good activity towards coke oxidation were transformed into coatings on a metallic substrate and evaluated for their oxidation activity. This chapter describes how the coatings were synthesized and their performance towards coking resistance and oxidation.

5.2 Materials and Synthesis

Catalytic coatings were prepared on metallic substrates with Ni, Fe, Cr as a constituent as the steam cracking reactors are made up of these elements, among others. The aim was to try and find a substrate that could match with the alloy used in industrial

cracking furnaces. This section describes in detail the substrate chosen and the synthesis of the coatings.

5.2.1 Choice of Metallic Substrate for Coatings

The steam cracking operation is carried out at very high temperatures. Choice of the metallic substrate is largely dependent upon the thermal stability of the material at these high temperatures. The material that was chosen as a substrate in this case was Incoloy800, which is thermally stable up to a temperature of 850 °C. It is an alloy of Ni – 30-35%, Cr 19-23% and Fe 39.5%. The Incoloy 800 sheets were 12 in x 12 in in size. These sheets were then cut into multiple coupons (1 cm x 1 cm). The weight of each coupon was ~ 800 mg.

5.2.2 Synthesis of Coatings

Coatings were synthesized in two steps. First, α-alumina was coated on the fresh Incoloy 800 followed by coating of ceria on top of the α-alumina layer. The α-alumina slurry consisted of a solvent (Toluene (84 mL, Sigma Aldrich) + IPA (42 mL, Sigma Aldrich)), a plasticizer - dibutyl phthalate (0.7 mL, Sigma Aldrich), a dispersant - fish oil (0.4 mL, Sigma Aldrich), a homogenizer Triton-X (0.5 mL, Sigma Aldrich), a binder - poly (vinyl butyral-co-vinyl-alcohol co-vinyl acetate) 0.7 g, Sigma Aldrich, α-Al_2O_3 nano powder (~ 100 nm, 13.3 g, Inframat Advanced Materials). The slurry was prepared by mixing all the ingredients in a ball mill with the help of zirconia balls of 1 mm size bought from Inframat Advanced Materials. The Incoloy coupon was dipped in the α-alumina slurry for 30 s and dried for 1 min. This was done two times before each sintering step. The dried coupon was sintered in three steps:

1. calcination at 800 °C for 2 h
2. calcination at 800 °C for 2 h
3. calcination at 850 °C for 48 h

Once the α-alumina coating was ready, ceria was dip-coated on top in two ways.

1. Precursor method: This method involved forming a solution of cerium nitrate hexahydrate (3 g) in methanol (15 mL)
2. Sol-gel method: It involved preparing a 0.5 M aqueous ceria sol by use of ceria particles (~10 nm) involved preparing a 0.5 M aqueous ceria sol by use of ceria particles (~10 nm)

For control experiments, ceria was deposited directly on a fresh Incoloy substrate and calcined at 550 °C to assess the importance of the α-alumina layer. This coating is denoted as CeO_2-Incoloy. Another control experiment involved synthesizing a α-alumina coating without the ceria layer on Incoloy (α-Al_2O_3-Incoloy). The coatings that are prepared by the precursor method are named as Pre_CeO_2_α-Al_2O_3-Incoloy whereas the ones prepared by the sol gel method were called as SG_ CeO_2_α-Al_2O_3-Incoloy. An oxidized Incoloy sample was prepared as a sample that had undergone the same thermal treatment before coke oxidation evaluation as the CeO_2_α-Al_2O_3-Incoloy coatings. An unsupported ceria film was synthesized by the sol-gel method to investigate the effect of the substrate on the ceria coated layer.

5.2.3 Material Characterization

Catalyst samples were characterized by X-ray diffraction, scanning electron microscopy, energy dispersive spectroscopy. The powders were characterized by X-ray diffraction (XRD) using Cu K α radiation. The instrument was operated at 40 mA and coated substrate samples were attached to the sample holder with the help of a tape. For SEM measurements, the Incoloy substrate was placed on the mounts with the help of carbon tape. Gold sputtering of 60 s was done on the sample before observing it under the microscope. SEM and EDS measurements were carried out on LEO 1530 thermally-assisted field emission scanning electron microscope, with an acceleration voltage of 10 kV, in the Center for Nanostructure Characterization, Georgia Institute of Technology.

5.2.4 Coking and Decoking Experiments

For *in-situ* coke deposition, the uncoated or coated Incoloy 800 substrate was placed in the measurement holder of the custom made NETZSCH TGA furnace. The TGA furnace was then heated to 800 °C in helium flow. Coking experiments were limited to 800 °C due to the thermal stability limit of the substrate. Once the desired temperature was reached, 2 mol% ethylene in helium was introduced into the system for 6 h. The reaction time was chosen to be 6 h to have a measurable amount of coke being deposited on the substrate. After 6 h, the ethylene flow was stopped and the furnace was allowed to cool while under helium flow. The coking rate and the amount of coke deposited were measured by the TGA. Coke deposited on the measurement head was removed completely prior to oxidation of the coked substrate, by temperature programmed oxidation in air up to 800

°C. Coke deposited on the substrate was oxidized after every cycle before the next coking cycle began.

5.3 Results and Discussion

5.3.1 Material Characterization

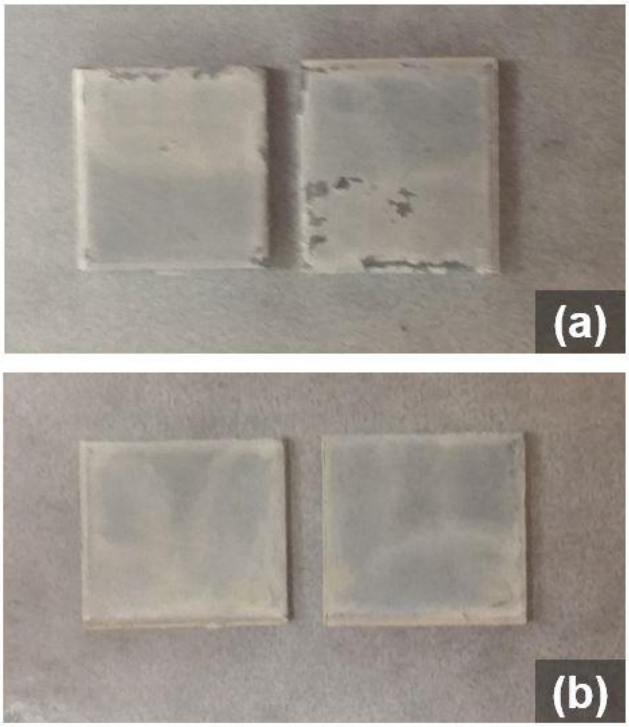

Figure 5.1 Visual inspection of CeO_2 coatings prepared by precursor and sol-gel methods

A visual inspection of the samples coated by two different methods was done to look for defects in the film. Figure 5.1a shows an image of pieces of the ceria coated on top of the α-alumina layer by the cerium nitrate method. Significant flaking was observed on the samples made by the nitrate method where the coating was detached from the substrate, causing exposure of the substrate to the reactive gases. Figure 5.1b shows two

sample pieces of the ceria coated by the sol-gel method. Sol-gel method resulted in negligible flaking of the coating.

Figure 5.2 shows the SEM image of ceria coated on top of α-alumina using the nitrate precursor method. As illustrated, the coating was not smooth and the appearance was similar to the α-alumina coatings alone. The particles were quite large and passage of hydrocarbon molecules through them was quite plausible. In contrast, the particles of the coating made by sol-gel method were smaller in size. Figure 5.3 shows SEM image ceria coated using the sol-gel method on top of the α-alumina layer. The coating was also cracked and the crack was of the width of ~ 100 nm.

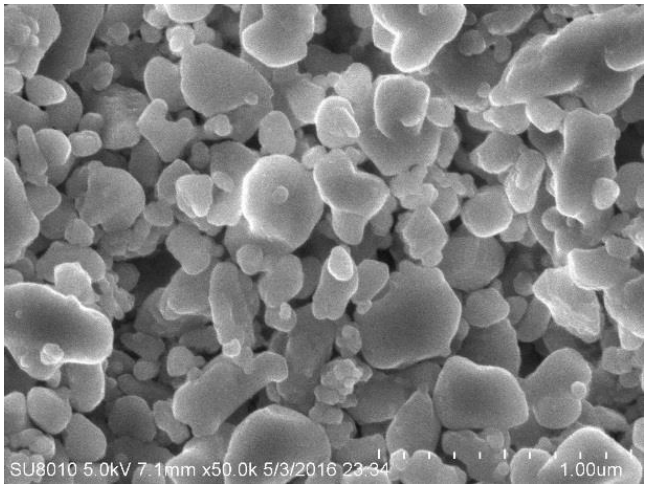

Figure 5.2 SEM analysis of Pre_CeO_2-α-Al_2O_3-Incoloy coating synthesized by the precursor method

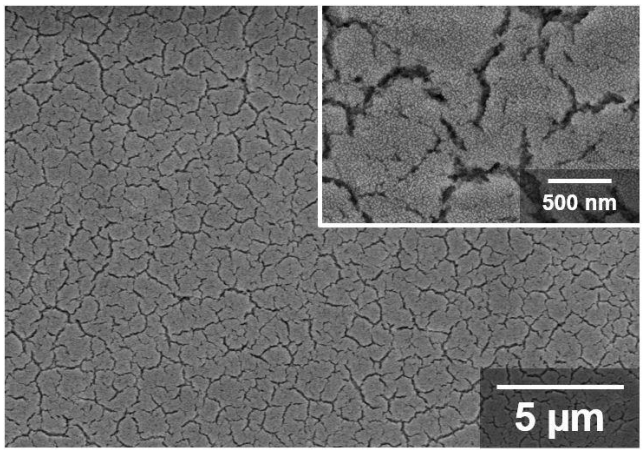

Figure 5.3 SEM analysis of SG_CeO_2-α-Al_2O_3-Incoloy coating synthesized by the sol-gel method

XRD pattern for the various substrates and coatings before the coking experiments is displayed in Figure 5.4. Bare Incoloy without pre-treatment showed two sharp peaks at 44° and 52°. When the Incoloy substrate undergoes oxidation to the same extent as the α-alumina coated layer, the XRD pattern was maintained and no changes were observed. An α-alumina coated Incoloy substrate showed peaks of α-alumina at 26°, 35° and 57° as well as the substrate peaks. When ceria was coated on top of the α-alumina layer with cerium nitrate as the precursor, a sharp peak at 28° was observed which is the 111 peak of CeO_2. The XRD pattern of the coating prepared by the sol-gel method gives a much broader peak at 28° indicating smaller CeO_2 particles as compared to the nitrate method.

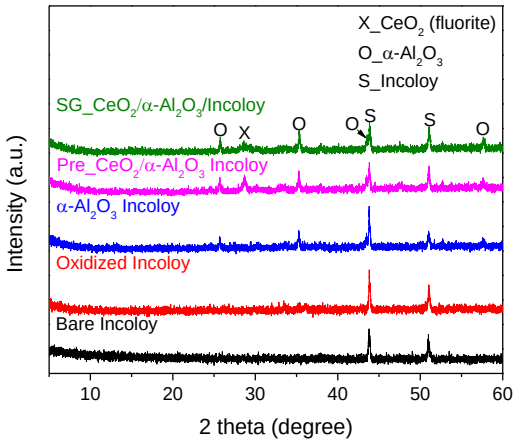

Figure 5.4 XRD pattern of substrate with or without coatings

Elemental mapping was done on the α-Al_2O_3 coating to understand the distribution of different metals in the coating and the substrate and is displayed in Figure 5.5. A significant concentration of Al was found in the coating which was expected. The coating itself was ~ 6 – 7 μm thick. The mapping of Cr showed large concentration in the coating too indicating diffusion of Cr from the substrate to the α-alumina coating during the calcination process. Most of the Fe was restricted to the substrate and no diffusion was observed. A small concentration of Ni was also seen in the coating, implying some diffusion for Ni atoms too.

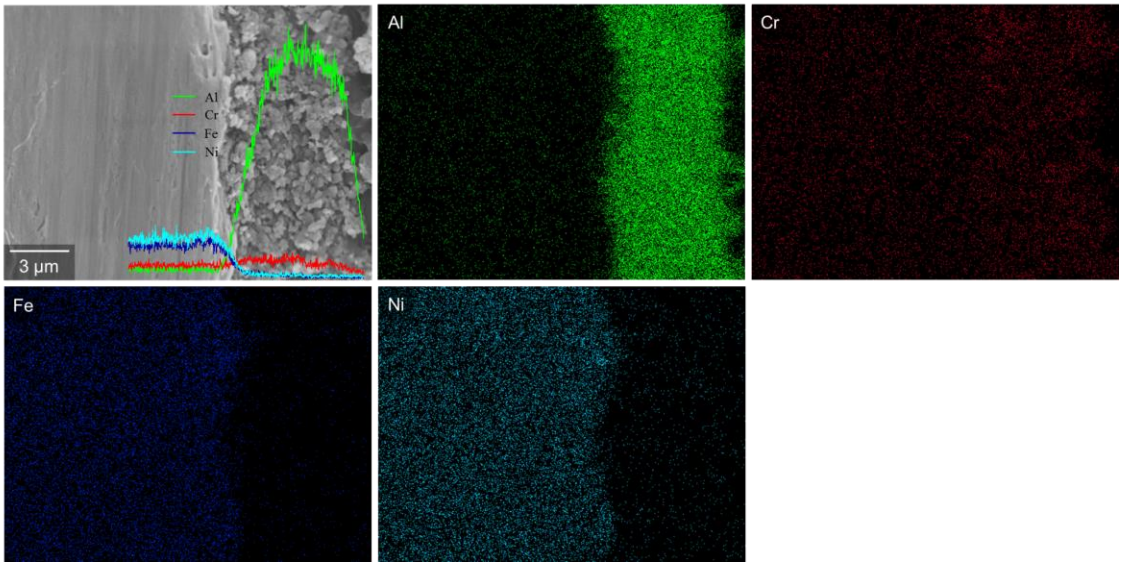

Figure 5.5 Elemental mapping of α-Al_2O_3-Incoloy coating using SEM-EDS

5.3.2 Coke Formation on Coatings

The aim of the coatings is to not only help in the oxidative removal of coke but also in minimizing coke formation. Hence, coking studies were performed on various coated and uncoated substrates to investigate the ability of the coatings to reduce coke formation.

5.3.2.1 Coking Studies on Bare Incoloy Substrate

Figure 5.6 shows scanning electron microscopy (SEM) images of the fresh Incoloy substrate. As can be seen that the surface of Incoloy was rough and there were numerous loose particles.

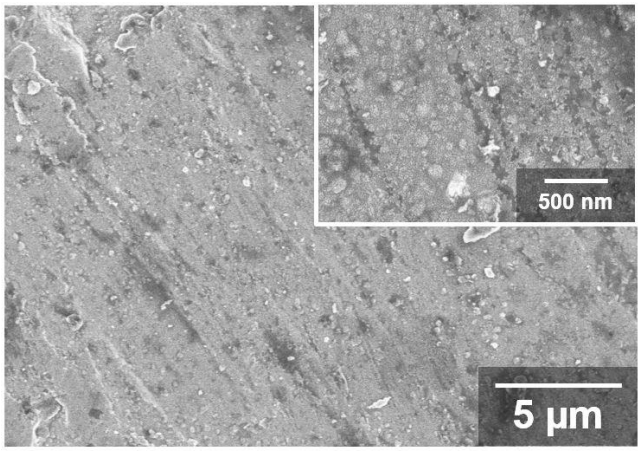

Figure 5.6 SEM analysis of fresh Incoloy800 substrate

The catalytic coke formed on the Incoloy after 25 min of the fourth coking cycle was observed under SEM. Two different regions were analysed on the substrate. Figure 5.7a shows smaller filaments formed and some particles. Figure 5.7b shows larger formation of carbon filaments. This filamentous coke formation is consistent with the previous knowledge of the morphology of catalytic coke as described in Section 1.2.1.

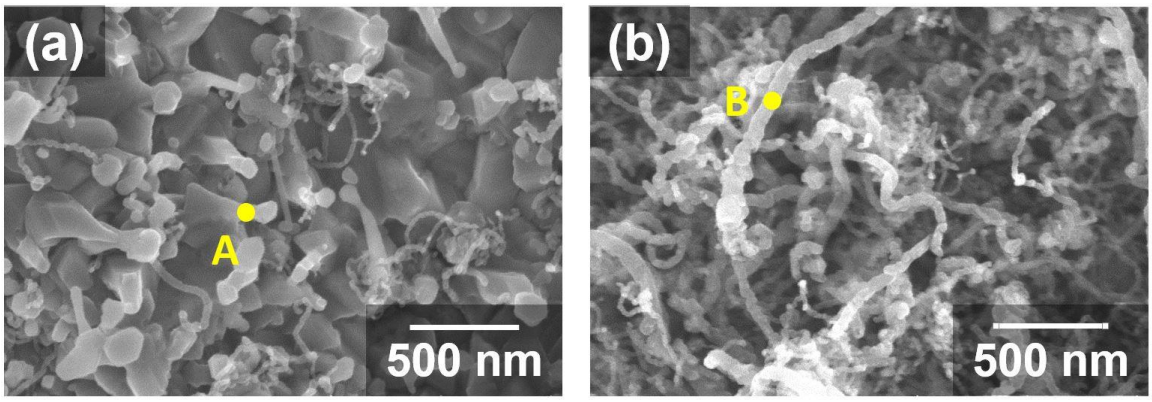

Figure 5.7 SEM analysis of coke formed on bare Incoloy substrate after 25 min of coking

Two points shown the in the figures on the coke species formed on bare Incoloy substrate without coating, were analysed for their elemental content using energy-dispersive X-ray spectroscopy (EDS) to provide a better understanding of the species

present. Table 5-1 provides the metallic, oxygen and carbon content for these two points. Point A constituted significant O, Cr and Mn. This could be attributed to the formation of chromia scales on the surface due to the diffusion of chromium from the bulk of the substrate to the surface. The high amount of oxygen could be due to the presence of metal oxides like chromium oxide, manganese oxide, iron oxide, nickel oxide, or due to the surface carbon oxygen complexes. Point B, which is a point on the filamentous coke, showed a large amount of carbon, as expected.

Table 5-1 Elemental analysis of different coke species formed on bare Incoloy substrate after 25 min of coking

Element (%)	Point A	Point B
C	2.31±0.71	74.96±2.38
O	64.78±4.72	17.07±1.35
Cr	18.59±0.93	0.30±0.15
Mn	10.83±3.10	0.46±0.16
Fe	1.78±0.46	4.33±0.57
Ni	0.35±0.05	1.84±0.59
Ti	1.23±0.42	0.65±0.04

5.3.2.2 Coking Studies on Oxidized Incoloy

Coke deposited on oxidized Incoloy 800 for a period of 6 h over a period of four cycles is displayed in Figure 5.8. The value in the parentheses gives the coke deposited x 10^{-4} per mg of coupon. As seen in the data, in the initial stage of coking up to 50 min, the coking rate was quite high. This rate also increased with every cycle. This behaviour is representative of catalytic coking, which takes place due to the exposed metallic species in the Incoloy 800 substrate. After the catalytic coking phase the metallic species were blocked and most of the coke that was formed was radical in nature and deposited at a rate that was linear in time.

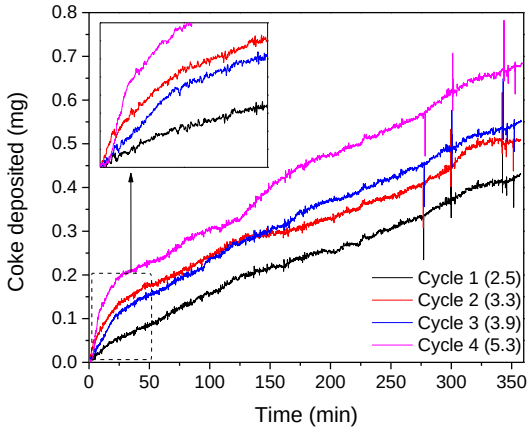

Figure 5.8 TG curves for coke deposition cycles on oxidized Incoloy substrate

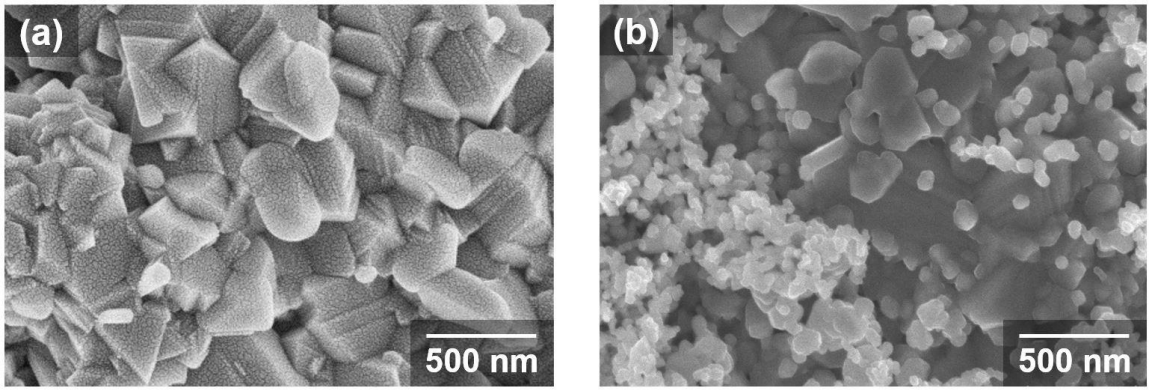

Figure 5.9 SEM analysis of oxidized Incoloy substrate a) before coking and b) after coking

Figure 5.9a shows SEM analysis of the fresh oxidized Incoloy substrate. A lot of large particles can be observed on the surface, which appear like metal oxide scales formed during the oxidation of the substrate. After four coking cycles (Figure 5.9b), smaller particles were seen on top of the scales. These particles were probably the coke particles deposited during the coking cycle.

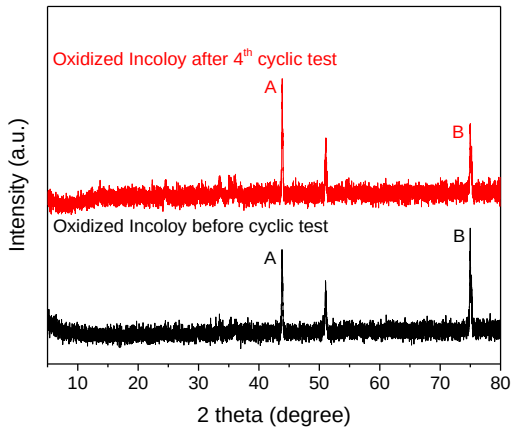

Figure 5.10 XRD pattern for oxidized Incoloy substrate before and after coking cycles

In the XRD patterns for the oxidized Incoloy before and after coking and decoking cycles Figure 5.10, all the three peaks correspond to the Incoloy substrate. After coking cycles, the ratio of the peaks A and B changed indicating a change in the orientation of the crystal planes due to the thermal treatment during the coking cycle.

5.3.2.3 Coking Studies on α-Al_2O_3-Incoloy

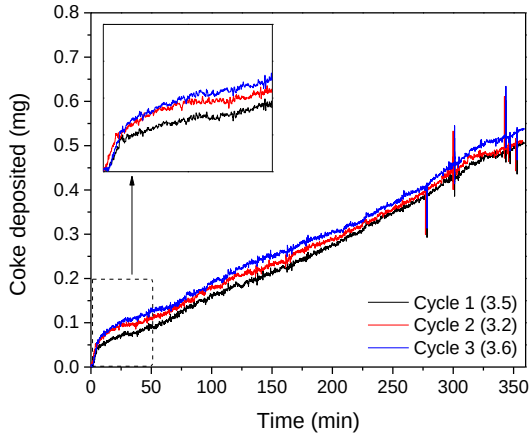

Figure 5.11 TG curves for coke deposition cycles on α-Al_2O_3-Incoloy substrate

Figure 5.11 shows the coking cycles for the α-Al_2O_3-Incoloy substrate. As can be seen, the catalytic coking in the initial part of the coking experiment was minimal, indicating the α-Al_2O_3 layer acted as a barrier between the hydrocarbon gas and the metallic species in the Incoloy. After three cycles, the catalytic coking slightly increased but it was still less than that observed on oxidized Incoloy.

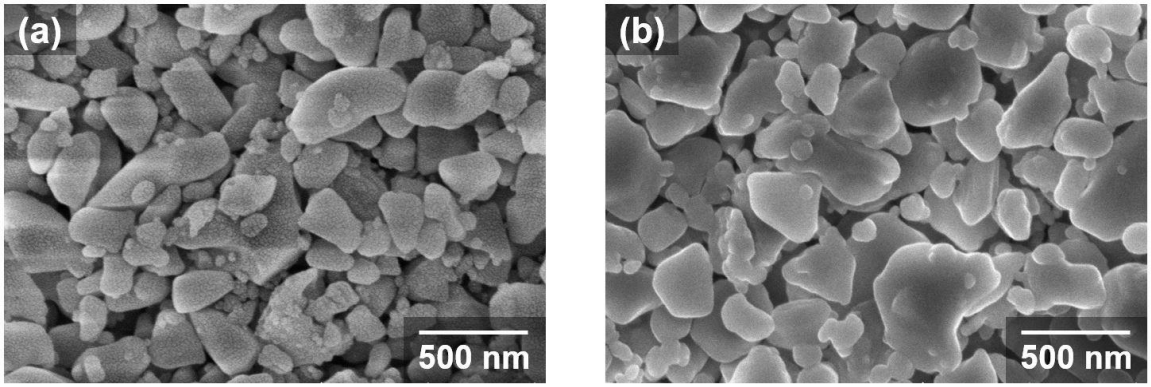

Figure 5.12 SEM analysis of α-Al_2O_3-Incoloy coating a) before and b) after coking cycles

As shown in Figure 5.12a, the coating looks quite uniform on the freshly coated α-alumina layer on top of the Incoloy 800. Evidently, the coating was not fully continuous and intergrown, and individual particles can be seen in the figure. Hence, the coating might not be a perfect barrier to stop the hydrocarbon gases from reaching the Incoloy surface and causing carburization. Figure 5.12b shows the SEM image of the α-Al_2O_3 layer after being exposed to coking cycles. The particles grew larger after the coking cycle due to the exposure to high temperature for a prolonged period of time.

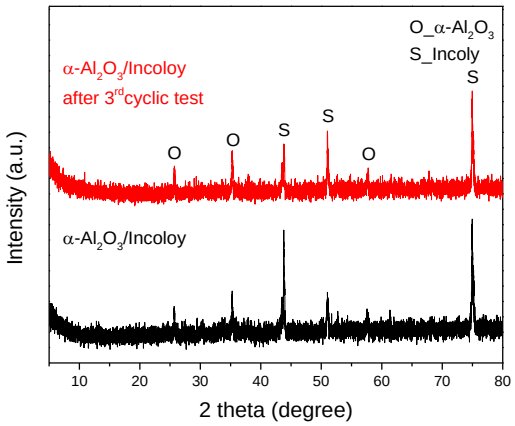

Figure 5.13 XRD pattern for α-Al_2O_3-Incoloy coating before and after coking cycles

Figure 5.13 displays the effect of coking cycles on the crystalline nature of the α-Al_2O_3-Incoloy coatings. Similar to the oxidized Incoloy tests, a change in the crystallinity of the substrate was seen after exposure to coking cycles. The peak ratio of the 44° and 75° peaks changed but the trend was opposite to that observed in oxidized Incoloy. This behaviour suggests some influence from the α-alumina coating on the crystallinity of the substrate.

5.3.2.4 Coking Studies on SG_CeO_2-Al_2O_3-Incoloy

Figure 5.14 shows the coke deposited on SG_CeO_2-α-Al_2O_3-Incoloy for a period of 6 h over a period of four cycles. The value in the parentheses gives the coke deposited per 10^{-4} mg of coupon. As seen, in the initial stage of coking up to 50 min, the coking rate was almost the same as the rate later on in the process. This behaviour implies the minimization of catalytic coking in the presence of the ceria coating. After four cycles, a smaller amount of coke was deposited on the coated substrate (3.1) than on the uncoated one (5.3). Hence, the coating not only helped in minimizing catalytic coking but it also

helped in lowering the total amount of coke deposited. This activity can help in prolonging the lifetime of a hypothetical cracking tube.

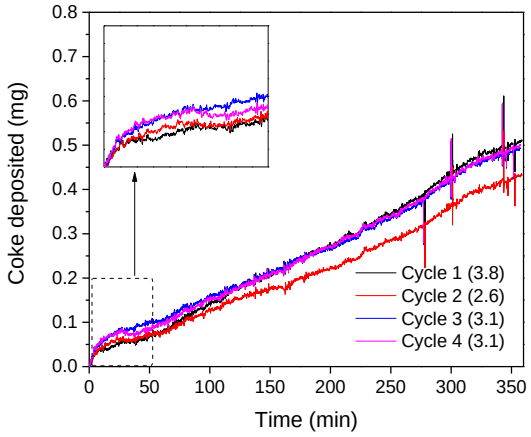

Figure 5.14 TG curves for coke deposition cycles on SG_ CeO_2-α-Al_2O_3-Incoloy

To understand the importance of the ceria layer on the coke deposition, a coking study was carried out with and without a ceria coating. After three coking cycles, the amount of coke deposited on the ceria coated substrate was slightly lower than the α-alumina coated substrate, as observed in Figure 5.15. This observation might be attributed to the ability of ceria to release oxygen to the coke for oxidation. Due to the large amount of time taken by the coking and decoking cycles, this cycling study was limited to one run. Hence, the obtained result may or may not be statistically significant. For reliable results, further analysis of this effect is necessary by repeating the runs.

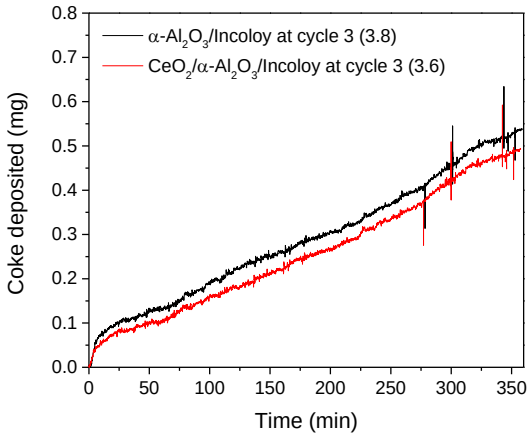

Figure 5.15 TG curves for comparison of coke deposition with and without ceria layer

The coke that was deposited on the SG_CeO_2-α-Al_2O_3-Incoloy was analyzed using SEM again at two different regions of the substrate. Figure 5.16a shows the rupture of the coating where catalytic filamentous coke appeared to have built up in a crack due to the exposure of the metallic species underneath the coating. Figure 5.16b shows another region where cracks were present on the coating. Comparing this to the analysis of the fresh coating, not much difference was observed. This is mostly because of the absence of high amounts of catalytic coke.

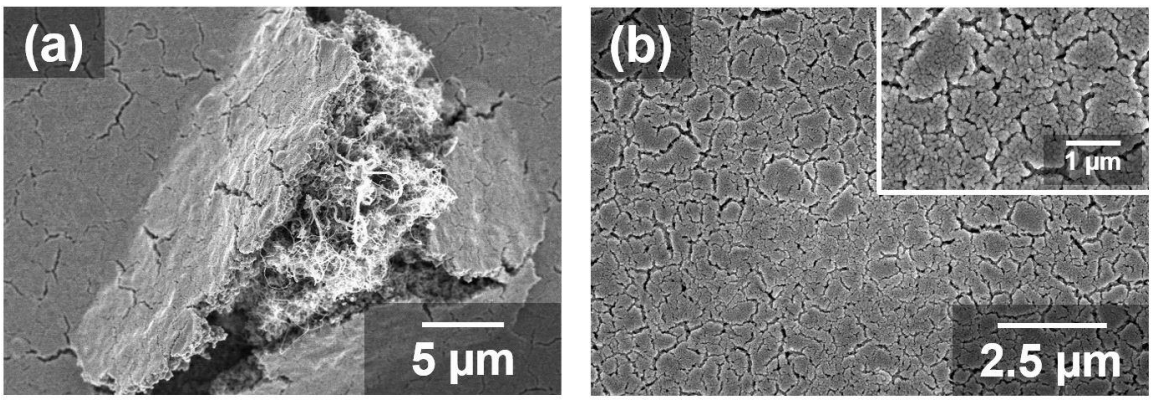

Figure 5.16 SEM analysis of coke deposited on SG_CeO_2-α-Al_2O_3-Incoloy coating

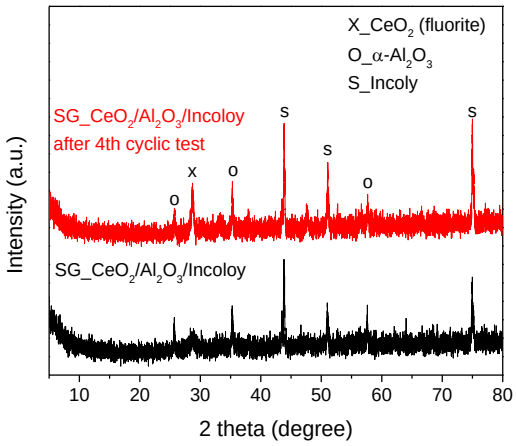

Figure 5.17 XRD pattern of SG_CeO_2-α-Al_2O_3-Incoloy coating before and after coking cycles

When XRD analysis was performed on SG_CeO_2-α-Al_2O_3-Incoloy coating, the ceria 111 peak at 28° showed a sharper peak after the coking cycle as compared to the freshly coated sample (Figure 5.17). Due to the high temperature exposure the ceria particles in the coating sintered leading to growth of the particles. There was a change in the intensities of the peaks related to the substrate, an observation similar to what was observed previously with the oxidized and α-alumina coated substrates

5.3.2.5 Elemental Analysis of Various Substrates with and without Coating

Table 5-2 provides the elemental percentages for different cases of the substrate with coatings. Since EDS is a surface technique, the values represent the phenomena happening on the surface alone and the results should be interpreted in a similar way. The bare Incoloy substrate showed a high amount of Cr, Fe and Ni on the surface, as expected. When the Incoloy was oxidized under the same conditions as the ceria and α-alumina coated Incoloy, the amount of Cr increased ~ 4 times. This is attributed to the diffusion of

Cr to the Incoloy surface and forming chromia scales which are known to help in reducing carbonization of the substrate.[40,41]

Table 5-2 Elemental analysis of substrates with or without coatings

Substrate	Al	Ti	Cr	Fe	Ni	Ce
Incoloy	3.8±0.7	0.9±0.7	19.8±0.6	43.7±0.8	31.7±0.6	-
Oxidized_Incoloy	4.0±0.5	2.5±0.3	68.7±2.8	20.8±4.0	4.0±2.1	-
Oxidized_Incoloy 4th cycle	2.6±0.6	2.8±2.7	83.8±3.5	7.7±2.0	3.1±0.7	-
CeO_2-Incoloy	5.6±1.4	1.1±0.5	11.8±1.1	25.9±5.3	8.5±1.0	47.1±3.4
CeO_2-Incoloy, 4th cycle	3.6±0.5	2.6±0.9	24.0±5.1	17.0±1.5	7.0±1.0	45.8±4.7
α-Al_2O_3-Incoloy	96.7±0.3	0.3±0.1	1.3±0.3	0.9±0.2	0.8±0.2	-
α-Al_2O_3-Incoloy, 4th cycle	98.1±0.2	0.1±0.1	1.1±0.2	0.5±0.2	0.3±0.3	-
SG_CeO_2/ α-Al_2O_3-Incoloy	43.2±1.4	0.1±0.1	2.0±0.3	1.8±1.0	0.6±0.8	52.2±1.8
SG_CeO_2/ α-Al_2O_3-Incoloy, 4th cycle	43.7±1.2	0.2±0.2	2.6±0.5	3.1±0.1	2.6±0.7	47.9±1.3

After the end of the fourth cycle the Cr concentration on the surface increased even more indicating more diffusion of the Cr. When ceria was coated directly on Incoloy, some amount of Cr was still present on the surface, denoting that the ceria coating was not uniform and continuous. There was also a greenish layer seen on the ceria coated Incoloy, which could be related to the formation of chromium oxides. On the other hand, when α-alumina was coated directly on Incoloy, a negligible amount of Cr was detected on the surface, implying complete coverage of the Incoloy surface with the coating. This is the reason that after fourth cycle the Cr amount remained negligible for the α-alumina coating while the Cr diffused towards the surface of the ceria coating, causing the Cr content to increase. Although the α-alumina was not crack-free, it was effective in minimizing the Cr diffusion towards the ceria layer. When ceria was coated on top of the α-alumina layer,

insignificant amounts of Cr were observed on the surface, indicating hindered diffusion of Cr atoms.

5.3.2.6 Importance of α-Alumina as the Buffer Layer

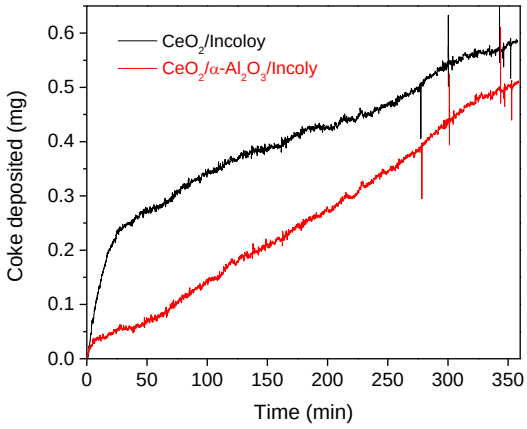

Figure 5.18 TG curves for comparison of coke deposition with and without α-alumina layer

Coking tests for ceria coatings on Incoloy with and without α-alumina are shown by the TG curves in Figure 5.18. As observed, the presence of α-alumina minimized catalytic coking in the region t = 0 to 50 min. This catalytic coking was significantly higher in the absence of the α-alumina layer. This could be attributed to the large amount of metal content on the surface of the CeO_2-Incoloy as stated in Table 5-2.

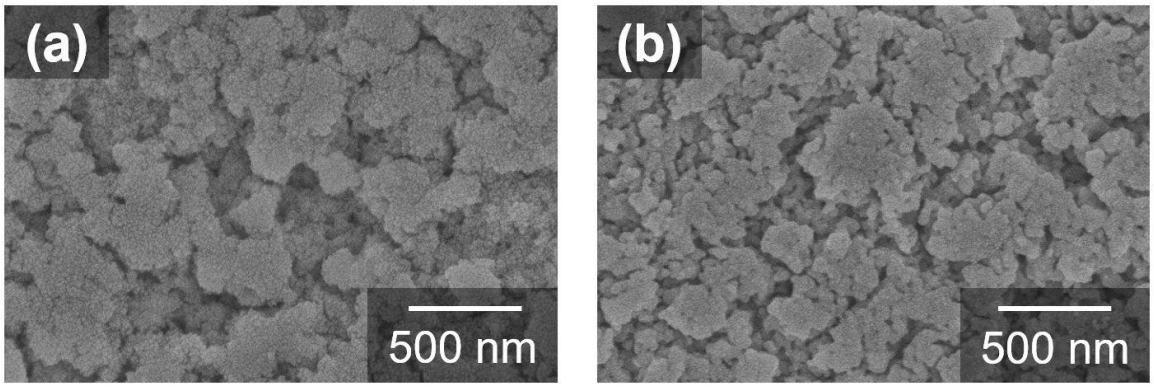

Figure 5.19 SEM analysis of SG_CeO_2-Al_2O_3-Incoloy coating 1) before and 2) after coking

Scale formation was observed on the CeO_2-Incoloy surface when α-alumina was not used as a buffer layer, as displayed in the SEM analysis in Figure 5.19. As compared to the SG_CeO_2-Al_2O_3-Incoloy, larger gaps were seen among the particles indicating a lack of continuity.

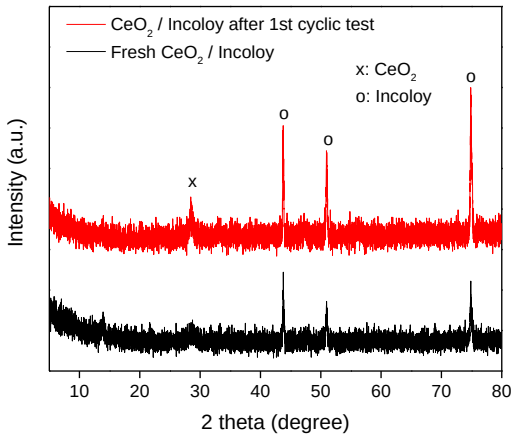

Figure 5.20 XRD pattern for CeO_2-Incoloy coating before and after coking

As shown in Figure 5.20, after cycling the XRD patterns revealed increase in crystallite size of the ceria particles on the CeO_2-Incoloy coating implying sintering of the coating due to exposure to a high temperature treatment. As expected, the peak ratio of the two sharp peaks of the substrate also changed after the coking cycle.

5.3.3 Catalytic Activity of Coatings towards Coke Oxidation

5.3.3.1 Oxidized Incoloy

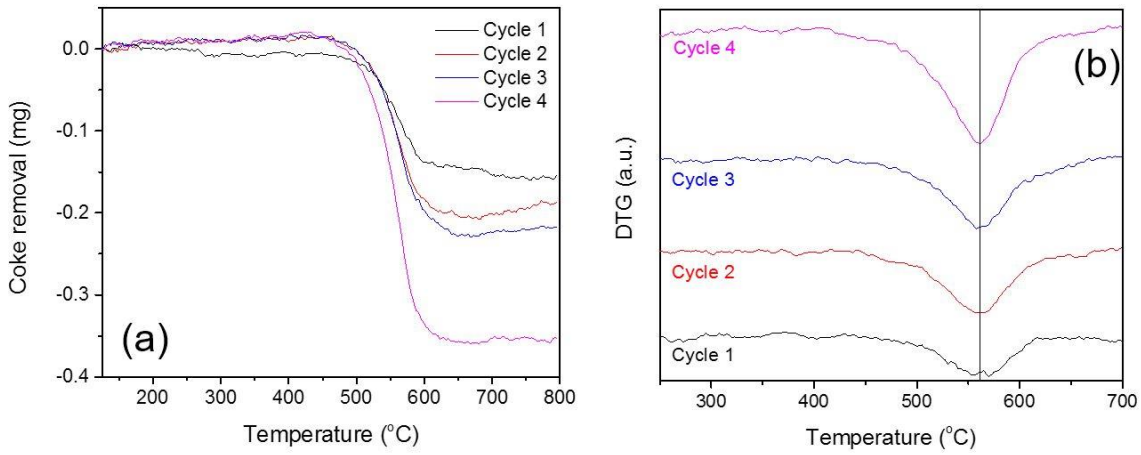

Figure 5.21 TPO curves for coke deposited on oxidized Incoloy

The oxidative capability of the coke deposited on the oxidized Incoloy substrate was assessed by temperature programmed oxidation experiments in the presence of air. Figure 5.21a shows the weight loss of coke with respect to temperature, which can be used to measure the amount of coke lost during oxidation. As seen in Figure 5.21a, the amount (mg) of coke oxidized after every cycle changed because a different amount of coke was deposited in every cycle. The mass of coke oxidized actually increased with every cycle. This behaviour could be attributed to two things: 1) more catalytic coke was formed with every cycle as shown earlier in Figure 5.8 and catalytic coke is easier to oxidize as compared to radical coke, 2) catalytic coke is formed due to exposure of metallic species that can also help catalyse coke oxidation, hence increase in coke oxidation rate.

Figure 5.21b gives the derivative of weight loss with respect to temperature, which tells the peak oxidation temperature needed to compare the oxidation activity over different

cycles. The coke was oxidized at ~ 560 °C during the decoking cycle (see Figure 5.21b). With every decoking cycle, the peak oxidation temperature also remained the same. This indicates no major degradation of the oxidized Incoloy substrate took place over a total of four coking and decoking cycles.

5.3.3.2 α-Al_2O_3-Incoloy

Figure 5.22a shows the weight loss curve for the coke deposited on the alumina coated Incoloy substrate. The amount (mg) of coke oxidized after every cycle remained the same for the α-alumina coating (see Figure 5.22a). This might be attributed to the same mass of coke deposited in every cycle as shown earlier in Figure 5.11.

The derivative of mass loss with respect to temperature is shown in Figure 5.22b. It is used to measure the peak oxidation temperature of coke after every cycle. The coke deposited on the α-alumina coated Incoloy oxidized at ~ 510 °C during the decoking cycle, which was 50 °C less than the peak oxidation temperature of the oxidized Incoloy temperature (Figure 5.21b). The peak of the oxidation DTG curve became broader with every cycle, indicating possible deterioration of the α-alumina coating.

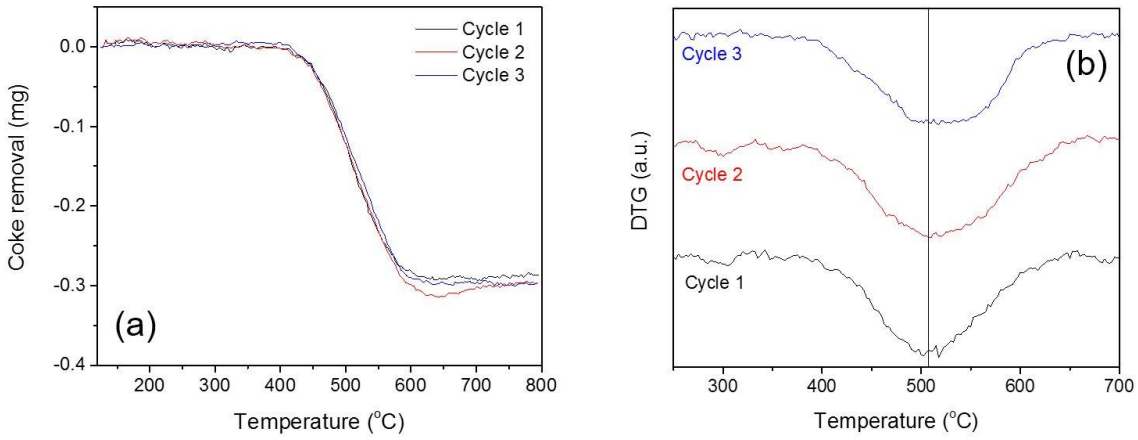

Figure 5.22 TPO curves for coke oxidation on α-Al_2O_3-Incoloy

5.3.3.3 CeO_2-α-Al_2O_3-Incoloy

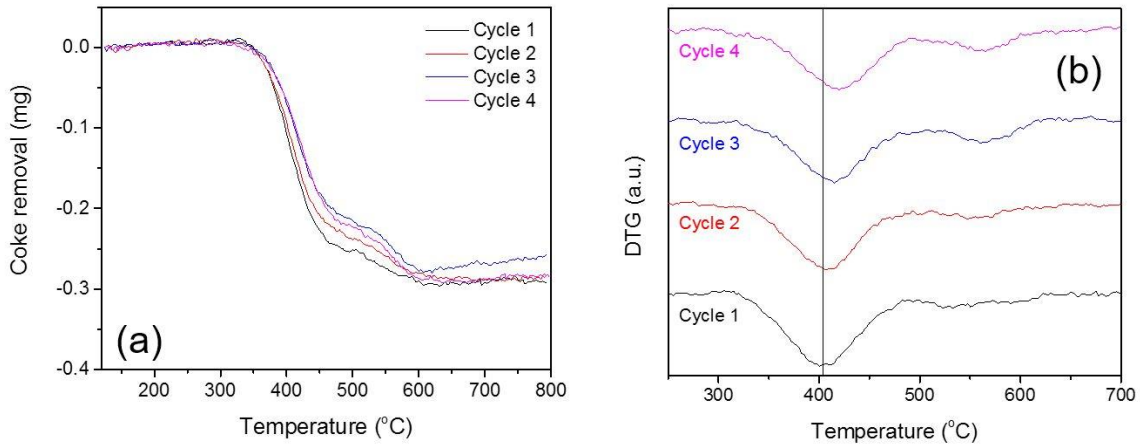

Figure 5.23 TPO curves for coke oxidation on SG_CeO_2-α-Al_2O_3-Incoloy

Similar to the previous two sections, the weight loss curve and the derivative of the weight loss for coke deposited on the SG_CeO_2-α-Al_2O_3-Incoloy were measured. Figure 5.23a shows the weight loss curve with respect to temperature. Similar to the α-alumina coating, the amount (mg) of coke oxidized after every cycle was the same for the SG_CeO_2-α-Al_2O_3 coating (Figure 5.23a).

The derivative of mass loss is shown in Figure 5.23b. The coke deposited on SG_CeO_2-α-Al_2O_3-Incoloy oxidized at ~ 400 °C during the decoking cycle, which was 160 °C less than the oxidized Incoloy peak oxidation temperature (Figure 5.23b). This decreased temperature is likely due to the high catalytic activity of ceria. The peak of the derivative of mass loss curves in Figure 5.23b shifted to the right with every cycle suggesting deterioration of the ceria coating which decreased the redox capability of ceria. This deterioration was shown earlier in Figure 5.17, in the form of sintered ceria particles after high temperature treatment during multiple coking and decoking cycles.

5.3.3.4 Comparison of Activity of Different Coatings

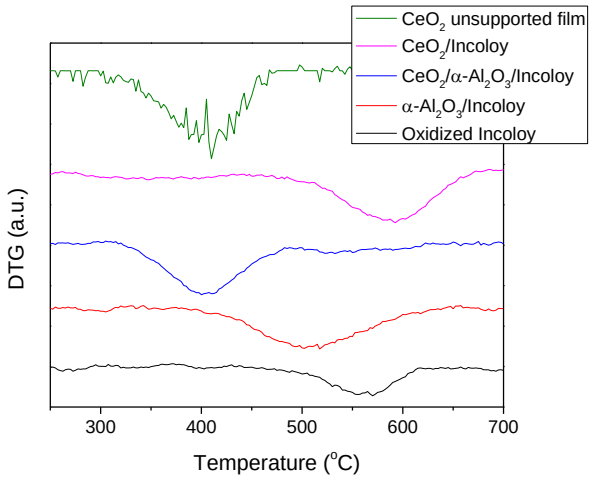

Figure 5.24 Comparison of peak oxidation temperature for various coatings

As we saw earlier, the SG_CeO_2-α-Al_2O_3-Incoloy coating showed the best catalytic activity by reducing the peak oxidation temperature of coke by 160 °C as compared to the Incoloy-substrate without coating. To understand the importance of the different components of the coating, it is important to compare the oxidation activities of the substrate with and without the individual components. Figure 5.24 compares the derivative

of the mass loss for these different cases. When the α-alumina buffer layer was absent (CeO_2-Incoloy), the coke oxidation temperature was more than that for the oxidized Incoloy case (Figure 5.24). This could be attributed to the formation of ceria chromate species, which blocked the release of oxygen from the ceria matrix and hence reduced its catalytic activity. These chromate species may also block access to the metallic sites, which can help in oxidizing coke. Thus the importance of the alumina layer is clear.

When an unsupported film of CeO_2 was prepared, the peak oxidation temperature was the same as the supported CeO_2-Al_2O_3-Incoloy coating, indicating no interaction between CeO_2 and Incoloy took place when α-Al_2O_3 was present as a median layer. Thus the presence of both ceria and alumina is essential for the high coke oxidation activity for the coatings.

5.4 Conclusions

Catalytic CeO_2 coatings were successfully synthesized on an Incoloy800 substrate. A sol-gel preparation method gave smaller particles of CeO_2 as well as negligible flaking as compared to the precursor method of preparation. A buffer layer of α-alumina was found to be essential to hold Cr atoms that might diffuse from the metallic substrate in place and stop them from diffusing into the active ceria layer. When Cr diffused into the ceria layer it reduced the activity of the ceria catalyst. No difference was found in the activity of the supported CeO_2 layer and the unsupported CeO_2 film, indicating negligible interaction between the coated ceria layer and the Incoloy substrate due to the presence of the intermediate alumina layer. The ceria layer was necessary to reduce the peak oxidation temperature of the coke by almost 160 °C as compared to the oxidized Incoloy substrate.

Along with reduction of the oxidation temperature, the coating also minimized catalytic coking by acting as a barrier and blocking access of much of the hydrocarbon molecules to the metallic sites. Some deterioration was observed in the ceria coating after four coking and decoking cycles, which increased the oxidation temperature by 10 °C. While the coatings are not perfectly continuous, the data demonstrate that even defective CeO_2-Al_2O_3 coatings give greatly enhanced coke reduction capabilities.

CHAPTER 6. SUMMARY AND FUTURE WORK

6.1 Key Contributions of this Work

This work focuses on being able to develop a methodology to minimize coke formation and reducing the oxidation temperature during decoking, in the steam cracking application. Specifically, the work involves forming radical coke species and also developing ceria catalysts that help in reducing the oxidation temperature of coke species in the presence of air as well as reducing the steam gasification temperature in presence of steam.

The key contributions of this work are:

CHAPTER 1: An extremely comprehensive review of the types of carbon deposits, their mechanism of formation and the different types of catalysts used for oxidation of carbonaceous deposits was published. Along with the regular qualitative comparison of the catalysts, a quantitative comparison was done by calculating the reaction rates of these catalysts under varied operating conditions. This review would be useful for future researchers to screen catalysts easily based on the reaction rates for their given application.

CHAPTER 2: A detailed *in-situ* methodology was developed for forming radical coke deposits directly on the catalytic supports and thus improving the coke-catalyst contact. This method provided a better representation of the coke catalyst contact than the physical mixtures or the tight contact method. Thermally aging the coke species increased the hardness of the coke.

CHAPTER 3: α-alumina supported ceria catalysts were highly active for coke oxidation as compared to bulk ceria. 50 mol% Ce catalyst showed activity four times more than the uncatalyzed coke oxidation at 500 °C. Ceria and α-alumina did not show any interactions implying presence on independent ceria domains on α-alumina surface. *In-situ* coke – catalyst contact showed similar mechanism of action as tight contact. A mechanism involving surface lattice active adsorbed oxygen species causing oxidation of coke particles was proposed.

CHAPTER 4: Doped (10 mol%) ceria catalysts with Gd, Mn and Sr as the dopants showed very high activity towards steam gasification of industrial coke. A reduction of ~ 65 °C was observed in the steam gasification temperature as compared to the uncatalyzed gasification with Gd. Gd and Mn also aided in the coke oxidation reaction using air while Sr proved to be a deterrent in the presence of air. Steam gasification was much slower as compared to air oxidation and the difference of peak temperature between them was ~ 200 °C.

CHAPTER 5: Catalytic coatings of ceria and α-alumina were successfully prepared on the metallic substrate of Incoloy 800 (an alloy of Ni, Fe, Cr). The α-alumina layer between the ceria and Incoloy layer was essential to minimize the chromium diffusion on the surface, which can potentially reduce the catalytic activity of ceria by forming inactive chromium oxides. A reduction of ~ 160 °C in the peak oxidation temperature of coke was achieved by the ceria coating as compared to the uncoated substrate.

6.2 Future Work

Potential directions in which this work can be continued are:

1) New alloys as substrate: Selection of new alloys that are stable up to 1100 °C would be important for obtaining data that is useful for high temperature industrial applications. The current study deals with coking studies at 800 °C due to the limitation on the stability of the substrate. The synthesis method of coatings will need tweaking to be stable at higher temperatures. The other important factor that can have a great effect on the stability of the coatings is the coefficient of thermal expansion (TEC). This factor can be changed by changing the composition of the substrate by having an Al, Cr or Ni rich alloy. These new alloys can be investigated for their effect on coking and decoking performance to have a better idea of the dependence of TECs on catalytic activity and stability.
2) Novel dopants: This work on coating synthesis focused on undoped ceria coatings. The next step would be to introduce dopants in the ceria matrix and then evaluate their performance and stability for both coke resistance and oxidation. Introduction of zirconia as a buffer layer could also be a potential way of minimizing catalytic coating and due to the different coefficient of thermal expansion, surface area, OSC, as compared to α-alumina, the activity observed might be different in the two cases.
3) Characterize coatings to determine thickness of the coating, extent of cracking, particle size, by use of novel techniques like TOF-SIMS, SEM, TEM-FIB.
4) Evaluating the coatings in the presence of steam: Since steam will be present in huge amounts during the coking as well as the decoking phase, it is important to test the activity and stability of the catalytic coatings in the presence of steam as well as steam – air mixtures. Presence of steam can also affect the morphology of the coatings and hence the activity.

5) Accelerated deactivation tests: Performing accelerated deactivation testing of coatings in the presence of steam - air mixtures, will help in studying the stability of the coatings over long time. The oxidation activity as well as the morphology of the coatings can be the important evaluations in determining the effect of the harsh conditions. This can help in prediction of life cycle of the cracking furnaces and can be the key to develop better coatings.

6) Develop a surrogate reaction for steam gasification of coke: To investigate the mechanism of carbon gasification in the presence of steam, a surrogate reaction of steam reforming of hydrocarbons, which mimic the H/C ratio of the industrial coke, will be studied. Tetralin, which contains both aliphatic (soft) and aromatic (hard) components, may act as a good model hydrocarbon to represent the carbon deposits formed during the initial stage of coking in the industrial furnaces. Extensive literature exists for reforming of tar as well as aromatic hydrocarbons (like benzene, toluene, naphthalene) on Ni catalysts (~500 articles). In contrast, very few studies have explored doped ceria catalysts (~ 50 articles) and none with coatings for steam reforming. The following directions can be taken:

    a. Conduct steam reforming of tetralin in a flow reactor, in the presence and absence of catalytic powders, measure the off gases using a GC-MS and determine any activity correlation to the coke gasification reaction (conducted in NETZSCH TGA)

    b. Dope ceria powders with alkali, transition and rare earth elements and assess reactivity

c. Investigate the reaction pathways for ceria catalyzed carbon gasification by characterizing catalysts with EXAFS, chemisorption, Raman spectroscopy, etc.

APPENDIX A. KINETICS OF COKE FORMATION

This appendix gives the details for the coking experiments and its kinetics.

A.1 Size and Shape of TGA Measuring Cup

As described in the chapter 2, the coking of supports was done in a measuring cup as shown in . The catalytic powder was measured in the cup, which was placed in the furnace. At high temperatures when hydrocarbon was passed on this sample cup, coke was formed on the cup as well as the catalytic powder. To remove the effect of the coke deposited on the cup, the catalytic support was taken out of the cup and an oxidation cycle was carried out on the empty coked cup. This cycle combusted all coke deposited on the cup and further analysis of the coked catalytic support was then carried out.

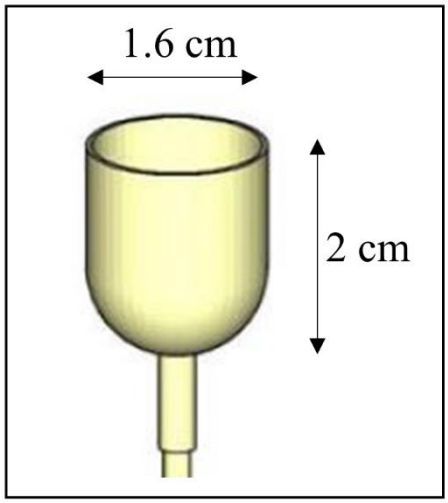

Figure A1 Size and Shape of TG Cell

A.2 Coke Formation Curve

Figure A2 TG profiles for coke deposition on 100 mg synthesized γ-alumina at 950 °C, 1 h shows a typical TGA coking curve. The coking is quite linear in time and when repeated is quite reproducible. The linear nature of the curve also denotes that coking is independent of any catalytic action. Catalytic coking seems to taper off with time as the catalytic sites are blocked due to coke formation.

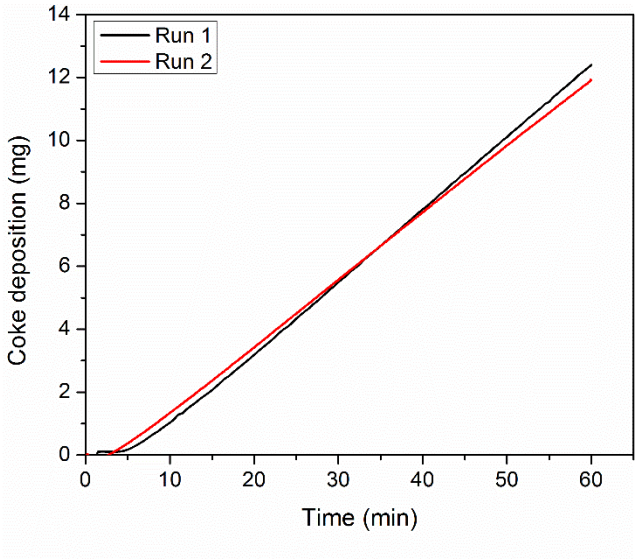

Figure A2 TG profiles for coke deposition on 100 mg synthesized γ-alumina at 950 °C, 1 h

A.3 Kinetics of Coke Formation in TGA

Table A1 and Table A2 give data for calculating the reaction order and activation energy for coke formation in the TGA, respectively. The values in these tables were plotted (Figure A3, Figure A4 and Figure A5) and the slope of the line was used to calculate the kinetic parameters. Separate analysis for reaction order was done for ethylene and propylene and an approximate value of 1 was obtained, denoting the radical nature of coke formation. The activation energy was found to be 91 kJ mol^{-1}. This energy is in the range

of energies for radical reactions to take place as shown in Table A3. It can be inferred from this observation that the coke formed in the TGA at high temperature is predominantly due to the radical reactions.

Table A1 Parameters for estimating reaction order for coke deposition using ethylene

ln (coking rate)	ln (concentration of ethylene)
-6.19626	-3.55338
-6.43371	-3.88985
-7.19853	-4.40067

Table A2 Parameters for estimating activation energy

ln (rate constant)	1/T x 10^4, K^{-1}
-11.39251	8.9
-10.47621	8.18
-9.9166	7.56

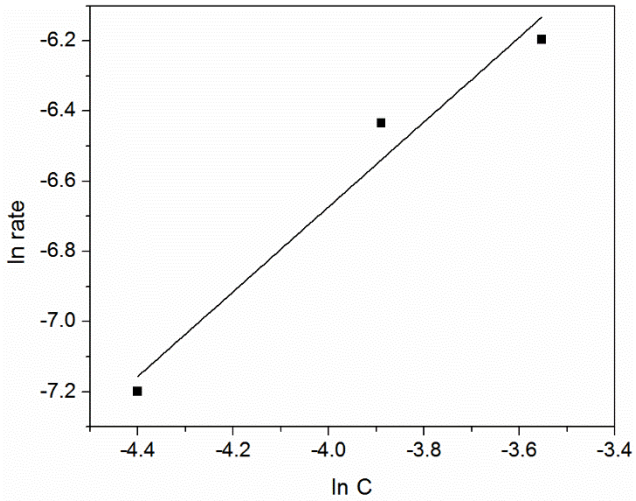

Figure A3 Reaction order analysis for ethylene for coke deposition on α-alumina

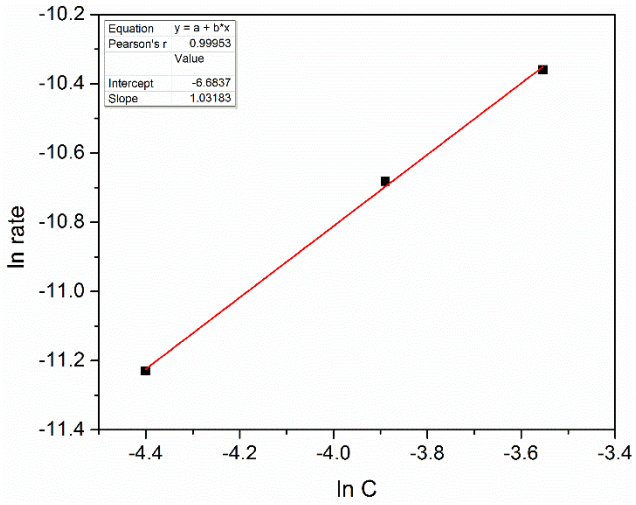

Figure A4 Reaction order analysis for propylene for coke deposition on α-alumina

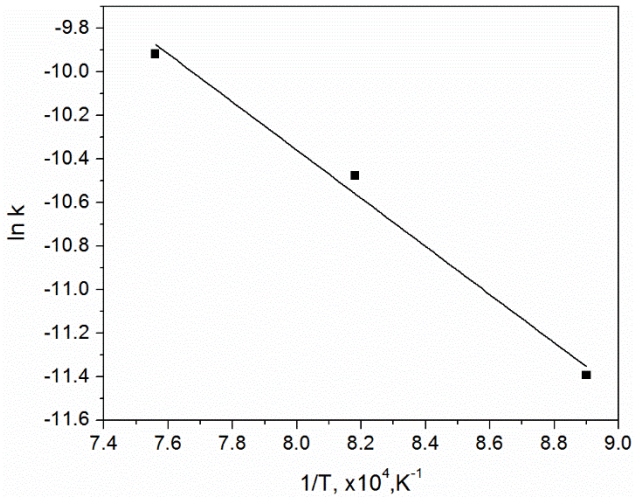

Figure A5 Arrhenius plot for coke deposition on α-alumina

Table A3 Activation energies of radical reactions for coking

Reaction forming coke	**Activation energy (kJ/mol)**
$C_4^+ \rightarrow$ coke	118[1]
H abstraction at benzene site	79.6[2]
H abstraction at naphthalene site	81.8[2]
H abstraction at anthracene site	84.6[2]
H abstraction at phenanthrene site	85.9[2]
Addition of allylic radical to ethene	70.5[3]
Addition of 1-methyl naphthanyl radical to ethene	70.1[3]
Addition of 9-methylanthracene radical to ethene	75.3[3]

.

APPENDIX B. EXAFS DATA FOR DOPED CERIA CATALYSTS

This appendix gives details EXAFS fitting for the undoped and doped ceria catalysts that were prepared by the one-pot synthesis.

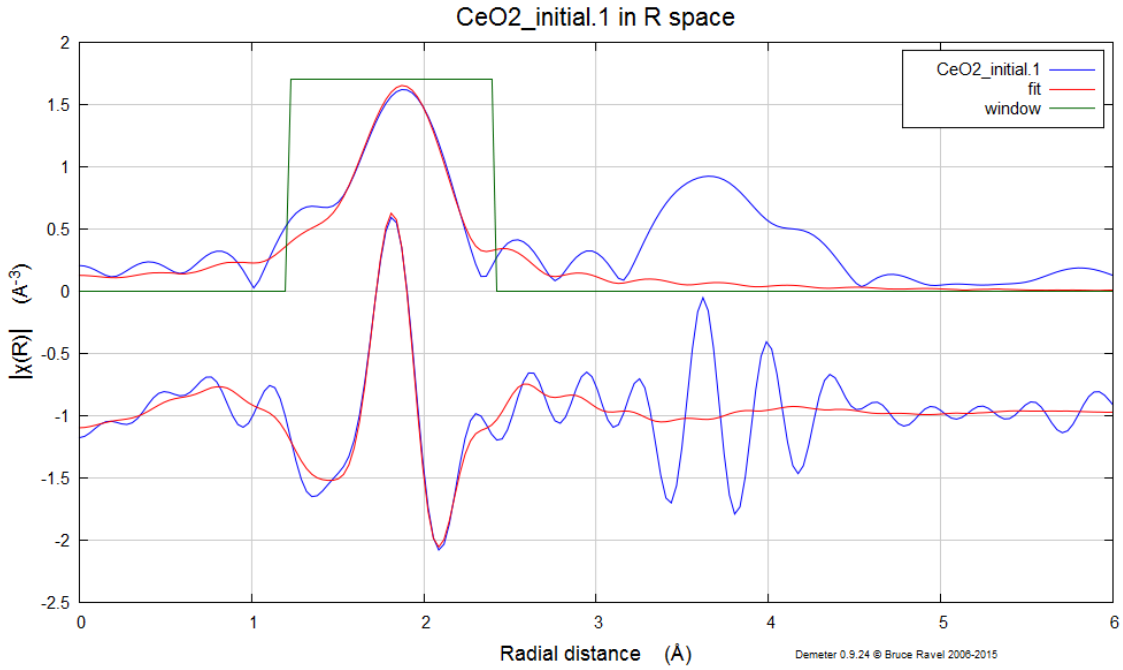

Figure B1 EXAFS fitting for standard CeO_2 sample

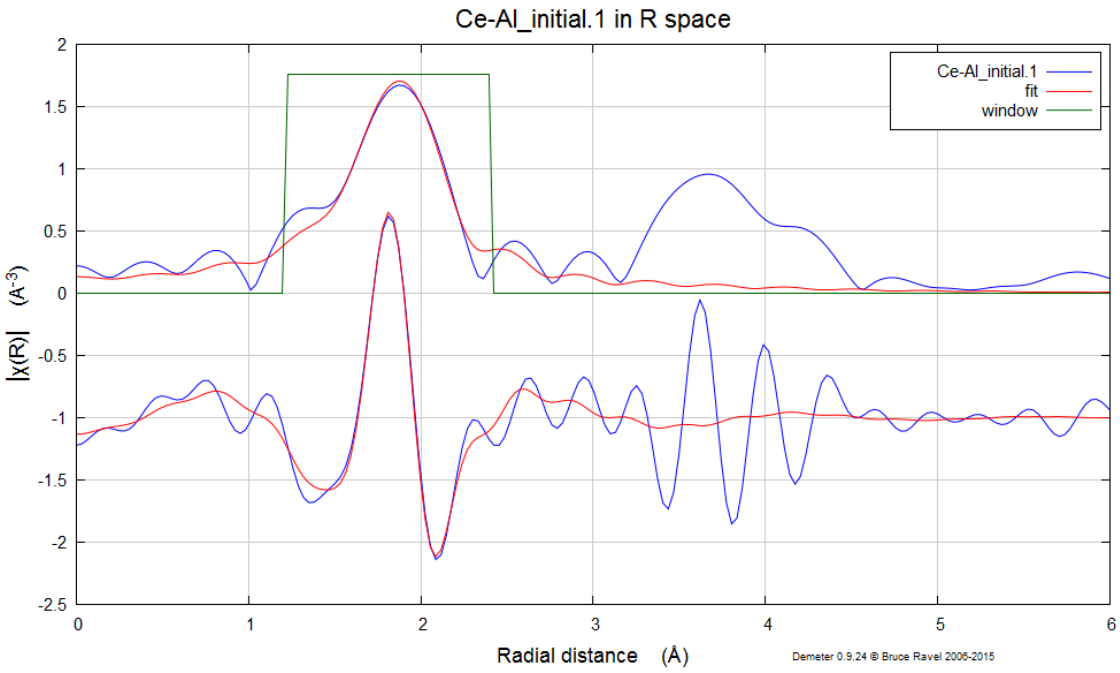

Figure B2 EXAFS fitting for CeAl catalyst

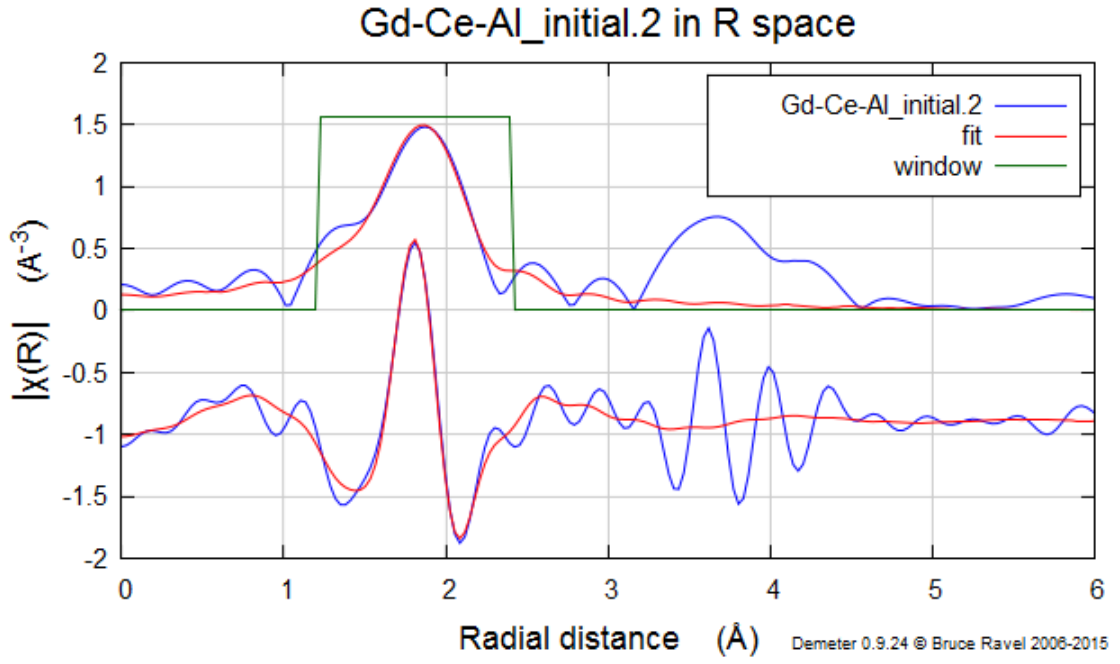

Figure B3 EXAFS fitting for 10GdCeAl catalyst

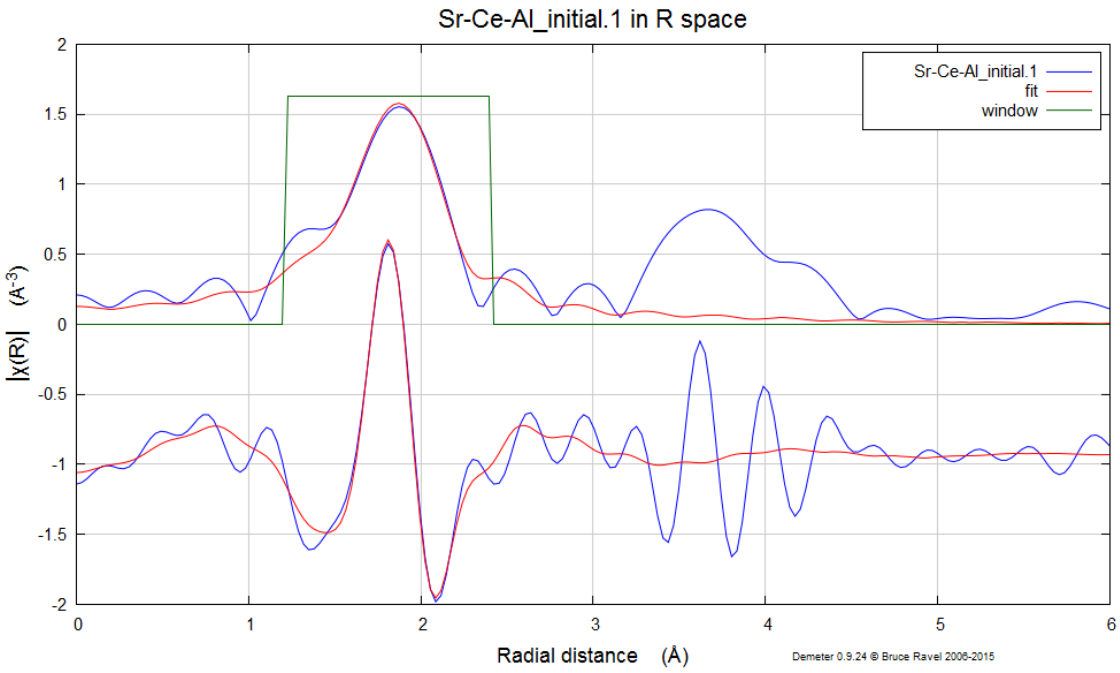

Figure B4 EXAFS fitting for 10SrCeAl catalyst

Acknowledgement: XAS studies were conducted using resources at the Advanced Photon Source, a U.S. Department of Energy (DOE) Office of Science User Facility operated for the DOE Office of Science by Argonne National Laboratory under Contract No. DE-AC02-06CH11357.

REFERENCES

(1) Stanmore, B. R.; Brilhac, J. F.; Gilot, P. The Oxidation of Soot: A Review of Experiments, Mechanisms and Models. *Carbon* **2001**, *39*, 2247.

(2) Prasad, R.; Bella, V. R. A Review on Diesel Soot Emission, Its Effect and Control. *Bull. Chem. React. Eng. Catal.* **2010**, *5* (2), 69.

(3) Forzatti, P.; Lietti, L. Catalyst Deactivation. *Catal. Today* **1999**, *52* (2-3), 165.

(4) Mann, R. Catalyst Deactivation by Coke Deposition: Approaches Based on Interactions of Coke Laydown with Pore Structure. *Catal. Today* **1997**, *37* (3), 331.

(5) Guisnet, M.; Magnoux, P. Deactivation by Coking of Zeolite Catalysts . Prevention of Deactivation . Optimal Conditions for Regeneration. *Catal. Today* **1997**, *36*, 477.

(6) Trimm, D. L. Catalysts for the Control of Coking during Steam Reforming. *Catal. Today* **1999**, *49*, 3.

(7) Abghari, S. Z. Investigation of Coke Formation in Steam Cracking of Atmospheric Gasoil. *J. Pet. Sci. Res.* **2013**, *2* (2), 82.

(8) Chan, K. Y. G.; Inal, F.; Senkan, S. Suppression of Coke Formation in the Steam Cracking of Alkanes : Ethane and Propane. *Ind. Eng. Chem. Res.* **1998**, *37*, 901.

(9) Kopinke, F. D.; Zimmermann, G.; Nowak, S. On the Mechanism of Coke Formation in Steam Cracking-Conclusions from Results Obtained by Tracer Experiments. *Carbon* **1988**, *26* (2), 117.

(10) Cai, H.; Krzywicki, A.; Oballa, M. C. Coke Formation in Steam Crackers for Ethylene Production. *Chem. Eng. Process. Process Intensif.* **2002**, *41* (3), 199.

(11) Frank, B.; Schuster, M. E.; Schlögl, R.; Su, D. S. Emission of Highly Activated Soot Particulate - The Other Side of the Coin with Modern Diesel Engines. *Angew. Chemie - Int. Ed.* **2013**, *52*, 2673.

(12) Lighty, J. S.; Veranth, J. M.; Sarofim, A. F. Combustion Aerosols: Factors Governing Their Size and Composition and Implications to Human Health. *J. Air Waste Manage. Assoc.* **2000**, *50* (9), 1565.

(13) Gärtner, C. A.; van Veen, A. C.; Lercher, J. A. Oxidative Dehydrogenation of Ethane: Common Principles and Mechanistic Aspects. *ChemCatChem* **2013**, *5*, 1.

(14) Ropital, F.; Broutin, P.; Reyniers, M.-F.; Froment, G. F. Anticoking Coatings for High Temperature Petrochemical Reactors. *Oil Gas Sci. Technol.* **1999**, *54* (3), 375.

(15) Mittal, K. G. Cracking Paraffinic Hydrocarbons to Make Alpha Olefins-a Review. *J. Chem. Technol. Biotechnol.* **1986**, *36*, 291.

(16) Shah, Y.; Stuart, E.; Sheth, K. Coke Formation during Thermal Cracking of N-Octane. *Ind. Eng. Chem. Process Des. Dev.* **1976**, *15* (4), 518.

(17) Niaei, A.; Salari, D.; Towfighi, J.; Chamandeh, A.; Nabavi R. Aluminized Steel and Zinc Coating for Reduction of Coke Formation in Thermal Cracking of Naphtha. *Int. J. Chem. React. Eng.* **2008**, *6*, 1.

(18) Sundaram, K. M.; Van Damme, P. S.; Froment, G. F. Coke Deposition in the Thermal Cracking of Ethane. *AIChE J.* **1981**, *27* (6), 946.

(19) Towfighi, J.; Sadrameli, M.; Niaei, A. Coke Formation Mechanisms and Coke Inhibiting Methods in Pyrolysis Furnaces. *J. Chem. Eng. Japan* **2002**, *35* (10), 923.

(20) Kopinke, F.-D.; Zimmermann, G.; Reyniers, G. C.; Froment, G. F. Relative Rates of Coke Formation from Hydrocarbons in Steam Cracking of Naphtha. 2. Paraffins, Naphthenes, Mono-, Di-, and Cycloolefins, and Acetylenes. *Ind. Eng. Chem. Res.* **1993**, *32*, 56.

(21) Albright, L. F.; Marek, J. C. Mechanistic Model for Formation of Coke in Pyrolysis Units Producing Ethylene. *Ind. Eng. Chem. Res.* **1988**, *27* (5), 755.

(22) Bond, G. C. The Role of Carbon Deposits in Metal-Catalysed Reactions of Hydrocarbons. *Appl. Catal. A Gen.* **1997**, *149*, 3.

(23) Kock, A. J. H. M.; Bokx, D. E.; Boellaard, E.; Klop, W.; Geus, J. W. The Formation

of Filamentous Carbon on Iron and Nickel Catalysts. *J. Catal.* **1985**, *96*, 468.

(24) Moodley, D. J. On the Deactivation of Cobalt-Based Fischer-Tropsch Synthesis Catalysts, 2008.

(25) Rostrup-Nielsen, J. R. Mechanisms of Carbon Formation on Nickel-Containing Catalysts. *J. Catal.* **1977**, *48*, 155.

(26) Guisnet, M.; Magnoux, P. Organic Chemistry of Coke Formation. *Appl. Catal. A Gen.* **2001**, *212* (1-2), 83.

(27) Yang, R.; Yang, K. Evidence for Temperature-Driven Carbon Diffusion Mechanism of Coke Deposition on Catalysts. *J. Catal.* **1985**, *93* (1), 182.

(28) Lahaye, J.; Badie, P.; Ducret, J. Mechanism of Carbon Formation during Steamcracking of Hydrocarbons. *Carbon* **1977**, *15* (2), 87.

(29) Niaei, A.; Salari, D.; Daneshvar, N.; Chamandeh, A.; Nabavi, R. Effect of Tube Materials and Special Coating on Coke Deposition in the Steam Cracking of Hydrocarbons. *World Acedemy Sci. Eng. Technol.* **2007**, *5*, 15.

(30) Zhou, J.; Xu, H.; Liu, J.; Qi, X.; Zhang, L.; Jiang, Z. Study of Anti-Coking Property of SiO_2/S Composite Coatings Deposited by Atmospheric Pressure Chemical Vapor Deposition. *Mater. Lett.* **2007**, *61* (29), 5087.

(31) Zhou, J.; Xu, H.; Luan, X.; Ling, X. Influence of the SiO_2/S Coating and Sulfur/phosphorus-Containing Coking Inhibitor on Coke Formation during Thermal Cracking of Light Naphtha. *Fuel Process. Technol.* **2012**, *104*, 198.

(32) Zhou, J.; Xu, H.; Ma, Q.; Zhang, L.; Dai, Y.; Peng, B. Mechanical and Thermal Properties of SiO_2/S Composite Coating Prepared by APCVD. *Mater. Sci. Eng. A* **2008**, *491* (1-2), 147.

(33) Horsley, G. W.; Cairns, J. A. The Inhibition of Carbon Deposition on Stainless Steel by Prior Selective Oxidation. *Appl. Surf. Sci.* **1984**, *18*, 273.

(34) Redmond, T.; Bergeron, M. P. Tests Demonstrate Anticoking Capability of New Coating. *Oil and Gas Journal*. 1999.

(35) Choi, A.; Yang, I.; Kang, S. SK Corporation. *Theor. Appl. Chem. Eng.* **2002**, *1*.

(36) BASF. *CAMOL Catalytic Coatings for Steam Cracker Furnace Tubes*; 2012.

(37) Petrone, S.; Deuis, R. L.; Kong, F.; Unwin, P. Catalyzed-Assisted Manufacture of Olefins (CAMOL): Year-(4) Update on Commercial Furnace Installations. In *AIChE Spring National Meeting*; 2010.

(38) Petrone, S.; Deuis, R. L.; Kong, F.; Sherwood, Y. C. Catalytic Surfaces and Coatings for the Manufacture of Petrochemicals, 2015.

(39) Zychlinski, W.; Wynns, K. A.; Ganser, B. Characterization of Material Samples for Coking Behavior of HP40 Material Both Coated and Uncoated Using Naphtha and Ethane Feedstock. *Mater. Corros.* **2002**, *53* (1), 30.

(40) Schietekat, C. M.; Sarris, S. A.; Reyniers, P. A.; Kool, L. B.; Peng, W.; Lucas, P.; Van Geem, K. M.; Marin, G. B. Catalytic Coating for Reduced Coke Formation in Steam Cracking Reactors. *Ind. Eng. Chem. Res.* **2015**, *54* (39), 9525.

(41) McKimpson, M. G.; Albright, L. F. Future Coils for Ethylene Furnaces: Reduced or No Coking and Increaed Coil Longevity. *ACS Div. Fuel Chem. Prepr.* **2004**, *49* (2), 776.

(42) Cai, H.; Oballa, M. C. Passivation of Steel Surface to Reduce Coke Formation, 2011.

(43) Higgins, K. J.; Jung, H.; Kittelson, D. B.; Roberts, J. T.; Zachariah, M. R. Kinetics of Diesel Nanoparticle Oxidation. *Environ. Sci. Technol.* **2003**, *37*, 1949.

(44) Neeft, J. P. A.; Nijhuis, T. X.; Smakman, E.; Makkee, M.; Moulijn, J. A. Kinetics of the Oxidation of Diesel Soot. *Fuel* **1997**, *76* (12), 1129.

(45) Dernaika, B.; Uner, D. A Simplified Approach to Determine the Activation Energies of Uncatalyzed and Catalyzed Combustion of Soot. *Appl. Catal. B Environ.* **2003**, *40* (3), 219.

(46) López-Suárez, F. E.; Bueno-López, A.; Illán-Gómez., M. J. Cu/Al_2O_3 Catalysts for Soot Oxidation: Copper Loading Effect. *Appl. Catal. B Environ.* **2008**, *84* (3-4), 651.

(47) Vander Wal, R. L.; Tomasek, A. J. Soot Oxidation: Dependence upon Initial Nanostructure. *Combust. Flame* **2003**, *134* (1-2), 1.

(48) Bokova, M. N.; Decarne, C.; Abi-Aad, E.; Pryakhin, A. N.; Lunin, V. V.; Aboukaïs, A. Kinetics of Catalytic Carbon Black Oxidation. *Thermochim. Acta* **2005**, *428* (1-2), 165.

(49) Jung, J.; Lee, J. H.; Song, S.; Chun, K. M. Measurement of Soot Oxidation With NO_2-O_2-H_2O in a Flow Reactor Simulating Diesel Engine DPF. *Int. J. Automot. Technol.* **2008**, *9* (4), 423.

(50) Yezerets, A.; Currier, N. W.; Kim, D. H.; Eadler, H. A.; Epling, W. S.; Peden, C. H. F. Differential Kinetic Analysis of Diesel Particulate Matter (soot) Oxidation by Oxygen Using a Step–response Technique. *Appl. Catal. B Environ.* **2005**, *61* (1-2), 120.

(51) Darcy, P.; Da Costa, P.; Mellottée, H.; Trichard, J.-M.; Djéga-Mariadassou, G. Kinetics of Catalyzed and Non-Catalyzed Oxidation of Soot from a Diesel Engine. *Catal. Today* **2007**, *119* (1-4), 252.

(52) Fenimore, C. P.; Jones, G. W. Oxidation of Soot by Hydroxyl Radicals. *J. Phys. Chem.* **1967**, *71* (3), 593.

(53) Neoh, K. G.; Howard, J. B.; Sarofim, A. F. Particulate Carbon. In *Soot Oxidation in Flames*; Siegla, D., Smith, G., Eds.; Springer US, 1981; pp 261–282.

(54) Puri, R.; Santoro, R. J.; Smyth, K. C. The Oxidation of Soot and Carbon Monoxide in Hydrocarbon Diffusion Flames. *Combust. Flame* **1994**, *97* (2), 125.

(55) Feugier, A. Soot Oxidation in Laminar Hydrocarbon Flames. *Combust. Flame* **1972**, *19* (2), 249.

(56) Neoh, K. G.; Howard, J. B.; Sarofim, A. F. Effect of Oxidation on the Physical Structure of Soot. *Symp. Combust.* **1985**, *20* (1), 951.

(57) Sirignano, M.; Kent, J.; D'Anna, A. Modeling Formation and Oxidation of Soot in Nonpremixed Flames. *Energy & Fuels* **2013**, *27* (4), 2303.

(58) Mahamulkar, S.; Yin, K.; Agrawal, P. K.; Davis, R. J.; Jones, C. W.; Malek, A.; Shibata, H. Formation and Oxidation/Gasification of Carbonaceous Deposits: A Review. *Ind. Eng. Chem. Res.* **2016**, *55* (37), 9760.

(59) Kašpar, J.; Fornasiero, P.; Graziani, M. Use of CeO_2-Based Oxides in the Three-Way Catalysis. *Catal. Today* **1999**, *50*, 285.

(60) Jung, H.; Kittelson, D. B.; Zachariah, M. R. The Influence of a Cerium Additive on Ultrafine Diesel Particle Emissions and Kinetics of Oxidation. *Combust. Flame* **2005**, *142*, 276.

(61) Stratakis, G. A.; Stamatelos, A. M. Thermogravimetric Analysis of Soot Emitted by a Modern Diesel Engine Run on Catalyst-Doped Fuel. *Combust. Flame* **2003**, *132*, 157.

(62) Cassee, F. R.; van Balen, E. C.; Singh, C.; Green, D.; Muijser, H.; Weinstein, J.; Dreher, K. Exposure, Health and Ecological Effects Review of Engineered Nanoscale Cerium and Cerium Oxide Associated with Its Use as a Fuel Additive. *Crit. Rev. Toxicol.* **2011**, *41* (3), 213.

(63) Bueno-López, A.; Krishna, K.; Makkee, M.; Moulijn, J. Active Oxygen from CeO_2 and Its Role in Catalysed Soot Oxidation. *Catal. Letters* **2005**, *99* (3-4), 203.

(64) Machida, M.; Murata, Y.; Kishikawa, K.; Zhang, D.; Ikeue, K. On the Reasons for High Activity of CeO_2 Catalyst for Soot Oxidation. *Chem. Mater.* **2008**, *20*, 4489.

(65) Gross, M. S.; Sánchez, B. S.; Querini, C. A. Diesel Particulate Matter Combustion with CeO_2 as Catalyst. Part II: Kinetic and Reaction Mechanism. *Chem. Eng. J.* **2011**, *168* (1), 413.

(66) Gross, M.; Ulla, M. A.; Querini, C. A. Diesel Particulate Matter Combustion with CeO_2 as Catalyst. Part I: System Characterization and Reaction Mechanism. *J. Mol. Catal. A Chem.* **2012**, *352*, 86.

(67) Preda, G.; Pacchioni, G. Formation of Oxygen Active Species in Ag-Modified CeO_2 Catalyst for Soot Oxidation: A DFT Study. *Catal. Today* **2011**, *177* (1), 31.

(68) Keating, P. R. L.; Scanlon, D. O.; Watson, G. W. The Nature of Oxygen States on the Surfaces of CeO_2 and La-Doped CeO_2. *Chem. Phys. Lett.* **2014**, *608*, 239.

(69) Krishna, K.; Bueno-López, A.; Makkee, M.; Moulijn, J. A. Potential Rare-Earth Modified CeO_2 Catalysts for Soot Oxidation Part III. Effect of Dopant Loading and Calcination Temperature on Catalytic Activity with O_2 and NO + O_2. *Appl. Catal. B Environ.* **2007**, *75* (3-4), 210.

(70) Aneggi, E.; de Leitenburg, C.; Llorca, J.; Trovarelli, A. Higher Activity of Diesel Soot Oxidation over Polycrystalline Ceria and Ceria–zirconia Solid Solutions from More Reactive Surface Planes. *Catal. Today* **2012**, *197* (1), 119.

(71) Aneggi, E.; Wiater, D.; de Leitenburg, C.; Llorca, J.; Trovarelli, A. Shape-Dependent Activity of Ceria in Soot Combustion. *ACS Catal.* **2014**, *4* (1), 172.

(72) Shen, Q.; Wu, M.; Wang, H.; He, C.; Hao, Z.; Wei, W.; Sun, Y. Facile Synthesis of Catalytically Active CeO_2 for Soot Combustion. *Catal. Sci. Technol.* **2015**, *5*, 1941.

(73) Piumetti, M.; Bensaid, S.; Russo, N.; Fino, D. Nanostructured Ceria-Based Catalysts for Soot Combustion: Investigations on the Surface Sensitivity. *Appl. Catal. B Environ.* **2015**, *165*, 742.

(74) Krishna, K.; Bueno-López, A.; Makkee, M.; Moulijn, J. A. Potential Rare Earth Modified CeO_2 Catalysts for Soot Oxidation I. Characterization and Catalytic Activity with O_2. *Appl. Catal. B Environ.* **2007**, *75* (3-4), 189.

(75) Bueno-López, A.; Krishna, K.; van der Linden, B.; Mul, G.; Moulijn, J. A.; Makkee, M. On the Mechanism of Model Diesel Soot-O_2 Reaction Catalysed by Pt-Containing La_{3+}-Doped CeO_2 A TAP Study with Isotopic O_2. *Catal. Today* **2007**, *121* (3-4), 237.

(76) Bueno-López, A.; Krishna, K.; Makkee, M.; Moulijn, J. Enhanced Soot Oxidation by Lattice Oxygen via La^{3+}-Doped CeO_2. *J. Catal.* **2005**, *230* (1), 237.

(77) Atribak, I.; Bueno-López, A.; García-García, A. Thermally Stable Ceria–zirconia Catalysts for Soot Oxidation by O_2. *Catal. Commun.* **2008**, *9* (2), 250.

(78) Liu, J.; Zhao, Z.; Liang, P.; Xu, C.; Duan, A.; Jiang, G.; Lin, W.; Wachs, I. E. Study on the Reaction Mechanism for Soot Oxidation over TiO_2 or ZrO_2-Supported Vanadium Oxide Catalysts by Means of In-Situ UV-Raman. *Catal. Letters* **2008**, *120* (2), 148.

(79) Reddy, B. M.; Bharali, P.; Thrimurthulu, G.; Saikia, P.; Katta, L.; Park, S.-E. Catalytic Efficiency of Ceria–Zirconia and Ceria–Hafnia Nanocomposite Oxides for Soot Oxidation. *Catal. Letters* **2008**, *123* (3-4), 327.

(80) Aneggi, E.; de Leitenburg, C.; Trovarelli, A. On the Role of Lattice/surface Oxygen in Ceria–zirconia Catalysts for Diesel Soot Combustion. *Catal. Today* **2012**, *181* (1), 108.

(81) Dhakad, M.; Mitshuhashi, T.; Rayalu, S.; Doggali, P.; Bakardjiva, S.; Subrt, J.; Fino, D.; Haneda, H.; Labhsetwar, N. Co_3O_4–CeO_2 Mixed Oxide-Based Catalytic Materials for Diesel Soot Oxidation. *Catal. Today* **2008**, *132* (1-4), 188.

(82) Shan, W.; Ma, N.; Yang, J.; Dong, X.; Liu, C.; Wei, L. Catalytic Oxidation of Soot Particulates over MnO_x-CeO_2 Oxides Prepared by Complexation-Combustion Method. *J. Nat. Gas Chem.* **2010**, *19* (1), 86.

(83) Aneggi, E.; de Leitenburg, C.; Dolcetti, G.; Trovarelli, A. Promotional Effect of Rare Earths and Transition Metals in the Combustion of Diesel Soot over CeO_2 and CeO_2–ZrO_2. *Catal. Today* **2006**, *114* (1), 40.

(84) Liu, J.; Zhao, Z.; Xu, C.; Duan, A.; Wang, L.; Zhang, S. Synthesis of Nanopowder Ce-Zr-Pr Oxide Solid Solutions and Their Catalytic Performances for Soot Combustion. *Catal. Commun.* **2007**, *8*, 220.

(85) Dulgheru, P.; Sullivan, J. A. Rare Earth (La, Nd, Pr) Doped Ceria Zirconia Solid Solutions for Soot Combustion. *Top. Catal.* **2013**, *56*, 504.

(86) Gu, Z.; Sang, X.; Wang, H.; Li, K. Structure and Catalytic Property of CeO_2-ZrO_2-Fe_2O_3 Mixed Oxide Catalysts for Diesel Soot Combustion: Effect of Preparation Method. *J. Rare Earths* **2014**, *32* (9), 817.

(87) Durgasri, D. N.; Vinodkumar, T.; Lin, F.; Alxneit, I.; Reddy, B. M. Gadolinium Doped Cerium Oxide for Soot Oxidation: Influence of Interfacial Metal–support Interactions. *Appl. Surf. Sci.* **2014**, *314*, 592.

(88) Małecka, M. A.; Kepiński, L.; Miśta, W. Structure Evolution of Nanocrystalline CeO_2 and $CeLnO_x$ Mixed Oxides (Ln = Pr, Tb, Lu) in O_2 and H_2 Atmosphere and Their Catalytic Activity in Soot Combustion. *Appl. Catal. B Environ.* **2007**, *74*, 290.

(89) Wu, X.; Liu, S.; Weng, D.; Lin, F. Textural–structural Properties and Soot Oxidation Activity of MnO_x-CeO_2 Mixed Oxides. *Catal. Commun.* **2011**, *12* (5), 345.

(90) Wu, X.; Liang, Q.; Weng, D.; Lu, Z. The Catalytic Activity of CuO–CeO_2 Mixed Oxides for Diesel Soot Oxidation with a NO/O_2 Mixture. *Catal. Commun.* **2007**, *8* (12), 2110.

(91) Liang, Q.; Wu, X.; Weng, D.; Xu, H. Oxygen Activation on Cu/Mn–Ce Mixed Oxides and the Role in Diesel Soot Oxidation. *Catal. Today* **2008**, *139* (1-2), 113.

(92) Atribak, I.; Bueno-Lopez, A.; Garcia-Garcia, A. Further Insights into the Key Features of Ceria–Zirconia Mixed Oxides Governing the Catalysed Soot Combustion Under NOx/O2. *Top. Catal.* **2009**, *52* (13-20), 2088.

(93) Wei, Y.; Liu, J.; Zhao, Z.; Duan, A.; Jiang, G.; Xu, C.; Gao, J.; He, H.; Wang, X. Three-Dimensionally Ordered Macroporous $Ce_{0.8}Zr_{0.2}O_2$-Supported Gold Nanoparticles: Synthesis with Controllable Size and Super-Catalytic Performance for Soot Oxidation. *Energy Environ. Sci.* **2011**, *4*, 2959.

(94) Liu, S.; Wu, X.; Weng, D.; Ran, R. Ceria-Based Catalysts for Soot Oxidation: A Review. *J. Rare Earths* **2015**, *33* (6), 567.

(95) Djuričić, B.; Pickering, S. Nanostructured Cerium Oxide: Preparation and Properties of Weakly-Agglomerated Powders. *J. Eur. Ceram. Soc.* **1999**, *19* (11), 1925.

(96) Guillén-Hurtado, N.; Bueno-López, A.; García-García, A. Catalytic Performances of Ceria and Ceria-Zirconia Materials for the Combustion of Diesel Soot under NO_x/O_2 and O_2. Importance of the Cerium Precursor Salt. *Appl. Catal. A Gen.* **2012**, *437-438* (2), 166.

(97) Zhang, G.; Zhao, Z.; Liu, J.; Jiang, G.; Duan, A.; Zheng, J.; Chen, S.; Zhou, R. Three Dimensionally Ordered Macroporous $Ce_{1-x}Zr_xO_2$ Solid Solutions for Diesel Soot Combustion. *Chem. Commun.* **2010**, *46* (3), 457.

(98) Zaletova, N. V; Turakulova, A. O.; Lunin, V. V. *Hierarchical Porous Ce-Zr Materials for Oxidation of Diesel Soot Particulate*; Elsevier Masson SAS, 2011; Vol. 141.

(99) Shimokawa, H.; Kusaba, H.; Einaga, H.; Teraoka, Y. Effect of Surface Area of La-

K-Mn-O Perovskite Catalysts on Diesel Particulate Oxidation. *Catal. Today* **2008**, *139*, 8.

(100) Aneggi, E.; De Leitenburg, C.; Dolcetti, G.; Trovarelli, A. Promotion Effect of Surface Lanthanum in Soot Oxidation over Ceria-Based Catalysts. *Top. Catal.* **2007**, *42-43* (May), 319.

(101) Katta, L.; Sudarsanam, P.; Thrimurthulu, G.; Reddy, B. M. Doped Nanosized Ceria Solid Solutions for Low Temperature Soot Oxidation: Zirconium versus Lanthanum Promoters. *Appl. Catal. B Environ.* **2010**, *101* (1-2), 101.

(102) Gao, Y.; Wu, X.; Liu, S.; Weng, D.; Zhang, H.; Ran, R. Formation of $BaMnO_3$ in $Ba/MnO_x–CeO_2$ Catalyst upon the Hydrothermal Ageing and Its Effects on Oxide Sintering and Soot Oxidation Activity. *Catal. Today* **2015**, *253*, 83.

(103) Sánchez Escribano, V.; Fernández López, E.; Gallardo-Amores, J. M.; del Hoyo Martínez, C.; Pistarino, C.; Panizza, M.; Resini, C.; Busca, G. A Study of a Ceria-Zirconia-Supported Manganese Oxide Catalyst for Combustion of Diesel Soot Particles. *Combust. Flame* **2008**, *153*, 97.

(104) Zou, G.; Xu, Y.; Wang, S.; Chen, M.; Shangguan, W. The Synergistic Effect in Co–Ce Oxides for Catalytic Oxidation of Diesel Soot. *Catal. Sci. Technol.* **2015**, *5*, 1084.

(105) Harrison, P. G.; Ball, I. K.; Daniell, W.; Lukinskas, P.; Céspedes, M.; Miró, E. E.; Ulla, M. A. Cobalt Catalysts for the Oxidation of Diesel Soot Particulate. *Chem. Eng. J.* **2003**, *95* (1-3), 47.

(106) Liang, Q.; Wu, X.; Weng, D.; Lu, Z. Selective Oxidation of Soot over Cu Doped Ceria/ceria–zirconia Catalysts. *Catal. Commun.* **2008**, *9* (2), 202.

(107) Nakagawa, K.; Ohshima, T.; Tezuka, Y.; Katayama, M.; Katoh, M.; Sugiyama, S. Morphological Effects of CeO_2 Nanostructures for Catalytic Soot Combustion of CuO/CeO_2. *Catal. Today* **2015**, *246*, 67.

(108) Reddy, B. M.; Rao, K. N. Copper Promoted Ceria-Zirconia Based Bimetallic Catalysts for Low Temperature Soot Oxidation. *Catal. Commun.* **2009**, *10* (9), 1350.

(109) Rao, K. N.; Venkataswamy, P.; Reddy, B. M. Structural Characterization and Catalytic Evaluation of Supported Copper-Ceria Catalysts for Soot Oxidation. *Ind.*

Eng. Chem. Res. **2011**, *50*, 11960.

(110) Muroyama, H.; Hano, S.; Matsui, T.; Eguchi, K. Catalytic Soot Combustion over CeO_2-Based Oxides. *Catal. Today* **2010**, *153*, 133.

(111) Cousin, R.; Capelle, S.; Abi-Aad, E.; Courcot, D.; Aboukaïs, A. Copper-Vanadium-Cerium Oxide Catalysts for Carbon Black Oxidation. *Appl. Catal. B Environ.* **2007**, *70*, 247.

(112) Ozawa, M.; Hattori, M.; Yamaguchi, T. Thermal Stability of Ceria Catalyst on Alumina and Its Surface Oxygen Storage Capacity. *J. Alloys Compd.* **2008**, *451* (1-2), 621.

(113) Di Monte, R.; Kasˇpar, J. On the Role of Oxygen Storage in Three-Way Catalysis. *Top. Catal.* **2004**, *28* (1-4), 47.

(114) Reddy, B. M.; Khan, A. Nanosized CeO_2–SiO_2, CeO_2–TiO_2, and CeO_2–ZrO_2 Mixed Oxides: Influence of Supporting Oxide on Thermal Stability and Oxygen Storage Properties of Ceria. *Catal. Surv. from Asia* **2005**, *9* (3), 155.

(115) Boaro, M.; Giordano, F.; Recchia, S.; Santo, V. D.; Giona, M.; Trovarelli, A. On the Mechanism of Fast Oxygen Storage and Release in Ceria-Zirconia Model Catalysts. *Appl. Catal. B Environ.* **2004**, *52* (3), 225.

(116) Neeft, J. P. A.; Makkee, M.; Moulijn, J. A. Catalytic Oxidation of Carbon Black - I . Activity of Catalysts and Classification of Oxidation Profiles. *Fuel* **1998**, *77* (3), 111.

(117) Zhang, Y.; Zou, X. The Catalytic Activities and Thermal Stabilities of Li/Na/K Carbonates for Diesel Soot Oxidation. *Catal. Commun.* **2007**, *8*, 760.

(118) An, H.; McGinn, P. J. Catalytic Behavior of Potassium Containing Compounds for Diesel Soot Combustion. *Appl. Catal. B Environ.* **2006**, *62*, 46.

(119) Castoldi, L.; Matarrese, R.; Lietti, L.; Forzatti, P. Intrinsic Reactivity of Alkaline and Alkaline-Earth Metal Oxide Catalysts for Oxidation of Soot. *Appl. Catal. B Environ.* **2009**, *90*, 278.

(120) Mul, G.; Kapteijn, F.; Moulijn, J. A. Catalytic Oxidation of Model Soot by Metal Chlorides. *Appl. Catal. B Environ.* **1997**, *12*, 33.

(121) Hleis, D.; Labaki, M.; Laversin, H.; Courcot, D.; Aboukaïs, A. Comparison of Alkali-Promoted ZrO_2 Catalysts towards Carbon Black Oxidation. *Colloids Surfaces A Physicochem. Eng. Asp.* **2008**, *330*, 193.

(122) Doggali, P.; Waghmare, S.; Rayalu, S.; Teraoka, Y.; Labhsetwar, N. Transition Metals Supported on Mesoporous ZrO_2 for the Catalytic Control of Indoor CO and PM Emissions. *J. Mol. Catal. A Chem.* **2011**, *347* (1-2), 52.

(123) Dhakad, M.; Joshi, A. G.; Rayalu, S.; Tanwar, P.; Bassin, J. K.; Kumar, R.; Lokhande, S.; Subrt, J.; Mitsuhashi, T.; Labhsetwar, N. Alumina Supported Co-K-Mo Based Catalytic Material for Diesel Soot Oxidation. *Top. Catal.* **2009**, *52*, 2070.

(124) Royer, S.; Duprez, D.; Can, F.; Courtois, X.; Batiot-Dupeyrat, C.; Laassiri, S.; Alamdari, H. Perovskites as Substitutes of Noble Metals for Heterogeneous Catalysis: Dream or Reality. *Chem. Rev.* **2014**, *114*, 10292.

(125) Fino, D.; Russo, N.; Saracco, G.; Specchia, V. The Role of Suprafacial Oxygen in Some Perovskites for the Catalytic Combustion of Soot. *J. Catal.* **2003**, *217*, 367.

(126) Wang, X.; Zhang, Y.; Li, Q.; Wang, Z.; Zhang, Z. Identification of Active Oxygen Species for Soot Combustion on $LaMnO_3$ Perovskite. *Catal. Sci. Technol.* **2012**, *2*, 1822.

(127) Ifrah, S.; Kaddouri, A.; Gelin, P.; Bergeret, G. On the Effect of La-Cr-O- Phase Composition on Diesel Soot Catalytic Combustion. *Catal. Commun.* **2007**, *8*, 2257.

(128) Xiao, P.; Zhong, L.; Zhu, J.; Hong, J.; Li, J.; Li, H.; Zhu, Y. CO and Soot Oxidation over Macroporous Perovskite $LaFeO_3$. *Catal. Today* **2015**, *258*, 660.

(129) Neeft, J. P. A.; Makkee, M.; Moulijn, J. A. Catalysts for the Oxidation of Soot from Diesel Exhaust Gases. I. An Exploratory Study. *Appl. Catal. B Environ.* **1996**, *8* (1), 57.

(130) van Setten, B. A. A. L.; Schouten, J. M.; Makkee, M.; Moulijn, J. A. Realistic Contact for Soot with an Oxidation Catalyst for Laboratory Studies. *Appl. Catal. B Environ.* **2000**, *28* (3-4), 253.

(131) Shimokawa, H.; Kurihara, Y.; Kusaba, H.; Einaga, H.; Teraoka, Y. Comparison of Catalytic Performance of Ag- and K-Based Catalysts for Diesel Soot Combustion. *Catal. Today* **2012**, *185* (1), 99.

(132) Neeft, J. P. A.; van Pruissen, O. P.; Makkee, M.; Moulijn, J. A. Catalysts for the Oxidation of Soot from Diesel Exhaust Gases. II. Contact between Soot and Catalyst under Practical Conditions. *Appl. Catal. B Environ.* **1997**, *12*, 21.

(133) Jelles, S. J.; van Setten, B. A. A. L.; Makkee, M.; Moulijn, J. A. Molten Salts as Promising Catalysts for Oxidation of Diesel Soot: Importance of Experimental Conditions in Testing Procedures. *Appl. Catal. B Environ.* **1999**, *21* (1), 35.

(134) van Setten, B. A. A. L.; van Dijk, R.; Jelles, S. J.; Makkee, M.; Moulijn, J. A. The Potential of Supported Molten Salts in the Removal of Soot from Diesel Exhaust Gas. *Appl. Catal. B Environ.* **1999**, *21* (1), 51.

(135) van Setten, B. A. A. L.; Bremmer, J.; Jelles, S. J.; Makkee, M.; Moulijn, J. A. Ceramic Foam as a Potential Molten Salt Oxidation Catalyst Support in the Removal of Soot from Diesel Exhaust Gas. *Catal. Today* **1999**, *53* (4), 613.

(136) Bassou, B.; Guilhaume, N.; Lombaert, K.; Mirodatos, C.; Bianchi, D. Experimental Microkinetic Approach of the Catalytic Oxidation of Diesel Soot by Ceria Using Temperature-Programmed Experiments. Part 2: Kinetic Modeling of the Impact of the Ceria/Soot Contacts on the Rate of Oxidation. *Energy & Fuels* **2010**, *24* (9), 4781.

(137) Simonsen, S. B.; Dahl, S.; Johnson, E.; Helveg, S. Ceria-Catalyzed Soot Oxidation Studied by Environmental Transmission Electron Microscopy. *J. Catal.* **2008**, *255* (1), 1.

(138) Matarrese, R.; Castoldi, L.; Lietti, L.; Forzatti, P. Soot Combustion: Reactivity of Alkaline and Alkaline Earth Metal Oxides in Full Contact with Soot. *Catal. Today* **2008**, *136*, 11.

(139) Yamazaki, K.; Sakakibara, Y.; Dong, F.; Shinjoh, H. The Remote Oxidation of Soot Separated by Ash Deposits via Silver-Ceria Composite Catalysts. *Appl. Catal. A Gen.* **2014**, *476*, 113.

(140) Obeid, E.; Lizarraga, L.; Tsampas, M. N.; Cordier, A.; Boréave, A.; Steil, M. C.; Blanchard, G.; Pajot, K.; Vernoux, P. Continuously Regenerating Diesel Particulate

Filters Based on Ionically Conducting Ceramics. *J. Catal.* **2014**, *309*, 87.

(141) Mahamulkar, S.; Yin, K.; Davis, R. J.; Shibata, H.; Malek, A.; Jones, C. W.; Agrawal, P. K. In Situ Generation of Radical Coke and the Role of Coke-Catalyst Contact on Coke Oxidation. *Ind. Eng. Chem. Res.* **2016**, *55* (18), 5271.

(142) Jeguirim, M.; Tschamber, V.; Brilhac, J. F.; Ehrburger, P. Oxidation Mechanism of Carbon Black by NO_2: Effect of Water Vapour. *Fuel* **2005**, *84* (14-15), 1949.

(143) Arnal, C.; Alzueta, M. U.; Millera, A.; Bilbao, R. Influence of Water Vapor Addition on Soot Oxidation at High Temperature. *Energy* **2012**, *43* (1), 55.

(144) Peralta, M. A.; Milt, V. G.; Cornaglia, L. M.; Querini, C. A. Stability of Ba,K/CeO_2 Catalyst during Diesel Soot Combustion: Effect of Temperature, Water, and Sulfur Dioxide. *J. Catal.* **2006**, *242*, 118.

(145) Badini, C.; Saracco, G.; Valentina, S.; Specchia, V. Suitability of Some Promising Soot Combustion Catalysts for Application in Diesel Exhaust Treatment. *Appl. Catal. B Environ.* **1998**, *18* (1-2), 137.

(146) Mckee, D. W.; Chatterji, D. The Catalyzed Reaction of Graphite with Water Vapor. *Carbon* **1978**, *16* (1), 53.

(147) Freriks, I. L. C.; van Wechem, H. M. H.; Stuiver, J. C. M.; Bouwman, R. Potassium-Catalysed Gasification of Carbon with Steam: A Temperature-Programmed Desorption and Fourier Transform Infrared Study. *Fuel* **1981**, *60* (6), 463.

(148) Moulijn, J. A.; Cerfontain, M. B.; Kapteijn, F. Mechanism of the Potassium Catalysed Gasification of Carbon in CO_2. *Fuel* **1984**, *63* (8), 1043.

(149) Meijer, R.; Kapteijn, F.; Moulijn, J. A. Kinetics of the Alkali-Carbonate Catalysed Gasification of Carbon: 3. H_2O Gasification. *Fuel* **1994**, *73* (5), 723.

(150) Linares-Solano, A.; Almela-Alarcon, A.; de Lecea, C. S.-M. CO_2 Chemisorption to Characterize Calcium Catalysts in Carbon Gasification Reactions. *J. Catal.* **1990**, *125* (2), 401.

(151) Atribak, I.; Bueno-Lopez, A.; Garcia-Garcia, A. Thermally Stable Ceria – Zirconia

Catalysts for Soot Oxidation by O_2. *Catal. Commun.* **2008**, *9* (2), 250.

(152) Alinezhadchamazketi, A.; Khodadadi, A. A.; Mortazavi, Y.; Nemati, A. Catalytic Evaluation of Promoted CeO_2-ZrO_2 by Transition, Alkali, and Alkaline-Earth Metal Oxides for Diesel Soot Oxidation. *J. Environ. Sci.* **2013**, *25* (12), 2498.

(153) Mogensen, M.; Sammes, N. M.; Tompsett, G. A. Physical, Chemical and Electrochemical Properties of Pure and Doped Ceria. *Solid State Ionics* **2000**, *129*, 63.

(154) Trovarelli, A. Catalytic Properties of Ceria and CeO_2 - Containing Materials. *Catal. Rev. Sci. Eng.* **1996**, *38* (4), 440.

(155) Aneggi, E.; Boaro, M.; Leitenburg, C. De; Dolcetti, G.; Trovarelli, A. Insights into the Redox Properties of Ceria-Based Oxides and Their Implications in Catalysis. *J. Alloys Compd.* **2006**, *408-412*, 1096.

(156) Wu, X.; Liu, S.; Weng, D.; Lin, F.; Ran, R. MnO_x-CeO_2-Al_2O_3 Mixed Oxides for Soot Oxidation: Activity and Thermal Stability. *J. Hazard. Mater.* **2011**, *187* (1-3), 283.

(157) Sun, S.; Chu, W.; Yang, W. Ce-Al Mixed Oxide with High Thermal Stability for Diesel Soot Combustion. *Chinese J. Catal.* **2009**, *30* (7), 685.

(158) Gorte, R. J. Ceria in Catalysis: From Automotive Applications to the Water-Gas Shift Reaction. *AlChE J.* **2010**, *56*, 1126.

(159) Soykal, I. I.; Sohn, H.; Singh, D.; Miller, J. T.; Ozkan, U. S. Reduction Characteristics of Ceria under Ethanol Steam Reforming Conditions: Effect of the Particle Size. *ACS Catal.* **2014**, *4* (2), 585.

(160) Bunluesin, T.; Putna, E. S.; Gorte, R. J. A Comparison of CO Oxidation on Ceria-Supported Pt, Pd, and Rh. *Catal. Letters* **1996**, *41*, 1.

(161) Chaikittisilp, W.; Kim, H.-J.; Jones, C. W. Mesoporous Alumina-Supported Amines as Potential Steam-Stable Adsorbents for Capturing CO_2 from Simulated Flue Gas and Ambient Air. *Energy & Fuels* **2011**, *25* (11), 5528.

(162) Zhang, Z.; Pinnavaia, T. J. Mesoporous γ-Alumina Formed Through the Surfactant-Mediated Scaffolding of Peptized Pseudoboehmite Nanoparticles. *Langmuir* **2010**, *26* (12), 10063.

(163) Fulvio, P. F.; Brosey, R. I.; Jaroniec, M. Synthesis of Mesoporous Alumina from Boehmite in the Presence of Triblock Copolymer. *ACS Appl. Mater. Interfaces* **2010**, *2* (2), 588.

(164) Van Damme, P. S.; Narayanan, S.; Froment, G. F. Thermal Cracking of Propane and Propane-PropyIene Mixtu Rest Pilot Plant Versus Industrial Data. *AIChE J.* **1975**, *21* (72), 1065.

(165) Ervin, K.; Gronert, S.; Barlow, S.; Gilles, M.; Harrison, A.; Bierbaum, V. M.; Depuy, C. H.; Lineberger, W. C. Bond Strengths of Ethylene and Acetylene. *J. Am. Chem. Soc.* **1990**, *112* (1), 5750.

(166) G.F. Froment; Steene, V. De. Thermal Cracking of Ethylene, Propylene and Light Hydrocarbon Mixtures. In *Kinetics Technology International, The Hague, The Netherlands*; pp 134–162.

(167) Van Speybroeck, V.; Reyniers, M. F.; Marin, G. B.; Waroquier, M. Modeling Elementary Reactions in Coke Formation from First Principles. *ACS Div. Fuel Chem. Prepr.* **2004**, *49* (2), 781.

(168) Sadezky, A.; Muckenhuber, H.; Grothe, H.; Niessner, R.; Pöschl, U. Raman Microspectroscopy of Soot and Related Carbonaceous Materials: Spectral Analysis and Structural Information. *Carbon* **2005**, *43*, 1731.

(169) Ivleva, N. P.; Messerer, A.; Yang, X.; Niessner, R.; Pöschl, U. Raman Microspectroscopic Analysis of Changes in the Chemical Structure and Reactivity of Soot in a Diesel Exhaust Aftertreatment Model System. *Environ. Sci. Technol.* **2007**, *41* (10), 3702.

(170) Lin, Y.; Zhan, Z.; Liu, J.; Barnett, S. Direct Operation of Solid Oxide Fuel Cells with Methane Fuel. *Solid State Ionics* **2005**, *176* (23-24), 1827.

(171) Yao, Y. U. Ceria in Automotive Exhaust Catalysts. *J. Catal.* **1984**, *86*, 254.

(172) Campbell, C. T.; Peden, C. H. F. Oxygen Vacancies and Catalysis on Ceria Surfaces.

Science (80-.). **2005**, *309*, 713.

(173) Park, S.; Vohs, J. M.; Gorte, R. J. Direct Oxidation of Hydrocarbons in a Solid-Oxide Fuel Cell. *Nature* **2000**, *404* (6775), 265.

(174) Yahiro, H. Electrical Properties and Reducibilities of Ceria-Rare Earth Oxide Systems and Their Application to Solid Oxide Fuel Cell. *Solid State Ionics* **1989**, *36* (1-2), 71.

(175) Adijanto, L.; Sampath, A.; Yu, A. S.; Cargnello, M.; Fornasiero, P.; Gorte, R. J.; Vohs, J. M. Synthesis and Stability of Pd@CeO_2 Core–Shell Catalyst Films in Solid Oxide Fuel Cell Anodes. *ACS Catal.* **2013**, *3* (8), 1801.

(176) Reddy, B. M.; Rao, K. N.; Reddy, G. K.; Khan, A.; Park, S. Structural Characterization and Oxidehydrogenation Activity of CeO 2 / Al 2 O 3 and V 2 O 5 /. *J. Phy. Chem.* **2007**, *111*, 18751.

(177) Damyanova, S.; Perez, C. A.; Schmal, M.; Bueno, J. M. C. Characterization of Ceria-Coated Alumina Carrier. *Appl. Catal. A Gen.* **2002**, *234* (1-2), 271.

(178) Martınez, A.; Ferna, M.; Conesa, J. C.; Soria, J. Structural and Redox Properties of Ceria in Alumina-Supported Ceria Catalyst Supports. *J. Phys. Chem. B.* **2000**, *104*, 4038.

(179) Shyu, J. Z.; Weber, W. H.; Gandhi, H. S. Surface Characterization of Alumina-Supported Ceria. *J. Phys. Chem.* **1988**, *92* (17), 4964.

(180) Bensalem, A.; Muller, J. C.; Bozon-Verduraz, F. From Bulk CeO_2 to Supported Cerium-Oxygen Clusters: A Diffuse Reflectance Approach. *J. Chem. Soc. Faraday Trans.* **1992**, *88* (1), 153.

(181) Echevsky, G. V; Ayupov, A. B.; Paukshtis, E. A. Coke Deactivation of Acid Sites on ZSM-5 Zeolite. *Catal. Deactiv. 2001, Proc.* **2001**, *139*, 77.

(182) Madier, Y.; Descorme, C.; Le Govic, A. M.; Duprez, D. Oxygen Mobility in CeO_2 and $Ce_{(x)}Zr_{(1-x)}O_2$ Compounds: Study by CO Transient Oxidation and $^{18}O/^{16}O$ Isotopic Exchange. *J. Phys. Chem. B* **1999**, *103* (50), 10999.

(183) Yin, K.; Mahamulkar, S.; Shibata, H.; Malek, A.; Jones, C. W.; Agrawal, P. K.; Davis, R. J. Catalytic Oxidation of Solid Carbon and Carbon Monoxide over Cerium-Zirconium Mixed Oxides. *AIChE J* **2017**, *63* (2), 725.

(184) Gamarra, D.; Munuera, G.; Hungría, A. B.; Fernández-García, M.; Conesa, J. C.; Midgley, P. A.; Wang, X. Q.; Hanson, J. C.; Rodríguez, J. A.; Martínez-Arias, A. Structure-Activity Relationship in Nanostructured Copper-Ceria-Based Preferential CO Oxidation Catalysts. *J. Phys. Chem. C* **2007**, *111* (29), 11026.

(185) Atkinson, A. Chemically-Induced Stresses in Gadolinium-Doped Ceria Solid Oxide Fuel Cell Electrolytes. *Solid State Ionics* **1997**, *95* (3-4), 249.

(186) Marina, O. A.; Bagger, C.; Primdahl, S.; Mogensen, M. A Solid Oxide Fuel Cell with a Gadolinia-Doped Ceria Anode: Preparation and Performance. *Solid State Ionics* **1999**, *123* (1-4), 199.

(187) Artini, C.; Pani, M.; Carnasciali, M. M.; Buscaglia, M. T.; Plaisier, J. R.; Costa, G. A. Structural Features of Sm- and Gd-Doped Ceria Studied by Synchrotron X-Ray Diffraction and μ-Raman Spectroscopy. *Inorg. Chem.* **2015**, *54* (8), 4126.

(188) Calvin, S.; Carpenter, E.; Ravel, B.; Harris, V.; Morrison, S. Multiedge Refinement of Extended X-Ray-Absorption Fine Structure of Manganese Zinc Ferrite Nanoparticles. *Phys. Rev. B* **2002**, *66* (22), 224405.

(189) Yin, K.; Mahamulkar, S.; Xie, J.; Shibata, H.; Malek, A.; Li, L.; Jones, C. W.; Agrawal, P.; Davis, R. J. Catalytic Reactions of Coke with Dioxygen and Steam over Alkaline-Earth-Metal-Doped Cerium-Zirconium Mixed Oxides. *Appl. Catal. A Gen.* **2017**, *535*, 17.

VITA

Shilpa Mahamulkar was born in Satara, India to Mr. Suresh and Mrs. Vasanti Mahamulkar. She received her elementary and secondary education in Mumbai, India. She completed her undergraduate studies and received a Bachelor of Technology degree in Pharamaceutical Chemistry and Technology at Institute of Chemical Technology, Mumbai, India, in 2010. She then pursued a Masters degree in Chemical Engineering from Indian Institute of Technology, Madras, Chennai, India from 2010 to 2012. In the fall of 2012, she arrived in the U.S. to pursue higher education. She enrolled in the School of Chemical & Biomolecular Engineering at Georgia Institute of Technology, to pursue a Doctor of Philosophy degree, under the guidance of Dr. Christopher Jones and Dr. Pradeep Agrawal.